University of Latvia
Faculty of Physics and Mathematics
Department of Physics

Microconvective effects in non-isothermal and inhomogeneous dispersions of magnetic nanoparticles

by Dmitry Zablotsky

supervised by Elmārs BLŪMS, Dr. Habil. Phys.

A Dissertation Submitted in Partial Fulfillment
Of the Requirements for the Degree Of
Doctor of Philosophy (Physics)

RIGA, 2012

This work has been supported by the European Social Fund within the project «Support for Doctoral Studies at University of Latvia».

Abstract

Ferrocolloids – stable dispersions of magnetic nanoparticles – possess notable magnetic properties, which become apparent in consequence of the application of the external magnetic fields and magnetic ordering of the nanoparticles. Non-isothermal colloidal systems in turn exhibit close coupling between the gradients of temperature and concentration of the dispersed phase – Soret effect - owing to the size difference between the components of the binary mixture. The interactions of the gradients of concentration and demagnetizing field in magnetizable medium contribute to the appearance of the magnetic forces affecting the regimes of heat and mass transfer.

The subject of this theoretical investigation is the emergence and evolution of the photoabsorptive convective-diffusive microstructures in ferrocolloid layers under the influence of the applied magnetic field. For this purpose a series of model problems is formulated in order to elucidate the principal mechanisms of the formation of magnetosolutal microconvection within the concentration microstructures induced by the absorption of the incident optical intensity and the consequent appearance of the thermal gradients. The magnetoadvective contributions to the effective mass transport coefficients are obtained by theoretical and numerical methods.

The secondary stability of the extended photoabsorptive microstructures is considered with respect to the variation of the control parameters. The destabilization of the extended gratings and the subsequent breaking of the translational symmetry are observed in numerical simulations. In turn, the loss of stability of the bidirectional grids is followed by the reduction of the order of the rotational symmetry.

The obtained theoretical results permit interpreting or reinterpreting some peculiarities of the real observations of the formation and evolution of the photoabsorptive concentration microstructures in the framework of magnetoadvective transport. The consideration of the influence of magnetosolutal microconvection in observable parameters has allowed describing the underlying microscopic mechanisms of some previously unexplained effects. In principle, the formation of the parasitic magnetic microconvection within the photoabsorptive microstructures under the action of the applied magnetic field is confirmed.

Preface

This investigation was conducted in the Laboratory of Heat and Mass Transfer of the Institute of Physics, University of Latvia between 2008 and 2012 under the supervision of Dr. habil. phys. Elmars Blums. I am deeply thankful to prof. Blums for suggesting a novel and interesting topic for research and for his valuable guidance of my work.

I am grateful to Dr. Ansis Mezulis for acquainting with the forced Rayleigh scattering technique and the peculiarities of formation and observation of photoabsorptive microstructures in magnetic dispersions.

I want to thank Mikhail Maiorov for sharing his knowledge and extensive experience on the magnetic effects and development of transport processes in ferrofluids.

The financial support of the European Social Fund within the project «Support for Doctoral Studies at University of Latvia» is gratefully acknowledged.

Contents

Introduction 7

Ferrofluids 7

Convective effects 9

Photoabsorptive transport 10

Overview 13

1. Physical model 15

1.1. Governing equations 15

1.1.1. Colloidal dispersions 15

1.1.2. Magnetic force 18

1.1.3. Drift of ferroparticles 21

1.2. Dimensional analysis 22

1.2.1. Dimensionless form of equations 22

1.2.2. Relationship between the scales 24

2. Photoabsorptive gratings 29

2.1. Definition of the problem 29

2.2. Thin ferrofluid layers 33

2.2.1. Base state 35

2.2.2. Linear stability problem 38

2.2.3. Nonlinear regime 44

2.2.4. Enhancement of mass transport 50

3. Extended microstructures 53

3.1. Formation 53

3.1.1. Transversal boundary 54

3.1.2. Stationary diffusive state 56

3.1.3. Secondary photoabsorption 62

3.1.4. Diffusive relaxation 65
3.1.5. Photoabsorptive microconvection 72
3.1.6. Normal field 83
3.1.7. Determination of transport coefficients 87
3.2. Stability 93
3.2.1. Definition of the problem 93
3.2.2. Instability in ∥ field 99
3.2.3. Instability in ⊥ field 103
3.2.4. Nonlinear regime 105
4. Microstructure grids 110
5. Localized structures 120
5.1. Diffusive state 121
5.2. Stationary microconvection 125
5.3. Azimuthal instability 127
Discussion 131
Final remarks 141
Bibliography 145

Introduction

Ferrofluids

The special properties of the magnetic liquids are determined by their structure. By composition ferrofluids are stabilized colloidal dispersions of ferromagnetic nanoparticles in liquid carrier - binary mixtures with magnetic properties introduced by the solid phase [1]. Depending on the circumstances and the amount of the necessary information, ferrofluids may be considered as single phase magnetizable fluids [2] or a multiphase medium [3]. Both approaches have been successfully employed and validated under different conditions. In fact, it seems appropriate to use the term *ferrofluid*, introduced by Rosensweig [4] for this purpose, when the continuum properties of these materials are under discussion. On the other hand, when the structure of the magnetic dispersion is emphasized they are more conveniently referred to as *ferrocolloids*. Still, the terms *ferrofluids*, *magnetic fluids* [5], *ferrocolloids*, *magnetic nanocolloids*, *magnetic nanosuspensions* or *magnetic dispersions* and other combinations are used more or less interchangeably in the literature.

The characteristic size of the dispersed phase in ferrofluids is in the nanometer range; consequently, the Brownian forces are normally sufficiently strong to prevent the sedimentation of the nanoparticles. In this respect ferrofluids are distinguished from the unstable magnetorheological fluids containing microsized magnetic particles.

For the purpose of protecting the dispersed phase from coagulation due to Vaan der Waals or magnetic interactions, the solvation layer is formed on the surface of the nanoparticles during the preparation process. The particular choice of the surfactant depends on the composition of the ferrofluid, but two types of stabilization are usually employed: the steric repulsion in organic solvents and ionic stabilization in polar solutions. Additionally, the chemical adsorption of the stabilizing agent may in a manner degrade the magnetic properties of the surface of the ferroparticle. In fact, the complex structure of the solvation shell and the solvent-particle interface has fundamental impact on the mass transport processes in non-isothermal ferrocolloids [6].

In the absence of the external magnetic fields the magnetic fluids behave in the similar manner as conventional colloidal dispersions. Naturally, the scope of applications of the ferrofluids is defined by their interactions with the applied field. The single-domain structure

of the ultrafine ferroparticles ensures the pronounced magnetic properties of the ferrocolloid. The application of the external magnetic field introduces a preferred direction to the suspended ensemble of the otherwise chaotically oriented magnetic nanoparticles. Macroscopically, ferrofluids behave as paramagnetic medium; the dispersed phase returns to the disordered state with no remanent magnetization upon the elimination of the applied field through a process known as rotary diffusion. Still, ferrofluids are distinguished from other typical paramagnetic materials by considerably greater magnetic susceptibility, frequently described in terms of *superparamagnetism* [7].

The complexity of the transport processes in magnetic dispersions ensues from their coupled and often nonlinear nature. The asymmetric size difference between the dispersed nanoparticles and the molecules of the solvent are the reason for the pronounced Soret effect in nonisothermal colloidal solutions [8]. Both normal [11] and anomalous [6] thermodiffusion have been observed in ferrofluids with different structure and stabilization. On the other hand, the reciprocal process – Dufour effect – is generally weak except in gas mixtures [9]-[10].

The spatial nonhomogeneity of the internal demagnetizing fields induced by the nonhomogeneity of the magnetic dispersion with respect to the concentration of the dispersed phase promotes the redistribution of the ferroparticles due to magnetophoresis in the self magnetic field upon the application of the external magnetic field. The magnetic particles are attracted to the regions of higher magnetic field strengths, but in turn, the accumulation of the ferroparticles weakens the external field through demagnetization. This self consistent interaction is conveniently described in terms of *magnetic diffusion* [53].

In nonisothermal ferrocolloids the thermal dependence of the magnetic susceptibility combines several factors of different nature. The thermal expansion of the ferrofluid and the thermal dependence of the saturation magnetization of the ferroparticles are in the essence of the thermomagnetic effect [1]. The consequent depletion of the magnetic nanoparticles from the regions of higher temperature can be interpreted in terms of the *magnetic thermophoresis* [12]-[15].

The existing and emerging applications of the magnetic fluids in engineering and technology require the complete understanding of the heat and mass transport processes occurring within the ferrofluid and actualize the problem of stability of the transport regimes under different operating conditions, in different environments and ranges of parameters.

Convective effects

It is generally regarded that the first systematic research into the buoyancy driven convection is due to Benard (1900) [16], who observed the formation of steady hexagonal convective cells above some critical threshold in a layer of liquid heated from below. Somewhat later, Strutt (1916) [17] obtained a theoretical solution for the model problem of convective stability in a layer with free boundaries. While a principal success of the hydrodynamic stability theory, it is now established that although the driving mechanism of convection due to Rayleigh and Benard are the same – thermal buoyancy, the convective patterns are different due to the influence of the thermocapillary forces in Benard's experiment [18].

The fundamental research by Benard and Rayleigh was not only the cornerstone of the theory of convective stability, but also one of the first scientific evidences of pattern formation and self-organization in nonequilibrium dissipative systems. The Rayleigh-Benard system has proven to be a convenient model problem for the investigation of the hydrodynamic stability and convective effects in spatially extended systems [19]. In fact, the mechanisms of structure formation and evolution in Rayleigh-Benard configuration share many common aspects with other nonlinear systems, even with different physical nature [20].

At present the theory of the hydrodynamic stability of the single component fluid is well established and the principal convective patterns and bifurcation scenarios in the Rayleigh-Bernard and other classical configurations have been the focal point of more than a century of intensive research. In turn, the Soret coupling in molecular binary mixtures has yielded a surprisingly rich pattern forming behavior of the thermogravitational convection [20]-[21]. The thermophoretic fluxes can have a stabilizing or destabilizing effect on the diffusive base state or the established convective state, depending on the orientation of the thermal gradient and the sign of the Soret effect [22]. The difference between the thermal and mass diffusivities in binary mixtures can lead to interesting dynamic effects in double diffusive convection. Apart from Bernard rolls, spatiotemporal structures like convective squares and crossrolls [23]-[24] as well as oscillatory [25] and wave-like regimes have been discovered [26]-[29].

In turn, strong asymmetry in size and mass between the constituents of colloidal dispersions as opposed to the molecular mixtures makes for large solutal buoyancy and low diffusive mobility of the dispersed phase [30]-[32]. The interplay between the thermal and solutal forces is weakened and the wave regimes become suppressed [37]. Sharp boundary layers and slow advancement of the concentration fronts complicate both the theoretical and

experimental analysis of the instabilities and bifurcation scenarios [30]-[36]. Still, to a large extent just the dynamics of the concentration field determine the mechanical equilibrium of the dispersion and the long-term stability of the convective regimes [30].

Apart from the thermogravitational buoyancy, the magnetic mechanism of destabilization occurs in non-isothermal ferrocolloids upon the application of the external magnetic field [38]-[39]. The internal gradients of the induced demagnetizing field can destroy the mechanical equilibrium of the conductive state of the ferrofluid layer even in uniform applied fields. In this respect, the influence of the thermomagnetic effect is perhaps described most thoroughly both from the theoretical point of view and experimentally, the scientific interest being guided by the potential in the prospective applications [41].

In turn, the magnetosolutal buoyancy appears in magnetizable dispersions due to the stratification by magnetophoretic [42]-[43] and thermophoretic forces [44]-[45] or gravitational sedimentation [46]-[48] in magnetic field. While the magnitude of the solutal effects is large in comparison with the thermoconvective destabilization, their dynamics is constrained by the slow diffusion timescale. The principal successes were achieved with account to the magnetoconvective instability in the magnetodiffusive evolution of the concentration fronts [49]-[51].

Still, it is clear that the convective-diffusive transport in non-isothermal and inhomogeneous magnetic dispersions is a complex process defined by the complicated and simultaneous coupled interactions of the gradients of temperature, concentration and the demagnetizing field. Only recently has emerged the understanding of the substantial influence of the concentration field on thermal and magnetic convection in magnetic dispersions.

Photoabsorptive transport

The discovery of the powerful sources of coherent radiation and the advances of the laser physics in the 60s and 70s necessitated the deeper understanding of the mechanisms of interaction of the electromagnetic radiation with matter. It has long been established that the propagation of the sufficiently powerful laser beams always causes the appearance of the thermogravitational convection in liquids or gasses [52]. Naturally, the investigation of the photoabsorptive transport processes and reciprocal effects between the beam and the medium of propagation was crucial for the design and application of lasers.

One of the most common and best studied effects is the formation of the thermal lens along the path of the laser beam. Based on the thermal dependence of the refractive index is the

Forced Rayleigh Scattering technique, developed for the purpose of studying the heat and mass transport processes in the medium. If a photoabsorptive thermal perturbation has a regular structure, such as, for example, formed by the focused interference pattern of two laser beams, than the regularity of the corresponding refractive index grating possesses the properties of a diffraction grating. The character of the relaxation dynamics of the secondary signal diffracted from the refractive index modulation gives valuable information about the evolution of the transport processes in the medium.

In binary mixtures with pronounced Soret effect the formation of the thermal gradient due to photoabsorption will inevitably initiate the emergence of the corresponding concentration gradient. In asymmetric mixtures such as colloidal dispersions or, in particular, ferrocolloids, even small temperature inhomogeneities create significant microscale variations of the concentration of the dispersed phase. Very low diffusive mobility of the dispersed phase in relation to the thermal diffusivity allows for the separation of the timescales and the thermal and concentration contributions to the modulation of the refractive index, so that the dynamics of the mass transport can be observed.

The theoretical description of the Soret effect estimates little influence of the external magnetic field on the transport process. In ferrocolloids, dispersions possessing magnetic properties, the magnetophoretic and dipolar interactions introduce notable contributions to the gradient diffusion [53]-[54] and thermophoresis [55] in the applied field. This result was effectively interpreted in terms of *magnetodiffusion* and *magnetic thermodiffusion*. An alternative hypothesis was expressed [56]-[57] that the observed peculiarities of the concentration dynamics in the FRS procedure are the consequence of the loss of stability of the advancing concentration front and the development of magnetoconvection. Independent measurements of the Soret effect in the thermodiffusion columns also point to a strong influence of the magnetic field [13]-[15].

By now extensive experimental investigations have been carried out with attempt to expose the role of the microconvective transport [58]-[62]. While it is possible to interpret the accumulated results in the framework of a phenomenological theory [63], no definite conclusion can be made with regard to the microscopic physical nature of the transport process.

The peculiarities in the evolution of the photoabsorptive microstructures due to the simultaneous action of the gradients of temperature, concentration and demagnetizing field

were also noted in [64]-[65]. The authors described dynamic oscillations of the thermal lens upon the application of the external magnetic field. A phoretic model [66]-[67] has been proposed to describe these effects. While the influence of the magnetic microconvection was not accommodated, its presence cannot be ruled out.

Perhaps for the first time the formation of the photoabsorptive magnetoconvection in ferrofluid layer within the beam spot of a laser was recognized in [68]-[69]. The authors report the observations of a novel magnetoconvective instability driven by the interactions of the thermophoretic and diffusive fluxes in the applied magnetic field. Interestingly, the observed deformation of the concentration microstructure allows for an alternative explanation in the framework of the phoretic effects alone [70]-[71]. The attempt to describe the driving force of the convective instability sparked a curious but controversial discussion on the form and range of validity of the magnetic force [72]-[75]. In fact, this issue is crucial to the present investigation and will be discussed in more detail in the appropriate section.

From the above, one may conclude that there exists an actual need of additional theoretical investigations of the complex microscale interactions between the gradients of temperature, concentration and the demagnetizing field in ferrodispersions to gain understanding of their role in the formation of the magnetic microconvection. The mechanisms of the emergence of microscale magnetoconvection are not clear at the moment and its presence or significance in the formation of the photoabsorptive microstructures is not yet apparent.

The ferrofluids, ferrodispersions attract considerable scientific interest by the possibility of magnetic control over the transport processes. Along with the traditional applications of the magnetic colloids essentially new ones are being put forward. Photoabsorptive microconvection is a prospective direction in biotechnology for the purpose of confining and manipulating macromolecules [76]-[77], efficient replication of DNA [77]-[79], growth of protein or colloidal crystals [80]. The photoabsorptive methods are most convenient for the formation of the concentration microstructures with the desired shape. The absorption of incident intensity by the ferroparticles allows transmitting the thermal energy to the whole volume of the ferrofluid layer within the penetration depth of the beam. The focusing of the optical radiation enables the creation of considerable thermal gradients and the corresponding concentration gradients even at moderate beam intensities and temperature differences. The possibility of forming localized or extended microstructures within the ferrofluid layer was demonstrated by different experimental arrangements. The combination of localized photoabsorption, thermophoretic depletion and magnetic effects in ferrocolloids allows great

degree of control over the processes in microscale systems. In this regard and in connection with the widening area of applications of the magnetic fluids in engineering and modern technology deep understanding of the fundamental transport processes is required; increases the level of significance of the problem of stability of the regimes of heat and mass transfer in ferrocolloids in different environments, operating conditions and ranges of parameters.

The *aim* of the current theoretical investigation is to elucidate through a series of model problems the role of the magnetoconvection in the formation and evolution of the photoabsorptive concentration microstructures in ferrocolloids in the presence of the applied magnetic field, consider the stability of these structures to the variation of parameters and to interpret some peculiar results of the available experimental measurements with account for the microconvective effects, to gain evidence of the presence of photoabsorptive magnetoconvection in real systems.

Overview

Structurally this dissertation consists of an introduction, five main sections describing the methodology and the obtained results, discussion and conclusions. In the *first section* the physical model governing the transport processes in non-isothermal and inhomogeneous magnetic dispersions, which will be used throughout the investigation, is developed on the basis of the mixture model approach and the principal approximations are introduced. The shape of the concentration microstructures is determined by the equilibrium of fluxes due to the gradient diffusion, thermophoresis, magnetophoresis and advection. The creeping microconvection driven by the magnetic ponderomotive forces is described in the Stokes approximation. The dimensionless form of the equations and the dimensionless parameters characterizing the problem are then obtained after the introduction of the characteristic scales.

In the *second section* the stability of a flat periodic concentration profile is considered in the presence of the applied magnetic field. This problem bears qualitative similarity to the formation and relaxation stages of the FRS procedure in thin ferrofluid layers. The linear analysis follows the approach of [56]-[57] and the determined parameters of the critical perturbation allow the subsequent considering of the nonlinear evolution of the concentration front above the threshold of the instability.

In the *third section* the transversal parasitic microconvection emerging within the photoabsorptive concentration microstructures is described as a possible mechanism of the development of convective currents. The consideration of the transversal direction reveals two

principal reasons for the formation of this type of magnetoconvection – the bulk contributions due to the interaction of the gradients of concentration and demagnetizing field and the boundary effects due to the discontinuity of the magnetization on the sidewalls of the layer. The influence of the convective fluxes is then considered as a perturbation of the diffusive base state. The calculation of the effective transport coefficients reveals the considerable role of advection in the mass transport processes within the photoabsorptive microstructures.

This section also deals with the problem of hydrodynamic stability of the extended convective-diffuse microstructures formed by photoabsorption. The instability due to the breaking of the translational symmetry and the resulting undulatory bending or peristaltic stratification of the concentration front is observed in numerical simulations. The corresponding linear stability problem is formulated and solved for the purpose of determining the threshold of the corresponding instabilities. The similarity and important distinction between this type of destabilization and the convective instability of a flat concentration front, considered in the previous section, is noted as well.

The *fourth section* describes the formation of the bidirectional periodic microstructures, concentration grids, with account for the magnetic microconvection. The evolution and eventual shape of the photoabsorptive grids is determined by numerical integration of the governing equations in real variables in the finite volume method formulation. The convective patterns forming within these microstructures resemble systems of toroidal vortices oriented along the external field. The destabilization of the array of convective-diffusive microstructures is observed at some parameters.

In the *fifth section* the problem of formation of localized microstructures embedded within the ferrofluid layer is considered on the example of the photoabsorption within the spot of a Gaussian beam. The role of the microconvective transport and the stability of the localized formations with respect to azimuthal perturbations of higher order are briefly discussed.

The *discussion* of the most significant results is offered in the corresponding section. Some experimental observations of photoabsorptive magnetic microstructures – gratings and bidirectional grids - available in the literature and otherwise are interpreted in the framework of the microconvective effects. Substantial evidence of the existence of *invisible* [70] magnetosolutal microconvection within the concentration microstructures is presented by comparison of the calculations and the results of real measurements.

Physical model

1.1. Governing equations

1.1.1. Colloidal dispersions

Depending on the circumstances and the ammount of the necessary information ferrofluids can be modeled either as homogeneous fluids with magnetic properties or colloidal dispersions of ferromagnetic nanoparticles in liquid carrier [4]. The dynamics of the solid constituent is usually not considered on conventional lengthscales due to the low mobility of the nanoparticles and as a consequence – extremely long diffusion timescales, so that the former approach is sufficient for the adequate description of the ferrofluid as a whole. On microscale the relative motion of the solid phase caused by thermal or magnetic forces becomes significant in many heat and mass transfer processes.

The postulate approaches [81] to the formulation of the dynamic models of the ferrocolloid are based on augmenting the classical single fluid equations by an additional balance equation and the appropriate constitutive relations. The form of the additional equations can frequently be based on the single fluid approximation and although the construction of such models possesses sound reasoning, it is in part guided by intuition.

It is clear that the mathematical formulation of the physical model governing the dynamics of the ferrocolloid has to be based on the fundamental conservation laws of mass, momentum and energy. The continuum approach to physical modeling requires the introduction of the formal spatial fields correlating with the physical quantities measurable in experiments. In the case of multiphase mixtures it is possible to initially formulate the balance and constituitive equations separately for each phase and complement them by the appropriate jump and boundary conditions. The general form of the balance equation for a mass-weighted quantity ψ_k for phase *k* in local instant formulation [82]

$$\frac{\partial}{\partial t}(\rho_k \psi_k) + \boldsymbol{\nabla} \cdot (\rho_k \psi_k \boldsymbol{u_k}) = -\boldsymbol{\nabla} \cdot J_k + \rho_k \phi_k \tag{1.1}$$

with interface efflux J_k, volume source ϕ_k is the basis of continuum mechanics.

In order to formally bring the separate continua of the phases into a “mixture of continua” or a single quasi-continuum the local field equations are subjected to spatial or time averaging.

The general averaged continuity and momentum balance equations have been formulated [81]-[82]

$$\frac{\partial}{\partial t}(\rho_k \varphi_k) + \boldsymbol{\nabla} \cdot (\rho_k \varphi_k \boldsymbol{u_k}) = \Gamma_\mathrm{k} \tag{1.2}$$

$$\frac{\partial}{\partial t}(\rho_k \varphi_k \boldsymbol{u_k}) + \boldsymbol{\nabla} \cdot (\rho_k \varphi_k \boldsymbol{u_k} \otimes \boldsymbol{u_k}) = -\varphi_k \boldsymbol{\nabla} p_k + \boldsymbol{\nabla} \cdot (\varphi_k \boldsymbol{\tau_k}) + \varphi_k \boldsymbol{f_k} \tag{1.3}$$

with φ_k - either a void-fraction or volume fraction depending on the form of averaging, Γ_k is the mass source of individual phases, p_k - partial pressure, $\boldsymbol{\tau_k}$ is the stress tensor and $\boldsymbol{f_k}$ – the momentum sources.

The averaged system of balance equations for a binary system consists of six balance equations complemented by the jump conditions describing the interaction of the phases. The separate description of the phase dynamics is excessively complicated. Alternatively, it is possible to consider the dynamics of the mixture as a whole.

The continuity equation for the mixture is obtained by summing over the continuity equations of the individual phases (1.2)

$$\frac{\partial \rho_m}{\partial t} + \boldsymbol{\nabla} \cdot (\rho_m \boldsymbol{u_m}) = 0 \tag{1.4}$$

with $\rho_m = \sum_\mathrm{k}^{\mathrm{s,p}} \varphi_k \rho_k$ and center-of-mass velocity $\boldsymbol{u_m} = \frac{1}{\rho_m} \sum_\mathrm{k}^{\mathrm{s,p}} \varphi_k \rho_k \boldsymbol{u_k}$. The quantities related to the solvent phase and the suspended particle phase are referred to by the corresponding indices s and p.

The momentum balance equation for the mixture results similarly from summing over the separate momentum equations for the individual phases

$$\frac{\partial}{\partial t}(\rho_m \boldsymbol{u_m}) + \boldsymbol{\nabla} \cdot (\rho_m \boldsymbol{u_m} \otimes \boldsymbol{u_m}) = -\boldsymbol{\nabla} p_m + \boldsymbol{\nabla} \cdot \boldsymbol{\tau_m} + \boldsymbol{f_M} - \boldsymbol{\nabla} \cdot \sum_{k=s,p} \varphi_k \rho_k \boldsymbol{U_{mk}} \otimes \boldsymbol{U_{mk}} \tag{1.5}$$

with $p_m = \sum_\mathrm{k}^{\mathrm{s,p}} \varphi_k p_k$, $\boldsymbol{\tau_m} = \sum_\mathrm{k}^{\mathrm{s,p}} \varphi_k \boldsymbol{\tau_k}$, $\boldsymbol{U_{mk}} = \boldsymbol{u_k} - \boldsymbol{u_m}$, $\boldsymbol{f_M} = \varphi_p \boldsymbol{f_p}$ – magnetic force, acting on the mixture.

The motion of the solid phase is described by equation (1.2) taking into account that the amount of the nanoparticles is conserved

$$\frac{\partial}{\partial t}(\rho_p \varphi_p) + \boldsymbol{\nabla} \cdot (\rho_p \varphi_p \boldsymbol{u_m}) = -\boldsymbol{\nabla} \cdot (\rho_p \varphi_p \boldsymbol{U_{mp}}) \tag{1.6}$$

Assuming that the mass of the ferroparticles is many times larger than the mass of the corresponding volume of the carrier phase, it is more convenient to rewrite equations (1.4)-(1.6) in terms of the mass fraction $c = \frac{\varphi_p \rho_p}{\rho_m}$ of the dispersed phase rather than the volume fraction. In fact, the expression for the volume fraction flow $\boldsymbol{J_\varphi} = \varphi_p \boldsymbol{U_{mp}}$, which is sometimes used, is accurate only in very dilute dispersions.

Introducing the slip velocity relative to the continuous phase as $\boldsymbol{U_{sp}} = \boldsymbol{u_p} - \boldsymbol{u_s}$ and assuming that the densities of the phase materials are constant except in the magnetic force term $\boldsymbol{f_M}$ (which is in essence the analogy of the Oberbeck-Boussinesq approximation) the system of equations is obtained

$$\boldsymbol{\nabla} \cdot \boldsymbol{u_m} = \frac{\rho_p - \rho_s}{\rho_p \rho_s} \boldsymbol{\nabla} \cdot \boldsymbol{J}_c \tag{1.7}$$

$$\rho_m \left[\frac{\partial c}{\partial t} + \boldsymbol{u_m} \cdot \boldsymbol{\nabla} c \right] = -\boldsymbol{\nabla} \cdot \boldsymbol{J}_c \tag{1.8}$$

$$\rho_m \left[\frac{\partial \boldsymbol{u_m}}{\partial t} + (\boldsymbol{u_m} \cdot \boldsymbol{\nabla}) \boldsymbol{u_m} \right] = -\boldsymbol{\nabla} p_m + \boldsymbol{\nabla} \cdot \boldsymbol{\tau_m} + \boldsymbol{f_M} - \boldsymbol{\nabla} \cdot \left[\boldsymbol{J_c} \otimes \boldsymbol{U_{sp}} \right] \tag{1.9}$$

The set of balance equations (1.7)-(1.9) for the mixture and the dispersed phase is usually referred to in the literature as the drift-flux model, the mixture model or the algebraic slip model depending on the author. The flux $\boldsymbol{J}_c = \rho_m c(1-c) \boldsymbol{U_{sp}}$ is therefore correspondingly referred to as the drift flux of the ferroparticles relative to the continuous phase and must be expressed through the constitutive relations.

In the case when the dispersed phase is solid it is reasonable to assume the existence of a common pressure field $p = p_m = p_k$. In turn, determining the contributions of the dispersed phase to the viscous shear stress tensor of the mixture $\boldsymbol{\tau_m}$ is a more complicated problem; the form of these contributions obviously depends on the structure of the dispersion and the operating conditions. Most commonly the carrier fluid is a Newtonian fluid, then in the absence of the external magnetic field and at moderate concentrations of the solid phase the non-Newtonian effects in ferrofluids are generally not significant. In the limit of infinite dilution the theoretical Einstein's relation is available for the viscosity of a suspension of spherical particles

$$\eta_\varphi = \eta\left(1 + 2.5\varphi_p\right) \tag{1.10}$$

At larger concentrations of the solid phase the collective hydrodynamic interactions of the ensemble of the particles become significant and higher terms in φ_p should be taken into

account. In most situations the empirical approach is adopted for this purpose. In this regard, the reader is referred to the pioneering works of Batchelor [83]-[84] on microhydrodynamics of dispersions.

In consequence of the application of the external magnetic field to a magnetic colloid several factors of different nature may contribute to the form of the shear stress tensor. The restriction of the internal degree of freedom – the internal rotations – and the consequent competition of the magnetic and hydrodynamic torque lie in the basis of the *magnetoviscous effect* [1]. While most considerable in oscillating fields, the mechanism of magnetic viscosity can become apparent in the interactions of the hydrodynamic vortices with stationary homogeneous fields. In turn, the considerable magnetic interactions of the ferroparticles can alter the internal structure of the ensemble and induce the formation of aggregates in concentrated ferrodispersions, leading to the appearance of non-Newtonian effects.

Still, the problem of structural evolution and rheology of the magnetic fluids is outside the scope of this investigation. The magnetic systems under consideration possess moderate concentrations of ferroparticles and are subjected to stationary homogeneous magnetic fields. The thermal variations are also not sufficient to induce substantial changes of viscosity and the intensity of convective motion is comparable with the diffusive mobility of the ferroparticles. In this regard, it is convenient to adopt the conventional form of the Newtonian viscous stress tensor corresponding to that of the isotropic and incompressible fluid with constant viscosity.

1.1.2. Magnetic force

In constant or slowly varying applied magnetic fields the system of Maxwell's equations reduces to those of magnetostatics. Disregarding the electric currents as ferrofluids are typically non-conducting, the configuration of the magnetic field within the magnetizable media is determined by the system

$$\boldsymbol{\nabla} \cdot \boldsymbol{B} = \boldsymbol{0} \tag{1.11}$$

$$\boldsymbol{\nabla} \times \boldsymbol{H} = \boldsymbol{0} \tag{1.12}$$

with auxiliary field $\boldsymbol{H}$ and magnetic induction $\boldsymbol{B} = \mu_0(\boldsymbol{H} + \boldsymbol{M})$.

In the presence of the external field the magnetic dispersions acquire magnetization $\boldsymbol{M}$, which is in principle a dynamic quantity requiring an additional dynamic equation. Still, its relaxation to the equilibrium state occurs mainly through the Brownian mechanism [5] and is characterized by the Brownian relaxation time, which is very small in comparison with the

diffusion time scale that is adopted throughout this investigation. It can then be assumed that the induced magnetization does not depend on time. The dynamic effects associated with the spontaneous reversals of the magnetic moments of the ferroparticles (Néel relaxation mechanism) will be omitted as well.

The form of the expression for the magnetic force $\boldsymbol{f_M}$ (1.5) acting on a polarizable medium has been a matter of debate recently. The partial reason for this controversy is that while the expression for the microscopic ponderomotive force acting in the external field $\boldsymbol{H}$ on an infinitesimal dipole $\boldsymbol{m}$ is well known and given by the Lorentz force $\mu_0(\boldsymbol{m}\boldsymbol{\nabla})\boldsymbol{H}$, the macroscopic averaged expression is not easily obtained.

The first consistent derivation based on the thermodynamic principles is attributed to Korteweg (1880) and Helmholtz (1882) [2]

$$\boldsymbol{f_M} = \boldsymbol{\nabla}\left[\frac{H^2}{2}\rho\left(\frac{\partial\mu}{\partial\rho}\right)_T\right] - \frac{H^2}{2}\boldsymbol{\nabla}\mu \tag{1.13}$$

where μ is the magnetic permeability.

The method was generalized by Cowley and Rosensweig [85] to account for the nonlinear dependence of the magnetization of ferrofluids

$$\boldsymbol{f_M} = -\boldsymbol{\nabla}\left[\mu_0\int_0^H\left(\frac{\partial Mv}{\partial v}\right)_{H,T}dH\right] + \mu_0(\boldsymbol{M}\boldsymbol{\nabla})\boldsymbol{H} \tag{1.14}$$

and v is the specific volume.

If the magnetic susceptibility does not depend on the applied field, i.e. for linearly magnetizable media, the expression due to Korteweg and Helmholtz is recovered after some transformations.

Owing to low compressibility of the solid phase the magnetostriction of the nanoparticles can be neglected [2] and the product Mv does not depend on v for dilute ferrocolloid. Alternatively, the approximation of incompressibility can be invoked once and the term containing the integral introduced into the pressure term of the momentum equation (1.9). Then the first term in (1.14) vanishes and the expression for the Kelvin-Helmholtz force is obtained

$$\boldsymbol{f_M} = \mu_0(\boldsymbol{M}\boldsymbol{\nabla})\boldsymbol{H} \tag{1.15}$$

The similarity of this result to the expression for the Lorentz force on a tiny dipole in a non-uniform field is quite remarkable.

The validity of relations (1.13)-(1.15) is not immediately recognized in stratified ferrocolloid with inhomogeneous distribution of ferroparticle concentration. In fact, an expression similar to (1.14) was obtained for a ferrosuspension [86] with the magnetostrictive term $\left(\frac{\partial Mv}{\partial v}\right)_{H,T} = M - \rho\left(\frac{\partial M}{\partial \rho}\right)_{H,T}$ replaced by a similar but not identical relation $M - n_m\left(\frac{\partial M}{\partial n_m}\right)_{H,T}$. Considering a more detailed mixture model [87] it appears that $\rho\left(\frac{\partial M}{\partial \rho}\right)_c = n_m\left(\frac{\partial M}{\partial n_m}\right)_{H,T}$ and the two formulations are equivalent. If the dipolar interactions can be neglected and the susceptibility of the magnetic dispersion is proportional to the number of the ferroparticles than the expression for the Kelvin-Helmholtz force (1.15) is again obtained.

The range of validity of the Kelvin-Helmholtz force was disputed again somewhat later [72] in a discussion following the observation of a novel microconvective instability induced in a layer of ferrofluid by photoabsorption under the action of the applied magnetic field [68]. The results of the experimental investigation by Luo, Du and Huang are of direct relevance to this work (see Discussion) so it is appropriate to consider the subject of the matter more closely.

It was pointed out that the alternative choice of the constitutive expression for the magnetic susceptibility $\boldsymbol{M} = \tilde{\chi}\boldsymbol{B}$ in terms of the macroscopic field $\boldsymbol{B}$ rather than the conventional definition $\boldsymbol{M} = \chi\boldsymbol{H}$ through the microscopic field results in a different formulation for the magnetic force. Making use of the expression due to Korteweg and Helmholtz (1.13)

$$\tilde{\boldsymbol{f}}_{\boldsymbol{M}} = \boldsymbol{\nabla}\left[\frac{B^2}{2}\rho\left(\frac{\partial \tilde{\chi}}{\partial \rho}\right)_T\right] - \frac{B^2}{2}\boldsymbol{\nabla}\tilde{\chi} \tag{1.16}$$

the relations (1.13) and (1.16) are physically equivalent. However, the expression for the Kelvin-Helmholtz force has been obtained on the grounds of the proportionality of the magnetic susceptibility to the density of the ferrofluid, which constitutes a dilute limit of non-interacting ferroparticles. Invoking the same assumption $\tilde{\chi}\sim\rho$ for (1.16) a similar but evidently distinct relation was given

$$\tilde{\boldsymbol{f}}_{\boldsymbol{M}} = \mu_0(\boldsymbol{M}\boldsymbol{\nabla})\boldsymbol{B} \tag{1.17}$$

The two formulations (1.15) and (1.17) for the Kelvin-Helmholtz force are in apparent contradiction. For the sake of consistency it was required that $\tilde{\chi} \approx \chi$ and then $\tilde{\boldsymbol{f}}_{\boldsymbol{M}} \approx \boldsymbol{f}_{\boldsymbol{M}}$, which limits the expression (1.15) to very dilute ferrofluids.

The issue was seemingly resolved by experimental measurements of the total magnetic force acting on a magnetizable body [74] invalidating (1.15) and confirming that (1.17) is the valid form of the Kelvin-Helmholtz force. The situation is not so certain, however.

It was pointed out [73] that while the approximations $\chi \sim \rho$ and $\tilde{\chi} \sim \rho$ define the range of validity of the corresponding expressions (1.15) and (1.17), it is not necessary that both are correct at the same time. In fact, the region of validity of (1.17) is much smaller than the one for (1.15) and the analysis of the pendulum experiment [74] employs the alternative formulation (1.17) outside its limited scope, but is nevertheless surprisingly accurate, while (1.15) is not. This contradiction was finally resolved by Engel [75], showing that the analysis of the pendulum experiment omits important contributions. Most importantly, the measurements of the *total* force cannot actually distinguish between the different formulations of the magnetic force *density* as the integral expression defining the macroscopic magnetic force on the container filled with ferrofluid can be decomposed in different ways.

The notable distinction between (1.15) and (1.17) is in the configurations of $\boldsymbol{B}$ and $\boldsymbol{H}$. If the external field is perpendicular to the ferrofluid layer, the magnetization and consequently the magnetic field experience a discontinuity on the layer boundary, while the magnetic induction is continuous. In the situation of induced nonuniformity of the magnetic susceptibility, the magnetic force defined by (1.17) is a bulk force, while (1.15) possesses important contributions concentrated in a narrow boundary layer. This causes peculiarities of the transport processes, which will be discussed later. Throughout this work the classical formulation (1.15) for the magnetic force density is assumed.

1.1.3. Drift of ferroparticles

In the absence of convection the phoretic transport of the magnetic nanoparticles in non-isothermal inhomogeneous ferrocolloids occurs due the presence of the gradients of concentration, temperature and the magnetically induced gradients of the demagnetizing field. The slip-flux $\boldsymbol{J_c}$ of the concentration of the solid constituent relative to the continuous phase is then comprised of the three principal components

$$\boldsymbol{J_c} = \boldsymbol{J_D} + \boldsymbol{J_T} + \boldsymbol{J_M} \tag{1.18}$$

i.e. the corresponding diffusive, thermophoretic and the magnetophoretic contributions.

The diffusive mass flux driven by the gradient of concentration is expressed by Fick's first law of diffusion $\boldsymbol{J_D} = -D\nabla c$, which also introduces the mass diffusivity D.

The convenient expression for the thermophoretic mass flux establishing the gradient of concentration in response to the thermal non-homogeneity is $\boldsymbol{J_T} = c(1-c)DS_T\nabla T$, which at same time defines the Soret coefficient S_T.

The magnetophoretic flux due to the non-uniform field can be obtained microscopically by considering the equilibrium of the Stokes' drag $6\pi\eta r\boldsymbol{U_{sp}}$ experienced by the spherical ferroparticle and the Kelvin's force $(\boldsymbol{m}\nabla)\boldsymbol{H}$ on a point dipole, which is associated with it. In strongly asymmetric solutions such as the colloidal dispersions the hydrodynamic argument is usually valid. Alternatively, a more general approach based on the thermodynamic principles can be employed [1]. Both give similar result $\boldsymbol{J_M} = \frac{m_g}{f_v}(1-c)\boldsymbol{f_M}$, where m_g is the mass of the particle and $f_v = 6\pi\eta r$ - the hydrodynamic drag coefficient.

1.2. Dimensional analysis

1.2.1. Dimensionless form of equations

The estimation of the relative importance of different terms in the balance equations can be carried out by the dimensional analysis. The following basic characteristic scales for the variables are introduced: L as the characteristic length scale - $\boldsymbol{r} = L\tilde{\boldsymbol{r}}$, diffusion time $\frac{L^2}{D}$, with D – the diffusivity of the suspended nanoparticles, as the characteristic time scale $t = \frac{L^2}{D}\tilde{t}$; characteristic temperature difference $\overline{\Delta T}$, concentration difference $\overline{\Delta c}$ and magnetic field difference $\overline{\Delta H}$. The rest of the scales follow from these definitions: velocity $\boldsymbol{u} = \frac{D}{L}\tilde{\boldsymbol{u}}$, mass flux of the suspended phase $\boldsymbol{J_c} = \rho_0\overline{\Delta c}\frac{D}{L}\tilde{\boldsymbol{J}}_{\boldsymbol{c}}$ with ρ_0 – reference density of the ferrocolloid, pressure $p = \rho_0\frac{D^2}{L^2}\tilde{p}$ and the measure for the force density $f = \frac{\eta D}{L^3}\tilde{f}$.

The set of equations (1.7)-(1.9) after the normalization becomes

$$\nabla\cdot\tilde{\boldsymbol{u}} = \frac{\rho_p-\rho_s}{\rho_p}\overline{\Delta c}\nabla\cdot\tilde{\boldsymbol{J}}_c \tag{1.19}$$

$$\left[\frac{\partial}{\partial t} + (\tilde{\boldsymbol{u}}\cdot\nabla)\right]\tilde{c} = -\nabla\cdot\tilde{\boldsymbol{J}}_c \tag{1.20}$$

$$\frac{1}{Sc}\left[\frac{\partial}{\partial t} + (\tilde{\boldsymbol{u}}\cdot\nabla)\right]\tilde{\boldsymbol{u}} = -\nabla\tilde{P} + \Delta\tilde{\boldsymbol{u}} + \tilde{\boldsymbol{f}}_{\boldsymbol{M}} - \frac{1}{Sc}\overline{\Delta c}\nabla\cdot\left(\tilde{\boldsymbol{J}}_c\otimes\tilde{\boldsymbol{U}}_{\boldsymbol{sp}}\right) \tag{1.21}$$

where the Schmidt number $Sc = \frac{\eta}{\rho_0 D}$ characterizes the ratio of momentum and mass diffusivities and prefactor Sc^{-1} was absorbed into the pressure term in (1.21).

In the dilute limit, when the characteristic concentration difference $\overline{\Delta c}$ is small, the system (1.19)-(1.21) allows making use of the pseudohomogeneous approximation for the description of the ferrocolloid [42]. The term on the right hand side of (1.19) disappears and the conventional form of the condition of divergence free velocity field for incompressible flow is recovered. The last term on the RHS of (1.21) vanishes as well. The set of mixture equations then indeed reduces to the equations of motion of a single component fluid with the Kelvin body force term, complemented by the concentration balance equation.

In turn, if the induced nonhomogeneities of the temperature, concentration and the demagnetizing field are not large, the magnetic susceptibility of the ferrocolloid can be linearized with respect to the deviations from the reference state (T_0, c_0, H_0)

$$\chi = \chi_0[1 + \chi_T(T - T_0) + \chi_c(c - c_0) + \chi_H(\boldsymbol{h}\cdot\boldsymbol{H} - H_0)] \tag{1.22}$$

with the expansion coefficients $\chi_Y = \frac{1}{\chi_0}\frac{\partial\chi}{\partial Y}$, χ_0 – reference susceptibility and $\boldsymbol{h}$ – unit vector in the direction of the applied magnetic field.

The normalized expression for the magnetic force density is then accordingly obtained after some transformations

$$\tilde{\boldsymbol{f}}_{\boldsymbol{M}} = \{Ga_m + Ra_m\tilde{T} + Rs_m\tilde{c} + Ar_m(\boldsymbol{h}\cdot\tilde{\boldsymbol{H}})\}\boldsymbol{\nabla}[(\boldsymbol{h} + r_H\tilde{\boldsymbol{H}})\cdot\tilde{\boldsymbol{H}}] \tag{1.23}$$

where $r_H = \frac{H}{2H_0}$.

The introduced dimensionless numbers characterize the relative strength of the magnetic buoyancy contributions due to thermal or solutal non-homogeneities or the consequent perturbations of the internal demagnetizing field: $Ra_m = \chi_T\overline{\Delta T}Ga_m$ is the magnetic thermal Rayleigh number, $Rs_m = \chi_c\overline{\Delta c}Ga_m$ - magnetosolutal Rayleigh number, $Ar_m = \chi_H\overline{\Delta H}Ga_m$ - magnetic Archimedes number and $Ga_m = \mu_0\chi_0H_0\frac{L^3}{\eta D}\frac{\overline{\Delta H}}{L}$ – magnetic Galilei number.

Assuming that the characteristic concentration scale $\overline{\Delta c}$ can be expressed in relation to the temperature perturbation $\overline{\Delta T}$ as $\overline{\Delta c} = c_0(1 - c_0)S_{MT}\overline{\Delta T}$ (here S_{MT} is the magnetic Soret coefficient, which will be formally introduced below) the drift flux (1.18) can then be expressed in normalized form

$$\tilde{\boldsymbol{J}}_c = -\boldsymbol{\nabla}\tilde{c} - s_m\boldsymbol{\nabla}\tilde{T} + \mathcal{M}_{ph}\boldsymbol{\nabla}[(\boldsymbol{h} + r_H\tilde{\boldsymbol{H}})\cdot\tilde{\boldsymbol{H}}] \tag{1.24}$$

with dimensionless magnetic Soret coefficient defined as $s_m = \frac{S_T}{S_{MT}}$ and the magnetophoretic number $\mathcal{M}_{ph} = \frac{\eta}{\rho_0 D}(1-c_0)\frac{m_g}{\eta f_\nu}\mu_0\chi_0 H_0 \frac{\overline{\Delta H}}{\overline{\Delta c}}$, which determines the relative mobility of the ferroparticles due to the magnetophoresis in the self-magnetic field.

The equations (1.11)-(1.12) permit to introduce the scalar potential of the self-magnetic field $\boldsymbol{H} - \boldsymbol{H_0} = -\boldsymbol{\nabla}\psi$, which allows for a more convenient treatment of the configuration of the induced demagnetizing field. The characteristic scale for this quantity follows from its definition $\overline{\Delta\psi} = \overline{\Delta H} \cdot L$ and the governing equation can be obtained without difficulty in dimensionless form

$$\Delta\tilde{\psi} = \boldsymbol{\nabla} \cdot \widetilde{\boldsymbol{M}} \tag{1.25}$$

In turn, the deviation of magnetization can be expressed omitting second order contributions

$$\boldsymbol{M} - \boldsymbol{M_0} \approx (\chi - \chi_0)\boldsymbol{H_0} + \chi_0(\boldsymbol{H} - \boldsymbol{H_0}) \tag{1.26}$$

and its proper characteristic scale is $\overline{\Delta H}$. In normalized form

$$\widetilde{\boldsymbol{M}} = \chi_0\widetilde{\boldsymbol{H}} + \left[\alpha_T\tilde{T} + \alpha_c\tilde{c} + \alpha_H\left(\boldsymbol{h}\cdot\widetilde{\boldsymbol{H}}\right)\right]\boldsymbol{h} \tag{1.27}$$

with dimensionless coefficients $\alpha_Y = \chi_Y\chi_0 H_0 \frac{\overline{\Delta Y}}{\overline{\Delta H}}$.

1.2.2. Relationship between the scales

In order to complete the proper normalization of the governing equations and find out the relative role of the contributing terms, it is necessary to determine the relationship between the thermal, concentration and magnetic scales $\overline{\Delta T}$, $\overline{\Delta c}$, $\overline{\Delta H}$. For this purpose it is appropriate to consider the drift flux $\boldsymbol{J_c}$ given by (1.18).

Given that a flat lateral temperature gradient $\boldsymbol{\nabla}T$ is induced in a layer of ferrocolloid in the presence of the similarly directed uniform applied magnetic field $\boldsymbol{H_0}$. After the establishing of the steady concentration profile the fluxes in the direction of the field obey the zero balance condition:

$$-\rho_0 D\frac{dc}{dx} - \rho_0 c(1-c)DS_T\frac{dT}{dx} + (1-c)\frac{m_g}{f_\nu}\mu_0 M_0\frac{dH}{dx} = 0 \tag{1.28}$$

From (1.11) $\frac{dH}{dx} = -\frac{dM}{dx}$ and the expansions (1.22) and (1.26) yield the stationary gradient of the magnetic field perturbation

$$\frac{dH}{dx} = -\frac{\chi_0 H_0}{1+\chi_0(1+\chi_H H_0)}\left[\chi_T\frac{dT}{dx} + \chi_c\frac{dc}{dx}\right] \tag{1.29}$$

Comparing the relations (1.28) and (1.29) allows determining the magnitude of the concentration perturbation

$$\frac{dc}{dx} = -\frac{S_T + \chi_T m_H}{1 + c_0(1-c_0)\chi_c m_H} c_0(1-c_0)\frac{dT}{dx} \tag{1.30}$$

The expression $\overline{\Delta c} = c_0(1-c_0)S_{MT}\overline{\Delta T}$ can then be recovered introducing the magnetic Soret coefficient [88]

$$S_{MT} = -\frac{S_T + \chi_T m_H}{1 + c_0(1-c_0)\chi_c m_H}, \text{ with } m_H = \frac{m_g}{f_\nu D c_0 \rho_0}\frac{\mu_0 M_0^2}{1 + \chi_0(1 + \chi_H H_0)} \tag{1.31}$$

where according to the Stokes-Einstein relation $f_\nu D = k_B T_0$.

In turn, similarly considering the dimensionless form of the drift flux (1.24) it is possible to obtain the relationship between the gradients

$$\left[1 + \frac{\tilde{\alpha}_c \mathcal{M}_{ph}}{1 + \tilde{\alpha}_H}\right]\frac{d}{dx}\tilde{c} = -\left[s_m + \frac{\tilde{\alpha}_T \mathcal{M}_{ph}}{1 + \tilde{\alpha}_H}\right]\frac{d}{dx}\tilde{T} \tag{1.32}$$

Because the gradients have been normalized, the coefficients on the right-hand side and on the left-hand side are equal. Clearly, the prefactor on the LHS is the effective diffusion coefficient d_m with the included contribution of magnetophoresis in the self-magnetic field. The coefficient on the RHS consists of two parts – first there is the magnetic Soret coefficient s_m, which has been similarly normalized to account for the presence of magnetophoresis. The second part follows from the thermomagnetic effect and the degradation of the ferrofluid magnetization in regions with higher temperature. The magnetic field thus contributes to the appearance of *magnetic thermophoresis*.

Table 1.1. Typical parameters of the ferrocolloid

Parameter	Value	
solvent density ρ_s	1000	kg m^{-3}
viscosity η	0.001	Pa s
thermal conductivity λ	0.1	W (m K)$^{-1}$
specific heat capacity c_p	2000	J (kg K)$^{-1}$
particle density ρ_p	5000	kg m^{-3}
diffusivity D	$3\cdot10^{-11}$	m^2 s^{-1}
Soret coefficient S_T	-0.16	K^{-1}
magnetic radius r_m	5	nm
spontaneous magnetization M_s	$5\cdot10^5$	A m^{-1}

The introduced dimensionless group is composed of the magnetic coefficients α_Y, mass transport coefficients - $\mathcal{M}_{ph}$, s_m and the dimensionless numbers governing the strength of the magnetic buoyancy contributions – Ra_m, Rs_m, Ar_m. The characteristic physical parameters for a typical ferrofluid based on organic solvent or water are summarized in Table 1.1.

The value of the phenomenological pyromagnetic coefficient χ_T can be experimentally measured by the method of magnetic granulometry and rarely exceeds *0.005* K^{-1} even for thermally sensistive ferrofluids. Consequently, the influence of the termomagnetic effect is rather weak and can be completely disregarded. In turn, the coefficient χ_H can also be obtained by magnetic measurements in real ferrofluid samples, but if the concentration of the ferrocolloid is not too great the characteristic value of χ_H can be estimated from the Langevin approximation of the ferrofluid magnetic susceptibility:

$$\chi_L(H) = \frac{M_{sat}}{H} L[\xi(H)] \tag{1.33}$$

with the Langevin function $L(x) = \coth(x) - \frac{1}{x}$ and $\xi(H) = \mu_0 \frac{mH}{k_B T_0}$ - the Langevin parameter, describing the ratio of the magnetic and thermal energy of the ferroparticle with magnetic dipole moment m.

Then the expression for $\chi_H = \frac{1}{\chi_0} \frac{\partial \chi_L}{\partial H}$ is obtained after some transformations

$$\chi_H(H) = -\frac{\xi_0}{H_0} \left[L(\xi_0) + \frac{3}{\xi_0} - \frac{1}{L(\xi_0)} \right] \tag{1.34}$$

with $\xi_0 = \xi(H_0)$.

In the assumed dilute limit the interactions of the ferroparticles are neglected and the magnetic susceptibility of the ferrocolloid is proportional to the concentration of the dispersed phase $\chi_c = c_0^{-1}$.

In the definition of the dimensionless susceptibilities more convenient is to use the modified coefficients $\tilde{\alpha}_Y = \alpha_Y \epsilon^{-1}$ with $\epsilon = 1 + \chi_0$ - the nonlinearity of magnetization. With the characteristic ferrofluid parameters $\tilde{\alpha}_c \approx 1$ and depends little on the applied field. The magnitude of $\tilde{\alpha}_H$ is generally considerably smaller than $\tilde{\alpha}_c$ and can be disregarded. The corresponding contribution to the magnetic buoyancy is omitted as well.

Considering a typical ferrofluid sample with the volume fraction of the solid particles φ_p at 5%, the dimensionless parameters governing the relative intensity of the mass transport

processes can be calculated. Due to the nonlinearity of the ferrofluid magnetization they depend on the magnitude of the imposed field (Figure 1.1), but are independent of the applied thermal difference, which influences only the strength of the buoyant forces.

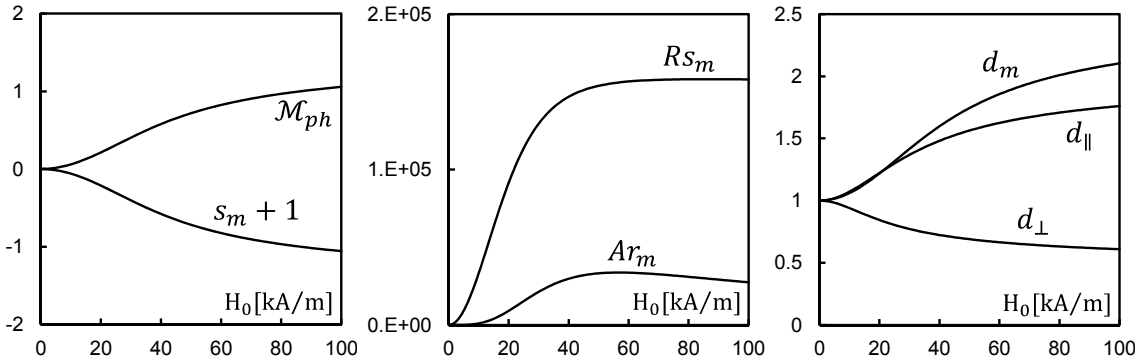

Figure 1.1. Dependence of the selected dimensionless parameters on the applied magnetic field

In turn, the magnetosolutal Rayleigh number is the principal control parameter describing the magnetic driving force of the microconvective transport. Even rather small thermal differences $\overline{\Delta T} \approx 1°K$ can produce sufficient temperature gradients so that the magnitude of Rs_m can reach significant values in the conditions of microscale transport $L \approx 50\mu m$. The value of the magnetic Rayleigh number implies a second order dependence on $\overline{\Delta T}$ and grows rapidly with the increase of the imposed thermal gradient (the estimations of the magnetosolutal Rayleigh numbers for some experimental investigations are available in [56]-[57]). This fact permits to expect the eventual formation of the magnetosolutal microconvection affecting the processes of mass transport.

From (1.32) and the presented arguments on the relative strength of the transport effects follows the definition of the bulk coefficient of magnetodiffusion in the direction of the applied field

$$d_m = 1 + \tilde{\alpha}_c \mathcal{M}_{ph} \tag{1.35}$$

The second term describes the magnetic contributions due to the magnetophoresis in the self-magnetic field of the stratified ferrocolloid. A more detailed calculation based on the thermodynamic arguments was performed [54] with account for the dipole-dipole interactions of the dispersed magnetic phase in the framework of the mean field model. The consideration of the second order terms shows that the magnetic action between the ferroparticles causes slight decrease of the effective diffusion coefficient both in the direction of the field $d_\parallel$ and in

the perpendicular direction $d_\perp$ (Figure 1.1). Still, the nonlinear magnetic diffusion is not the focus of this investigation and these effects are not considered.

In turn, it is evident that the Schmidt number Sc defined as a ratio of momentum and mass diffusivities $\frac{\eta}{\rho_0 D}$ is very large in ferrodispersions due to the relatively low diffusive mobility of the suspended nanoparticles. For the selected characteristic parameters (Table 1.1) Sc is of the order approximately $10^4 \ldots 10^5$. Consequently, the term divided by Sc vanishes from the rhs of (1.21) and so does the inertial term on the lhs. The microconvective flows are Stokes' flows.

Making use of the described simplifications the final form of the governing equations is obtained, omitting the accents over the normalized quantities

$$\boldsymbol{\nabla} \cdot \boldsymbol{u} = 0 \tag{1.36}$$

$$\left(\frac{\partial}{\partial t} + \boldsymbol{u} \cdot \boldsymbol{\nabla}\right) c = \Delta\left(c + s_m T - \mathcal{M}_{ph} H\right) \tag{1.37}$$

$$-\boldsymbol{\nabla} P + \Delta \boldsymbol{u} + R s_m c \boldsymbol{\nabla} H = \boldsymbol{0} \tag{1.38}$$

$$\Delta \psi = \tilde{\alpha}_c \boldsymbol{h} \boldsymbol{\nabla} c \tag{1.39}$$

where $H = \boldsymbol{h} \cdot \boldsymbol{H}$ is the component of the self magnetic field along the external field.

The following characteristic dimensionless parameters are used throughout this investigation if not explicitly mentioned otherwise: $\tilde{\alpha}_c = 1$, $s_m = -2$, $\mathcal{M}_{ph} = 1$.

The direction of the thermophoretic flux determined by the sign of the Soret coefficient s_m corresponds to that of the imposed thermal gradient. In that regard the dispersed ferroparticles migrate into the regions of higher temperature, the process known as *anomalous thermodiffusion*. While the mechanisms of the Soret effect in colloidal dispersions are not completely clear at the moment, the ferrocolloids stabilized by electrorepulsive forces generally exhibit negative Soret coefficients, as opposed to those with steric stabilization and consequently positive Soret effect. Still, considering the form of the equations (1.36)-(1.39) the change of sign of the concentration deviation formed by the imposed temperature gradient simply leads to the corresponding reversal of the demagnetizing field deviation and the product of the concentration deviation and the gradient of the demagnetizing field, which constitutes the magnetic force in (1.38), remains the same. Then the results of the investigation are equally applicable to both the situation of the normal and anomalous thermodiffusion and the sign of the Soret coefficient is a matter of convenience.

Photoabsorptive gratings

2.1. Definition of the problem

The experimental investigation of the microscale transport processes in real magnetic dispersions requires the controlled creation and observation of the concentration microstructures. Such task is most conveniently accomplished by optical methods. The forced Rayleigh scattering technique in the application to ferrocolloids implies the creation of a photoabsorptive thermal modulation within the ferrofluid layer leading to the emergence of the corresponding ferroparticle concentration grating due to the strong Soret effect. The induced regular perturbation of the refractive index possesses the properties of a diffraction grating and can be probed by the scanning laser. The intensity of the diffracted signal carries information about the shape of the photoabsorptive microstructure and the dynamics of its evolution.

To proceed with the description, it is first necessary to define the coordinates. For this purpose the notation of [53] is adopted. The *y*- axis is pointed in the direction of the imposed modulation and the direction corresponding to this axis will be called the parallel direction. In turn, the *x*- axis will be oriented in the perpendicular direction, but still within the plane of the layer, along the extent of the grating and is called the longitudinal direction. Finally, the *z*- axis pointed across the gap of the layer is the transversal or also perpendicular direction.

Given that a layer of ferrocolloid with thickness $\Delta z = 2Ll$ (where l - arbitrary constant) is illuminated by a light source with intensity I_0. The intensity of the incident light is not uniform but is instead modulated in the parallel direction $\sim \cos(k_y y)$ with wave-vector $k_y = \frac{\pi}{L}$. The carrier fluid is transparent and the absorption of the incident radiation takes place on the suspended nanoparticles. In turn, according to the Bouguer–Lambert–Beer law for the optical absorption by an ensemble of independent absorption centers the intensity of the illumination diminishes exponentially with the penetration depth

$$I(y,z) = \frac{1}{2} I_0 e^{-\varepsilon c z} \left[1 + \cos\left(\frac{\pi}{L} y\right)\right] \text{ with } z \in [0; 2l] \tag{2.1}$$

where ε is the appropriate extinction coefficient and $2L$ – the interfringe of the grating.

Assuming that only negligible part of the attenuation is due to scattering and the whole absorbed optical intensity is converted to the thermal energy of the ferroparticles, the

generation of heat within the layer due to the absorption of radiation is proportional to $-\frac{\partial I}{\partial z}$. More heat is generated near the upper surface of the layer than near the lower one due to the weakening of the beam and the average heat generation along the depth of the layer can be expressed as

$$\bar{q}(y) = \frac{1}{2}\overline{\Delta I}_0 \left(1 + f_c \frac{c - c_0}{c_0}\right)\left[1 + \cos\left(\frac{\pi}{L}y\right)\right] \tag{2.2}$$

with $\overline{\Delta I}_0 = I_0 \frac{1}{\Delta z}(1 - e^{-\varepsilon c_0 \Delta z})$ and $f_c = \frac{\varepsilon c_0 \Delta z}{e^{\varepsilon c_0 \Delta z} - 1}$, c_0 is the reference concentration of the ferroparticles.

In turn, the distribution of temperature within the layer of ferrocolloid can be described by introducing the modulated heat source (2.1) into the normalized temperature equation, employing the characteristic scales (section 1.2.1, taking the half-period of the modulation as the characteristic length L)

$$Le\left(\frac{\partial}{\partial t} + \boldsymbol{u}\cdot\boldsymbol{\nabla}\right)T = \Delta T + \frac{1}{2}\frac{L^2}{\lambda}\frac{\overline{\Delta I}_0}{\overline{\Delta T}}(1 + r_c c)[1 + \cos(\pi y)] \tag{2.3}$$

The prefactor $Le = \frac{D}{\kappa}$ is the Lewis number defined as the ratio of mass and thermal diffusivities. In dispersions of nanoparticles the diffusion coefficient is by several orders of magnitude smaller than the thermal diffusivity $\kappa = \frac{\lambda}{\rho_0 c_p}$. For the adopted characteristic parameters of a ferrocolloid (Table 1.1) the Lewis number can be estimated and is of the order of 10^{-3}. Consequently, the terms on the lhs of (2.3) can be disregarded – the microscale solutal convection is not sufficiently strong to deform the thermal field and the establishing of the temperature distribution occurs almost instantly on the diffusive timescale.

In turn, the introduced coefficient $r_c = f_c \frac{\overline{\Delta c}}{c_0}$ is tentatively dubbed the coefficient of secondary photoabsorption and describes the enhanced absorption of the optical intensity due to the influx of the ferroparticles into the heated region (or similarly – weakened absorption due to the depletion of the ferroparticles in the case of the positive Soret coefficient). It ensures the coupling of the temperature equation with the concentration balance equation. The role of this coefficient in the photoabsorptive mass transport will be determined later and for now the temperature field is decoupled from concentration ($r_c = 0$).

In order to solve the temperature equation for the layer, the formulation of the appropriate boundary conditions on the sidewalls is required. Still, at first it would be useful to consider

the adiabatically insulated layer. For this purpose the stationary solution of (2.3) in the absence of convection can be decomposed into the constant and the periodic component. The zero-order part of the solution is not defined for the adiabatic boundary conditions, but the first parallel mode yields the characteristic temperature difference

$$\overline{\Delta T}_0 = \frac{1}{\pi^2}\frac{L^2}{\lambda}\overline{\Delta I}_0 \tag{2.4}$$

The thermal deviation $\overline{\Delta T}_0$ was obtained under the assumption of the negligible heat diffusion through the transversal boundary. The validity of this approximation is not immediately apparent. Still, the expression (2.4) is useful for completing the proper normalization of the temperature equation (2.3)

$$\Delta T = -\frac{1}{2}\pi^2(1 + r_c c)[1 + \cos(\pi y)] \tag{2.5}$$

If the successful comparison with the experimental measurements is desired, the formulation of the necessary boundary conditions should accommodate the method of thermal stabilization of the photoabsorptive microstructure if such stabilization is employed. For the purpose of this investigation a general form of the Newton's law of cooling is convenient, which yields a boundary condition of the third type on the sidewall of the layer. In dimensionless form

$$\boldsymbol{n}\boldsymbol{\nabla}T + Bi \cdot T = 0 \tag{2.6}$$

where $\boldsymbol{n}$ – the boundary normal vector and the dimensionless thermal Biot number has been introduced $Bi = \frac{\alpha L}{\lambda}$ characterizing the intensity of heat dissipation through the transversal boundary of the layer, with α - the heat transfer coefficient. For convenience, the value $Bi = 1$ is used for numerical calculations throughout this investigation, corresponding to conductive heat transfer.

The solution of (2.5) with account for (2.6) for the stationary state with negligible advection is straightforward. Up to the leading parallel mode

$$T(y, z) = T_0(z) + T_1(z)\cos(\pi y) \tag{2.7}$$

with the corresponding expressions for the mode amplitudes in dimensionless form

$$T_0(z) = \frac{1}{4}\pi^2\left(l^2 + 2\frac{l}{Bi} - z^2\right) \tag{2.8}$$

$$T_1(z) = \frac{1}{2}\left[1 - \frac{Bi\cosh(\pi z)}{\pi\sinh(\pi l) + Bi\cosh(\pi l)}\right] \tag{2.9}$$

and the value of l corresponds to the aspect ratio of the element of the photoabsorptive thermal grating.

The characteristic temperature scale is then obtained by averaging of the temperature profile across the gap of the layer and is slightly different from (2.4)

$$\overline{\Delta T} = \overline{\Delta T}_0 f_T \quad \text{with} \quad f_T = 1 - \frac{1}{\pi + Bi\coth(\pi l)}\frac{Bi}{\pi l} \tag{2.10}$$

In principle, the measures (2.10) and (2.4) are sufficiently close if the thickness of the layer is not too small in comparison with the period of the induced grating. The diffusion of heat in the transversal direction then has little influence on the induced temperature difference, which is determined mainly by the parallel heat fluxes within the layer. Then the expression (2.4) is more convenient and will be used for the normalization of the thermal perturbation.

Making use of the adopted characteristic parameters of the ferrofluid (Table 1.1), it becomes possible to evaluate the coefficient r_c. For typical temperature difference in FRS experiments on the order of not more than $\overline{\Delta T} \approx 1°K$ the induced concentration differences are moderate and the secondary absorption is negligible $r_c \sim 5\% \ldots 10\%$. Still, the coefficient r_c implies a linear dependence on $\overline{\Delta T}$ and at higher optical intensities this effect should be taken into account.

The creation of the spatially extended thermal modulation within the layer of the ferrocolloid unavoidably initiates the formation of the corresponding grating of ferroparticle concentration by thermophoretic forces. The characteristic photoabsorptive temperature gradient in the parallel direction $\frac{\overline{\Delta T}}{L}$ is quite sufficient to induce measurable stratification of the ferrocolloid in the conditions of microscale transport. In turn, the application of external magnetic fields to such photoabsorptive formations leads to the appearance of demagnetizing effects – in the regions with enhanced ferroparticle concentration the external field is weakened, otherwise, it is enhanced where the ferroparticles are depleted by thermodiffusive fluxes. Apart from magnetodiffusive redistribution of the ferroparticles, the self-consistent interactions of the concentration and magnetic field perturbations may macroscopically entrain the carrier fluid and excite magnetoadvective fluxes.

It is apparent from (2.4) that the induced characteristic temperature difference scales as a square of the characteristic length L. In turn, the expression for the magnetosolutal Rayleigh number Rs_m implies a square dependence on $\overline{\Delta T}$ and L. Considering all factors the Rayleigh number scales as a sixth degree dependence on the characteristic length and can rapidly reach considerable values in the conditions of the FRS experiment upon the application of the external magnetic field.

2.2. Thin ferrofluid layers

The formation and observation of photoabsorptive microstructures generally takes place in thin layers with thickness ranging from approximately 10 to 100 micrometers. Rather than actual thickness, however, more important is the aspect ratio of the induced concentration variation. It seems reasonable to suppose that if the interfringe of the induced grating is much larger than the thickness of the layer $l \ll 1$ then the nonhomogeneity of the concentration profile across the gap of the layer would not play as significant a role in the lateral mass transport as the imposed parallel modulation. The transversal dimension of the convective-diffusive problem (1.36)-(1.39) can then be disregarded assuming the flat concentration profiles across the gap of the ferrofluid layer. For the detailed description of this situation the approach of [56]-[57] is adopted.

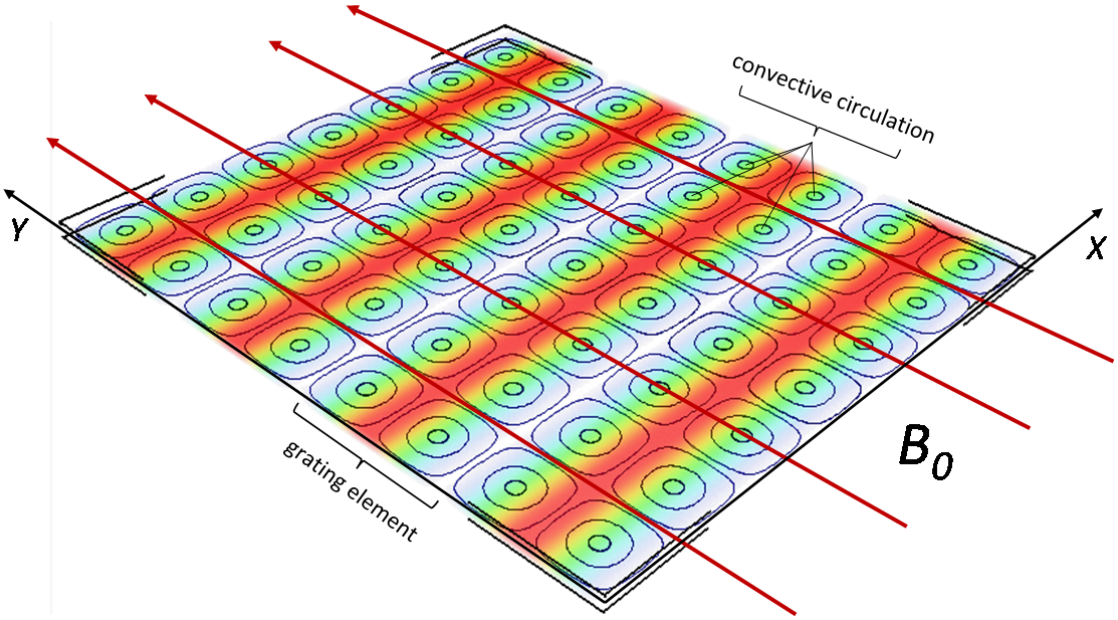

Figure 2.1. Definition of the problem: photoabsorptive concentration grating is induced within a thin ferrofluid layer under the action of the applied parallel magnetic field. The convective currents connect within the plane of the layer.

It is thus assumed that in thin ferrofluid layers the convective circulation can only be connected within the plane of the layer (Figure 2.1) and the possibility of the transversal currents is ignored for now. Still, the reduction of the transversal profile should be performed in a meaningful way. In this regard, the Stokes's equation (1.38) allows an important simplification for the plane parallel flow. If the velocity within the layer is parallel to the sidewalls, the parabolic profile such as that of the Poiseuille's law allows identically

satisfying the no-slip hydrodynamic boundary conditions on the sidewalls of the layer. Separating the coordinates in the following form

$$\boldsymbol{u} = \frac{3}{2}\left[1 - \left(\frac{z}{l}\right)^2\right]\langle \boldsymbol{u} \rangle_{\boldsymbol{z}} \tag{2.11}$$

where $\langle \boldsymbol{u} \rangle_{\boldsymbol{z}}$ is the velocity averaged along the gap of the layer, the dimensionless Stokes equation (1.38) becomes

$$-\nabla P + \frac{3}{2}\left[1 - \left(\frac{z}{l}\right)^2\right]\Delta_{\perp}\langle \boldsymbol{u} \rangle_{\boldsymbol{z}} - \beta \langle \boldsymbol{u} \rangle_{\boldsymbol{z}} + \boldsymbol{f_M} = 0 \tag{2.12}$$

with $\Delta_{\perp} = \partial_x^2 + \partial_y^2$ – the transverse Laplacian and $\beta = \frac{3}{l^2}$ is the dimensionless friction factor.

Assuming that the flow is irrotational $\boldsymbol{\nabla}_{\perp} \times \langle \boldsymbol{u} \rangle_{\boldsymbol{z}} = 0$ (meaning also that the magnetic force is potential $\boldsymbol{f_M} = -\boldsymbol{\nabla}_{\perp} P_M$) and incompressible $\boldsymbol{\nabla}_{\perp} \cdot \langle \boldsymbol{u} \rangle_{\boldsymbol{z}} = 0$ at least within the midplane of the layer, the second term in (2.12) vanishes and the form of the Darcy's law is obtained

$$-\boldsymbol{\nabla}_{\perp} P - \beta \langle \boldsymbol{u} \rangle_{\boldsymbol{z}} + \boldsymbol{f_M} = 0 \tag{2.13}$$

The potential of the magnetic force – the magnetic pressure P_M - can then be introduced into the total pressure gradient. Similar equation was used for the purpose of determining the stability and character of evolution of the magnetic formations in ferrofluid Hele-Shaw layers [96]-[99].

The limits of validity of the Darcy's law are not immediately apparent and the mechanisms of the momentum transport in thin layers were recognized only recently [100]-[101]. The equation (2.13) contains a single friction term $-\beta \langle \boldsymbol{u} \rangle_{\boldsymbol{z}}$ pertaining to the diffusion of momentum in the transversal direction, which describes the viscous interactions of the flow with the sidewalls of the layer on the length scale of the layer thickness Ll. In turn, the expected emergence of the lateral convective circulation would involve the appearance of the viscous shear stresses in the parallel and longitudinal directions due to the regular reversals of the flow. In that regard the viscous interactions within the convective pattern operate correspondingly on the length scales L and $L\frac{\lambda_x}{2}$ with λ_x – dominant longitudinal wavelength. Consequently, the two main regimes of momentum transport have been recognized: in the Darcy's limit of long wavelengths the lateral viscous friction is less pronounced than the corresponding transversal stresses and the equation (2.13) is quite accurate. In the opposite situation, the flow regime characterized mainly by the viscous stresses within the convective structure rather than the interactions with the sidewalls constitutes the short wavelength Stokes's regime. There are no terms in (2.13) accounting for the diffusion of momentum

within the plane of the ferrofluid layer and so the Darcy's law cannot correctly describe the character of the hydrodynamic motions in the latter situation.

In this regard, even if the interfringe of the grating considerably exceeds the thickness of the layer, it is not reasonable to assume that the scales of the convective motions would do so as well. The longitudinal wavelengths λ_x in general considerably depend on the magnitude of the buoyant forces [100] and the increase of the Rayleigh number would lead to the decrease of the scale of elementary hydrodynamic circulations and the eventual transition into the Stokes's regime. Nevertheless, the reduction of the transversal dimension is still possible in the Stokes's regime if a corresponding contribution accounting for the lateral diffusion of momentum could be added to (2.13). In fact the addition of the Brinkman's term $\Delta_\perp \langle \boldsymbol{u} \rangle_{\boldsymbol{z}}$ to account for the lateral viscous interactions yields the Darcy-Stokes equation

$$-\boldsymbol{\nabla}_\perp P + (\Delta_\perp - \beta)\langle \boldsymbol{u} \rangle_{\boldsymbol{z}} + \boldsymbol{f_M} = 0 \tag{2.14}$$

and permits successful qualitative predictions of the character of scaling of the resulting convective motions with regard to the thickness of the layer and the magnitude of the buoyant forces across both the Darcy's and Stokes's regimes of the flow [100]-[101].

Consequent numerical investigations with account to the full Stokes's equation and the transversal fluxes have also shown the existence of the "gap" regime at high magnitudes of the buoyant effects, characterized by the growth of the convective modes across the gap of the layer and the destruction of the parabolic profile [101]-[102]. For the time being the transversal currents will be disregarded and the existence of the parabolic profile (2.11) is assumed for the purpose of this investigation, the Brinkman's model (2.14) is adopted to account for the transport of momentum within the Hele-Shaw cell.

2.2.1. Base state

The phoretic evolution of the photoabsorptive grating in thin ferrofluid layer during the formation process or the relaxation stage of the FRS procedure after the switching off of the optical stimulation is described by the diffusion equation with changeable source

$$\frac{\partial c_0}{\partial t} = d_0 \frac{\partial^2}{\partial y^2} c_0 \overbrace{+ s_m \frac{\partial^2}{\partial y^2} \langle T \rangle_z}^{optical\ pumping} \tag{2.15}$$

and the corresponding initial conditions.

The exact shape of the concentration profile depends only on the reference point. It is convenient to choose the origin in such manner so that the grating would be symmetric and the transient base state can be written as

$$c_0(y,t) = \frac{1}{2}\left(e^{i\pi y} + e^{-i\pi y}\right)c(t) \tag{2.16}$$

with $c(t)$ expressed correspondingly either as $C_0\left(1 - e^{-d_0\pi^2 t}\right)$ or $C_0 e^{-d_0\pi^2 t}$ for the formation or relaxation process or just as C_0 for the stationary state, satisfying (2.15).

The corresponding configuration of the internal demagnetizing field induced within the layer by the application of external homogeneous magnetic field is determined by the equation (1.39). It can be put in the following form

$$H_0(y,t) = -\tilde{\alpha}_c c_0(y,t) f_0 \tag{2.17}$$

In the expression for the demagnetizing field (2.17) the contribution $-\tilde{\alpha}_c c_0$ comes from the lateral part $\Delta_\perp$ of the Laplacian in the equation (1.39) and accurately describes the distribution of the self magnetic field under the assumption of an infinitely thick layer. However, this assumption is in apparent contradiction with considering the thin layers and retaining just this contribution is not completely satisfactory because the transversal boundary effects (Section 3.1.1) can become substantial as the thickness of the layer is reduced. More detailed calculations performed in Section 3.1.2 (or similarly by the method of Green's function in [96]) demonstrate that for a concentration mode characterized by the wavenumbers k_y in the parallel direction and k_x in the longitudinal direction the corresponding gap averaged mode of the demagnetizing field should be multiplied by the factor $f_H(k_x, k_y)$, which is expressed either as

$$f_\parallel(k_x,k_y) = \frac{k_y^2}{k^2}\left[1 - f_\perp(k_x,k_y)\right] \text{ or } f_\perp(k_x,k_y) = e^{-kl}\frac{\sinh(kl)}{kl} \tag{2.18}$$

correspondingly for the parallel and perpendicular configurations of the external magnetic field, with $k = \sqrt{k_x^2 + k_y^2}$.

Considering (2.18), it is clear that the concentration modes possessing no variation in the parallel direction, i.e. $k_y = 0$, do not contribute to the formation of the demagnetizing field distribution in the parallel configuration of the external field. In turn, all concentration modes possess corresponding modes of the demagnetizing field in the perpendicular configuration of the applied field. In this regard, there is reason to expect that the behavior of the concentration microstructures would be considerably different in both these configurations.

In the limit of infinitely thick layer the factor $f_{\parallel}$ is determined only by the lateral variation of the concentration within the ferrofluid layer, on the other hand, in the opposite situation in layers with vanishing thickness $f_{\parallel}$ approaches zero. In turn, the factor $f_{\perp}$ for the perpendicular configuration of the external field vanishes in the former case and approaches unity in the latter, in very thin layers. The diverging behavior of the magnetic factors follows from the different mechanisms contributing to the formation of the configuration of the demagnetizing field and will be discussed in later sections (Section 3.1.2 and further). Still, at this point it is convenient to retain the generality with respect to the configuration of the external field and denote the corresponding factor as f_H. Consequently, for the single mode of the base state this factor is denoted as $f_0 = f_H(0, \pi)$ in (2.17).

The photoabsorptive formation of a modulated concentration profile eventually results in a stationary state, which is described by the equilibrium of diffusive, thermophoretic and magnetophoretic fluxes $\boldsymbol{\nabla} \cdot \boldsymbol{J_c} = 0$. The gap averaged dimensionless temperature profile (2.7) is expressed from (2.10)

$$\langle T \rangle_z(y) = 0.5 f_T \cos(\pi y) \tag{2.19}$$

In turn, the corresponding primary mode of the stationary photoabsorptive concentration distribution is described by a simple expression: $c_0(y) = C_0 \cos(\pi y)$ and with the employed normalization the equation (2.19) yields the required amplitude of the induced concentration grating $C_0 = -\frac{1}{2} f_T \frac{s_m}{d_0}$, where d_0 – is the coefficient of magnetic diffusion in thin layers, which is slightly different from its bulk value (1.35)

$$d_0 = 1 + \tilde{\alpha}_c \mathcal{M}_{ph} f_0 \tag{2.20}$$

In contrast with the definition (1.35) accounting for only the bulk contributions, the expression (2.20) accommodates the influence of the transversal boundary by means of the coefficient f_0 dependent on the configuration of the applied magnetic field and the thickness of the layer. From the previous discussions on the form of f_H it is apparent that d_0 approaches d_m in the limit of infinitely thick layers.

The base state (2.16)-(2.17) yields a potential magnetic force $c_0 \boldsymbol{\nabla}_{\perp} H_0$ and then the convective currents can only be induced through the mechanism of hydrodynamic destabilization of the concentration grating by laterally connecting circulation. Examining the linear stability of the miscible interfaces and arrays of concentration stripes it was ascertained that in fact both stages of the forced Rayleigh scattering procedure can be destabilized by the application of the external magnetic field [56]-[57]. In the present section the problem of linear stability and

the non-linear evolution of the regular photoabsorptive concentration microstructures in thin ferrofluid layers will be sequentially considered.

2.2.2. Linear stability problem

The system of equations (1.36)-(1.39) with the appropriate base state (2.16)-(2.17) and cyclic boundary conditions would describe the evolution of the concentration and hydrodynamic perturbations during the formation and relaxation stage of the FRS procedure. In thin layer approximation the equation (1.38) is replaced by (2.14) and assuming the flat profiles of concentration and demagnetizing field across the gap of the layer the magnetic force is accordingly expressed as $\boldsymbol{f_M} = Rs_m c\boldsymbol{\nabla}_\perp H$. The critical parameters of the hydrodynamic instability of the stationary state can be obtained by performing the linear stability analysis of the problem (1.37) and (2.14). For that purpose the equations are linearized in the vicinity of the appropriate base state (2.16)-(2.17)

$$-\boldsymbol{\nabla}_\perp P + (\Delta_\perp - \beta)\boldsymbol{u} + Rs_m(c_0\boldsymbol{\nabla}_\perp \delta H + \delta c\boldsymbol{\nabla}_\perp H_0) = 0 \tag{2.21}$$

$$\frac{\partial \delta c}{\partial t} + \boldsymbol{u}\boldsymbol{\nabla}_\perp c_0 = \Delta_\perp\left(\delta c - \mathcal{M}_{ph}\delta H\right) \tag{2.22}$$

with $\boldsymbol{u} = \langle \boldsymbol{u} \rangle_{\boldsymbol{z}}$. In turn, $\delta c = c - c_0$ and $\delta H = H - H_0$ are defined as the small perturbations of c_0 and H_0. A similar problem was considered for the sharp interface [56] and the periodic array of sharp stripes [57].

Expanding the perturbations $\boldsymbol{u}$, δc and δH into normal modes in the longitudinal direction in the regime of exponential amplification as $\delta X = X(y)e^{ik_x x + \omega t}$, where k_x is the longitudinal wave number of the perturbation and ω is the growth increment, the pressure term from equation (2.21) can be removed by applying the *curl* operator. The transversal component of the vorticity vector follows from the continuity condition – the divergence free velocity field

$$\{\boldsymbol{\nabla} \times \boldsymbol{u}\}_{\mathrm{z}} = -\frac{i}{k_x}\left(\frac{\partial^2}{\partial y^2} - k_x^2\right)V(y)e^{ik_x x + \omega t} \tag{2.23}$$

with $V(y)$ - the amplitude of the parallel velocity component u_y.

In turn, the parallel profiles $X(y)$ of velocity, concentration and demagnetizing field perturbation amplitudes can also be expanded in Fourier modes

$$X(y) = \sum_{n=-\infty}^{+\infty} x_n\, e^{iq_n y} \tag{2.24}$$

with $q_n = \frac{\pi n}{q}$, where each mode is denoted by an expansion index n and a parameter q.

The additional parameter describes the periodicity of the imposed perturbation. It has been introduced because the shape of the perturbations is not clear *a priori* due to the absence of the boundaries in the parallel direction and formal unboundedness of the flow. The dimensionless period $2q$ of the critical perturbation must then be determined from the eventually obtained dispersion relation. The employed expansion of the fields $\sim e^{i(k_x x+q_n y)}$ essentially corresponds to a periodic system of coordinated convective vortices with the rotation axes oriented along the transversal direction and different aspect ratios determined by wavenumbers k_x and q_n.

Making use of the expansion (2.24) with account for the factors (2.18) the Fourier coefficients of the demagnetizing field perturbation are expressed

$$h_n = -\tilde{\alpha}_c c_n \hat{f}_n e^{iq_n y} \tag{2.25}$$

with $\hat{f}_n = f_H(k_x, q_n)$ and the equations (2.21)-(2.22) are projected accordingly

$$v_n = -\frac{\tilde{\alpha}_c Rs_m C_0 k_x^2}{(q_n^2 + k_x^2)(q_n^2 + k_x^2 + \beta)} \frac{i\pi}{2} \left[(f_0 - \hat{f}_{n-q}) c_{n-q} - (f_0 - \hat{f}_{n+q}) c_{n+q} \right] \tag{2.26}$$

$$c_n = -\frac{C_0}{\hat{d}_n (q_n^2 + k_x^2) + \omega} \frac{i\pi}{2} (v_{n-q} - v_{n+q}) \tag{2.27}$$

where c_n and v_n are the corresponding Fourier modes (2.24) of concentration perturbation and parallel velocity. The introduced spectral coefficients $\hat{d}_n = d_H(k_x, q_n)$ have the form of a coefficient of magnetic diffusion

$$d_H(k_x, q_n) = 1 + \tilde{\alpha}_c \mathcal{M}_{ph} f_H(k_x, q_n) \tag{2.28}$$

The projected equations (2.26)-(2.27) allow obtaining the dispersion relation for the instability of the periodic grating

$$\frac{4\mathcal{M}_{ph} k_n^2 (k_n^2 + \beta)}{k_x^2 \pi^2 C_0^2 Rs_m} v_n - \frac{(d_0 - \hat{d}_{n-q})(v_n - v_{n-2q})}{\hat{d}_{n-q} k_{n-q}^2 + \omega} - \frac{(d_0 - \hat{d}_{n+q})(v_n - v_{n+2q})}{\hat{d}_{n+q} k_{n+q}^2 + \omega} = 0 \tag{2.29}$$

with $k_n^2 = q_n^2 + k_x^2$.

The necessary condition for the existence of the solution to (2.29) is the requirement that the coefficients v_n should form an infinite chained system of linear equations, which determines the stability of the problem. Also, the indices of the coefficients must be positive or negative integers. Taking this into account the coefficients can form a chain only if the condition

$$q = \frac{j}{2}, \text{ with } j = 1,2 \ldots \tag{2.30}$$

is fulfilled. This is a necessary requirement for the existence of a periodic solution.

The condition (2.30) is necessary but not sufficient for the existence of a nontrivial solution to the linearized stability problem (2.29). For this purpose, it is required that the determinant of the linear system (2.29) is equal to zero. This yields the desired dispersion relation for the determination of the critical parameters.

Also, it is clear that the system (2.29) can be decomposed. In fact, it consists of only $2q$ unique chains, each of the chains consisting of unique coefficients v_n, which do not contribute to other chains. Assuming that the stability of the system is determined by the stability of the leading mode, it makes sense to examine just the chain, which includes the coefficient v_1. The exact stability problem is thus reduced to the evaluation of the determinant of a tridiagonal matrix (2.29).

On the other hand, the coefficients on the main diagonal grow rapidly with n, especially at larger values of q. In this case, it is reasonable to attempt the first approximation of the dispersion relation

$$\frac{4\mathcal{M}_{ph}k_n^2(k_n^2+\beta)}{k_x^2\pi^2C_0^2Rs_m}-\left(\frac{d_0-\hat{d}_{n-q}}{\hat{d}_{n-q}k_{n-q}^2+\omega}+\frac{d_0-\hat{d}_{n+q}}{\hat{d}_{n+q}k_{n+q}^2+\omega}\right)=0 \tag{2.31}$$

The primary instability is stationary and the critical parameters can be found by setting the growth increment of the hydrodynamic mode to zero $\omega = 0$. The critical solutal Rayleigh can then be expressed

$$Rs_m^{crit}=\frac{4\mathcal{M}_{ph}}{\pi^2k_x^2C_0^2}\frac{\hat{d}_{n-q}\hat{d}_{n+q}k_{n-q}^2k_{n+q}^2k_n^2(k_n^2+\beta)}{(d_0-\hat{d}_{n-q})\hat{d}_{n+q}k_{n+q}^2+(d_0-\hat{d}_{n+q})\hat{d}_{n-q}k_{n-q}^2} \tag{2.32}$$

The relation (2.32) gives a good approximation of the critical parameters but loses an important aspect of the stability problem. To expose this drawback it is appropriate to consider the case $q = 1$, for which the expression (2.32) is not actually valid. Returning to (2.29) for $n = 1$, after truncating higher modes in fact two critical Rayleigh numbers are obtained

$$Rs_{1,p}^{crit}=\frac{4\mathcal{M}_{ph}}{\pi^2C_0^2}\frac{\hat{d}_0\hat{d}_2(4\pi^2+k_x^2)(\pi^2+k_x^2)(\pi^2+k_x^2+\beta)}{2(d_0-\hat{d}_0)\hat{d}_2(4\pi^2+k_x^2)+(d_0-\hat{d}_2)\hat{d}_0k_x^2} \tag{2.33}$$

and

$$Rs_{1,u}^{crit}=\frac{4\mathcal{M}_{ph}}{\pi^2C_0^2}\frac{\hat{d}_2(4\pi^2+k_x^2)(\pi^2+k_x^2)(\pi^2+k_x^2+\beta)}{(d_0-\hat{d}_2)k_x^2} \tag{2.34}$$

under the assumption that $v_1 = -v_{-1}$ and $v_1 = v_{-1}$. These two cases correspond accordingly to the perturbation modes referred to as the *peristaltic mode* and *undulation mode* [56]-[57].

The peristaltic $q = 1$ mode alternately stretches or compresses the initial concentration profile in the parallel direction. The undulation mode, on the other hand, attempts to bend the concentration "stripes". With larger parallel periodicities $2q$ the situation does not allow such simple interpretation anymore. It can be hypothesized that the endpoints of a *p*-mode must be located on the minima/maxima of the concentration profile, at the same time the endpoints of a hydrodynamic mode from the *u*- group are positioned on the fronts of the concentration field, implying a phase shift by $\frac{1}{2}$ in the parallel direction. This assumption is substantiated by the mode $q = \frac{1}{2}$, which belongs to the "u" group, but for which the coefficients v_n with positive and negative indices are decoupled.

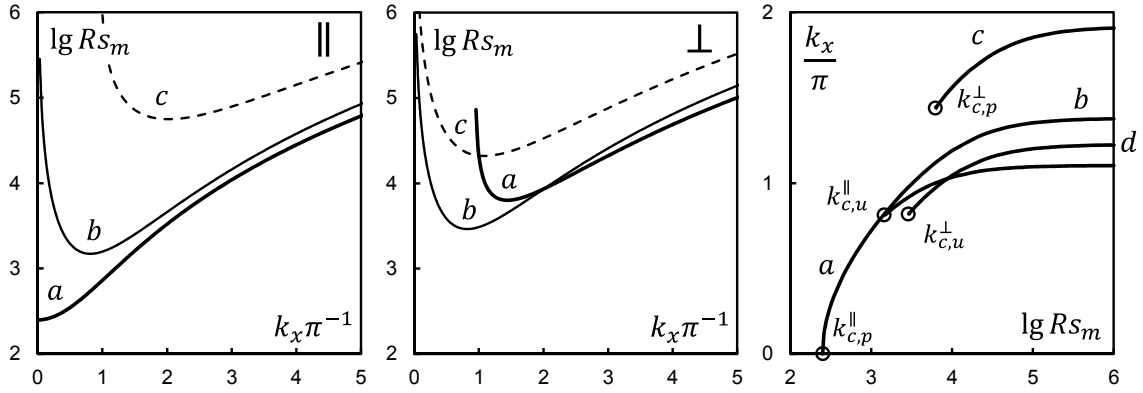

Figure 2.2. Critical parameters of the hydrodynamic instability at $\beta = 12$ - neutral curves for the parallel (left) and perpendicular (middle) orientations of the applied field: *p*-modes *(a)* $q = 1$, *(b)* $q \to \infty$ and *u*-mode *(c)* $q = 1$; right – dependence of the optimal longitudinal wave-number on the magnetosolutal Rayleigh number for different perturbations: *(a)* peristaltic mode *(b)* undulatory mode in parallel and *(c)-(d)* perpendicular configurations of the applied magnetic field.

In this regard, the calculations with respect to (2.33), (2.34) and the full system (2.29) for different values of the number q show that the *p*-modes are the least stable ones (Figure 2.2), so the *u*-modes will be disregarded. Comparing different *p*-modes it becomes apparent that in the parallel configuration of the applied field the critical hydrodynamic perturbation is periodic with the period of the induced concentration grating and corresponds to a coordinated system of convective vortices located on the fronts of the concentration profile, while convective currents spanning multiple grating periods are less likely.

From (2.33) with $k_x \to 0$ the exchange of stabilities takes place at the threshold given by

$$Rs_{\parallel}^{crit} = \frac{2}{C_0^2}\frac{\mathcal{M}_{ph}}{d_0 - 1}(\pi^2 + \beta) \tag{2.35}$$

In contrast, it is exactly the formation of larger vortices that is promoted by the applying of the external field in the perpendicular direction. The critical perturbation corresponds to narrow circulations strongly elongated along the parallel direction, essentially cross grating flows in the form of alternating shear currents. For larger parallel wavelengths $q \to \infty$, the critical threshold can then be expressed in simple form

$$Rs_{\infty}^{crit} = 2\frac{\mathcal{M}_{ph}}{C_0^2}\frac{d_H(k_x, \pi)}{d_0 - d_H(k_x, \pi)}(\beta + k_x^2)\left(1 + \frac{k_x^2}{\pi^2}\right) \tag{2.36}$$

The advective shear currents spanning the whole unbounded grating in fact would lead to the undulatory bending of the concentration stripes. To avoid confusion this single mode will be denoted as the undulatory mode, while the critical mode $q = 1$ of the parallel configuration of the applied field will be denoted as the peristaltic mode, because it leads to the peristaltic deformation of the grating. These are the two most unstable modes in the appropriate configurations of the external field.

In all cases the critical Rayleigh number grows with the dimensionless friction factor β and decreasing the thickness of the ferrofluid layer obviously increases the magnetoconvective stability of the photoabsorptive formations. In the situation with the applying of the external field perpendicularly to the ferrofluid layer, the increasing of β eventually leads to the replacement of the critical perturbation – at aspect ratios slightly lower than $l = 0.1$ the peristaltic perturbation with $q = 1$ becomes the most unstable just as in the case of the field applied in the parallel direction. Still, such narrow layers are rarely considered.

The longitudinal wavenumbers of the appropriate critical perturbations are determined by the condition

$$\frac{\partial Rs_m^{crit}}{\partial k_x} = 0 \tag{2.37}$$

In this regard the parameters of the peristaltic ($q = 1$) and undulatory ($q \to \infty$) modes of instability are most interesting with the corresponding longitudinal wavelengths denoted accordingly by $k_{c,p}$ or $k_{c,u}$ at threshold in both the parallel ($\parallel$) and perpendicular ($\perp$) configurations of the applied magnetic field. Clearly, the form of the critical peristaltic perturbation cannot be obtained from the shape of the neutral curve in the parallel

configuration of the applied field (Figure 2.2), because the whole band of such perturbations with sufficiently large longitudinal wavelengths becomes unstable at the threshold (2.35) and $k_{c,p}^{\parallel} \to 0$. In turn, if the magnetosolutal Rayleigh number Rs_m exceeds the appropriate critical one Rs_m^{crit}, the fastest growing hydrodynamic mode is determined by the condition of the maximum growth increment

$$\frac{\partial \omega}{\partial k_x} = 0 \tag{2.38}$$

The growth increments ω of the modes can be obtained from the relation (2.29), which yields a quadratic equation for the evaluation of the hydrodynamic growth rates for the peristaltic mode $q = 1$

$$\left(\frac{\omega}{d_0\pi^2}\right)^2 + \left[Q_2 + Q_0 - \left(3 - 2\frac{\hat{d}_0 - \hat{d}_2}{d_0 - \hat{d}_2}\right)Q_2 \frac{Rs_m}{R_{1,u}^{crit}}\right]\frac{\omega}{d_0\pi^2} + \left(1 - \frac{Rs_m}{R_{1,p}^{crit}}\right)Q_0 Q_2 = 0 \tag{2.39}$$

with $Q_n = \frac{\hat{d}_n k_n^2}{d_0\pi^2}$.

Also, for the critical undulatory perturbation $q \to \infty$ of the perpendicular configuration of the applied field the growth increments can be expressed in explicit form

$$\frac{\omega_\infty}{d_0\pi^2} = \frac{d_H(k_x, \pi)}{d_0}\left(\frac{Rs_m}{Rs_\infty^{crit}} - 1\right)\left(1 + \frac{k_x^2}{\pi^2}\right) \tag{2.40}$$

The optimal longitudinal wave numbers of the fastest growing perturbations above the threshold of the instability considerably depend on Rs_m (Figure 2.2), especially in thin ferrofluid layers, which can also lead to interesting transient phenomena in systems with time-dependent base state. Considering, for example, the relaxation process of the grating, in the leading parallel mode approximation the shape of the base state (2.16) remains unchanged and the dynamics of the concentration amplitude can thus be interpreted as the corresponding time-dependent evolution of the magnetic Rayleigh number $Rs_m(t)$. If the initially uniform concentration grating was somehow formed above the critical threshold of the convective instability, its relaxation can also be convectively unstable. As the amplitude of the concentration modulation is decreased, the magnitude of the Rayleigh number also deceases and a cascade of perturbation modes with higher and higher longitudinal wavelengths becomes progressively excited according to Figure 2.2. This effect was particularly noted in [50] and is characteristic for transient base states.

2.2.3. Nonlinear regime

The previously considered linear stability problem may be useful for ascertaining the possibility of destabilization of the photoabsorptive concentration grating by the external magnetic field and determining the threshold of the instability as well as the approximate shape of the emerging convective currents. Still, in the supercritical regime above the threshold the exponential amplification of the mode amplitudes is quickly saturated by the non-linear terms and the linear analysis does not yield any information on the eventual convective deformation of the photoabsorptive grating and cannot be used to quantitatively characterize the convective-diffusive stationary state.

In turn, the nonlinear regime of the development of the microconvective instability within the photoabsorptive formations in thin ferrofluid layers can be described by a suitable nonlinear model. The equations for the nonlinear convective-diffusive problem are summarized from (1.37) and (2.14) as previously, but retaining the nonlinear terms

$$-\nabla_\perp p + (\Delta_\perp - \beta)\boldsymbol{u} + Rs_m c \boldsymbol{\nabla}_\perp H = 0 \tag{2.41}$$

$$\frac{\partial c}{\partial t} + \boldsymbol{u}\boldsymbol{\nabla}_\perp c = \Delta_\perp\left(c - \mathcal{M}_{ph} H\right) \tag{2.42}$$

and complemented by the base-state (2.16)-(2.17) and periodic boundary conditions in parallel and longitudinal directions.

The solution of (2.41)-(2.42) can be obtained without difficulty by making use of the Galerkin method and expanding the fields in series of periodic functions in parallel and longitudinal direction, taking advantage of the cyclic boundary conditions. The time-dependence of the coefficients of the expansion can be resolved with the desired accuracy through numerical integration in time by, for example, Runge-Kutta method.

It is clear that for the purpose of numerical integration the expansions have to be truncated at some point. The truncation is usually performed increasing the number of contributing modes until the residual of the solution is localized in the desired interval, i.e. the solution has converged. There exists, however, a related family of nonlinear models distinguished by the assumption that not all contributing modes are equally useful in the expansion. The truncation of the field expansions is then performed by picking out the most significant modes. The nonlinear models thus obtained are generally weakly-nonlinear, because the problem of picking out the most significant modes loses relevance for fully-nonlinear models and the approaches to selecting these modes are not evidently generalized. The determination of the most significant modes is usually a postulate process based on general considerations,

intuition and experience. Good results have been obtained by considering the nonlinear term in the scalar transport equation $\boldsymbol{u}\boldsymbol{\nabla}_{\perp}c$, which is one of the main sources of nonlinearity.

The performed linear stability analysis of the stationary diffusive base state of the photoabsorptive concentration grating evidences that in the parallel field configuration the critical perturbation mode is periodic with the period of the induced grating along the direction of the applied magnetic field and it belongs to the group of peristaltic perturbations. The primary hydrodynamic mode is then expressed as

$$u_y = \hat{u}_{11}(t)\sin(\pi y)\sin(k_x x) \tag{2.43}$$

and it is the sole hydrodynamic mode retained from the expansion of the parallel component of velocity. The expression for the longitudinal component of velocity corresponding to this mode is obtained from the condition of the divergence free velocity field

$$u_x = \frac{\pi}{k_x}\hat{u}_{11}(t)\cos(\pi y)\cos(k_x x) \tag{2.44}$$

In turn, the critical hydrodynamic mode of the perpendicular configuration of the applied magnetic field corresponds to cross grating shear currents of alternating direction

$$u_y = \hat{u}_{10}(t)\sin(k_x x) \tag{2.45}$$

To be more precise, in very narrow layers ($l < 0.1$ at the assumed parameters) (2.43) once again becomes the critical perturbation also in perpendicular configuration of the external field, but this case is not very interesting and the analysis is similar, so this situation will not be considered here. For (2.45) the longitudinal component vanishes $u_x \to 0$ ensuring the continuity of the convective flow.

The different configurations of the flow ensue from the different mechanisms of the formation of the internal demagnetizing field in consequence of the application of external magnetic field to the regular microstructures of ferroparticle concentration. Due to these considerable differences, it is more convenient and evident to consider the two situations separately.

The linear stability analysis of the stationary state has yielded the two Fourier modes $\sim\sin(k_x x)$ and $\sim\cos(2\pi y)\sin(k_x x)$, which compose the critical mode of the concentration perturbation δc in parallel applied field as a weighed sum. The coefficients are determined by the equations of the linear problem and are not relevant in the following. In the expansion of concentration only the leading longitudinally k_x-periodic modes, which are generated by the nonlinear term $\boldsymbol{u}\boldsymbol{\nabla}_{\perp}c$, will be retained. The expression for the concentration perturbation is then obtained

$$c(x,y,t) = \hat{c}_{10}(t)\sin(k_x x) + [c(t) + \hat{c}_{01}(t)]\cos(\pi y) + \hat{c}_{12}(t)\cos(2\pi y)\sin(k_x x) \quad (2.46)$$

where $c(t)$ is defined from (2.16).

The corresponding demagnetizing field perturbation is determined from (2.25), taking into account that the factors f_H vanish in the parallel field for modes varying just in the longitudinal direction

$$H(x,y,t) = -\tilde{\alpha}_c\{[c(t) + \hat{c}_{01}(t)]f_0\cos(\pi y) + \hat{c}_{12}(t)f_H(k_x, 2\pi)\cos(2\pi y)\sin(k_x x)\} \quad (2.47)$$

Projecting the governing equations (2.41) and (2.42) onto the selected ansatz (2.43) and (2.46) and making use of (2.44) and (2.47) the system of dynamic equations for the mode amplitudes is obtained. For the hydrodynamic mode

$$\hat{u}_{11}(t) = \frac{(d_0 - 1)\pi k_x^2}{(\pi^2 + k_x^2)(\pi^2 + k_x^2 + \beta)}\frac{Rs_m}{\mathcal{M}_{ph}}[c(t) + \hat{c}_{01}]\left[\hat{c}_{10} - \frac{1}{2}\frac{d_0 - d_H(k_x, 2\pi)}{d_0 - 1}\hat{c}_{12}\right] \quad (2.48)$$

and the concentration modes

$$\hat{c}'_{10} = \frac{\pi}{2}\hat{u}_{11}(t)[c(t) + \hat{c}_{01}] - k_x^2\hat{c}_{10}(t) \quad (2.49)$$

$$\hat{c}'_{01} = -\frac{\pi}{2}\hat{u}_{11}(t)\left(\hat{c}_{10} - \frac{1}{2}\hat{c}_{12}\right) - d_0\pi^2\hat{c}_{01}(t) \quad (2.50)$$

$$\hat{c}'_{12} = -\frac{\pi}{2}\hat{u}_{11}(t)[c(t) + \hat{c}_{01}] - (4\pi^2 + k_x^2)d_H(k_x, 2\pi)\hat{c}_{12}(t) \quad (2.51)$$

Where the primes denote time derivatives and $c(t)$ is the time-dependent amplitude of the selected base state (2.16).

The obtained 4-mode Lorenz-type system of equations can be integrated numerically. The imposed longitudinal wave-number k_x is determined for the given value of the magnetic Rayleigh number Rs_m from the linear analysis by the relations (2.38) and (2.39) as k_x^ω for the fastest growing perturbation. Any possible time evolution of this wave number is then disregarded.

The calculated time-dependence of the amplitudes of the selected perturbation modes from the initial arbitrary fluctuation $\hat{c}_{10} = 0.01$ to the stationary state is plotted on Figure 2.3. These applied initial conditions can only influence the dynamics of the amplitudes but not the stationary values, which will be subsequently used in the determination of the relaxation behaviour, and are not important in the following. The obtained quantitative dynamics of the mode amplitudes (Figure 2.3) also evidence that the contribution of the mode $\hat{c}_{12}$ to the stationary state is not very significant.

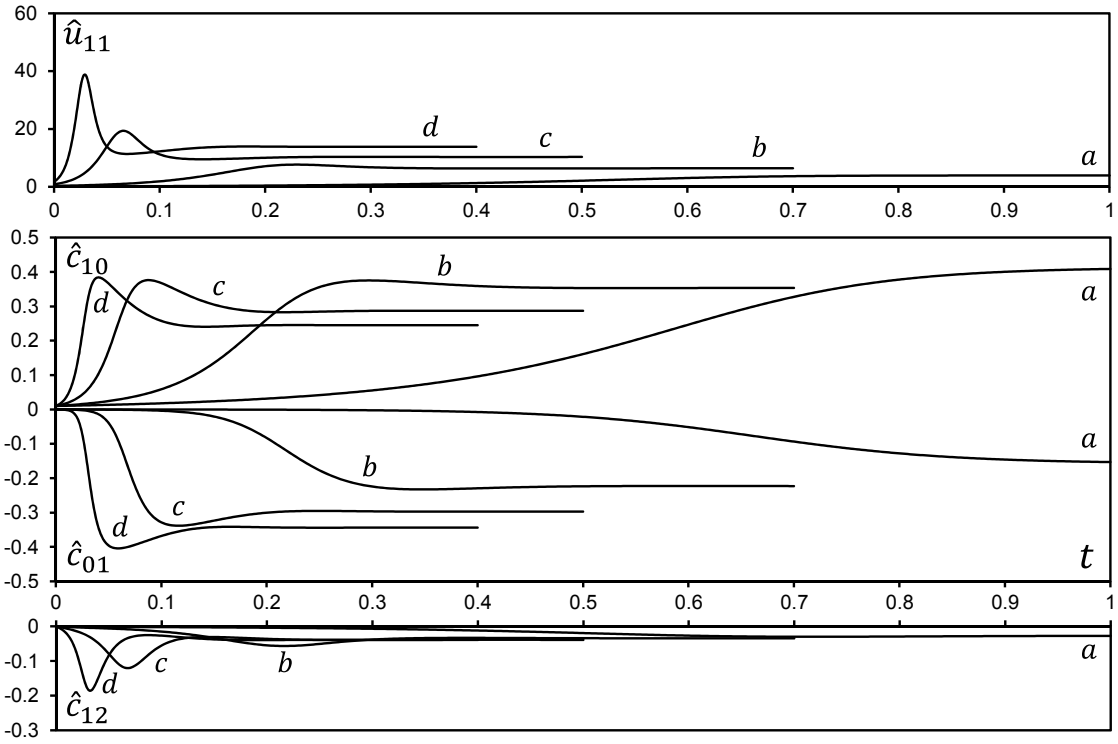

Figure 2.3. Evolution of the mode amplitudes $\hat{c}_{01}$, $\hat{c}_{10}$, $\hat{c}_{12}$ and $\hat{u}_{11}(t)$ from initial fluctuation to the stationary state at $\beta = 12$ and *(a)* $Rs_m = 1000$, *(b)* $Rs_m = 2000$, *(c)* $Rs_m = 5000$, *(d)* $Rs_m = 10\,000$.

The equations (2.48)-(2.51) can be solved for the eventual stationary regime and the stationary mode amplitudes $\hat{C}_{10}$, $\hat{C}_{01}$, $\hat{C}_{12}$ and $\hat{U}_{11}$ are obtained without difficulty in analytical form. For that purpose, the hydrodynamic perturbation (2.48) yields

$$\hat{U}_{11} = \frac{(d_0 - 1)\pi k_x^2}{(\pi^2 + k_x^2)(\pi^2 + k_x^2 + \beta)} \frac{Rs_m}{\mathcal{M}_{ph}} \left[C_0 + \hat{C}_{01}\right] \left[\hat{C}_{10} - \frac{1}{2} \frac{d_0 - d_H(k_x, 2\pi)}{d_0 - 1} \hat{C}_{12}\right] \tag{2.52}$$

In turn, from the solution of (2.49)-(2.51) the stationary concentration mode amplitudes are obtained

$$\hat{C}_{10} = \frac{\pi}{k_x} \sqrt{-d_0 (1 + 0.5\varepsilon_{12})^{-1} \hat{C}_{01} C_0 \sqrt{\frac{Rs_{1,p}^{crit}}{Rs_m}}}\,, \quad \hat{C}_{01} = -C_0 \left(1 - \sqrt{\frac{Rs_{1,p}^{crit}}{Rs_m}}\right) \tag{2.53}$$

$$\hat{C}_{12} = -\varepsilon_{12} \hat{C}_{10} \tag{2.54}$$

The introduced factor $\varepsilon_{12} = \frac{k_x^2}{d_H(k_x, 2\pi)\left(4\pi^2 + k_x^2\right)}$ is rather small, reflecting the small influence of the mode amplitude $\hat{C}_{12}$ on the stationary state. In principle, this mode can be neglected without notable consequences.

In turn, the shape of the emerging convective flow in the perpendicular configuration of the applied magnetic field corresponds to cross grating shear currents (2.45) and the associated critical concentration mode $\sim \sin(\pi y)\sin(k_x x)$. Retaining in addition only the leading longitudinally k_x-periodic modes generated by the nonlinear term $\boldsymbol{u}\boldsymbol{\nabla}_\perp c$ in the expansion of concentration

$$c(x,y,t) = [c(t) + \hat{c}_{01}(t)]\cos(\pi y) + \hat{c}_{11}(t)\sin(\pi y)\sin(k_x x) \tag{2.55}$$

the corresponding demagnetizing field perturbation is determined from (2.25)

$$H(x,y,t) = -\tilde{\alpha}_c\{[c(t) + \hat{c}_{01}(t)]f_0\cos(\pi y) + \hat{c}_{11}(t)f_H(k_x,\pi)\sin(\pi y)\sin(k_x x)\} \tag{2.56}$$

Projecting the governing equations (2.41) and (2.42) onto the selected modes again yields the equations for the mode amplitudes. For the hydrodynamic mode

$$\hat{u}_{10}(t) = \frac{\pi}{2}\frac{[d_0 - d_H(k_x,\pi)]}{k_x^2 + \beta}\frac{Rs_m}{\mathcal{M}_{ph}}[c(t) + \hat{c}_{01}]\hat{c}_{11} \tag{2.57}$$

and the concentration modes

$$\hat{c}'_{01} = -\frac{\pi}{2}\hat{u}_{10}(t)\hat{c}_{11} - d_0\pi^2\hat{c}_{01}(t) \tag{2.58}$$

$$\hat{c}'_{11} = \pi\hat{u}_{10}(t)[c(t) + \hat{c}_{01}] - (\pi^2 + k_x^2)d_H(k_x,\pi)\hat{c}_{11}(t) \tag{2.59}$$

where primes denote time derivatives and $c(t)$ is the time-dependent amplitude of the selected base state (2.16).

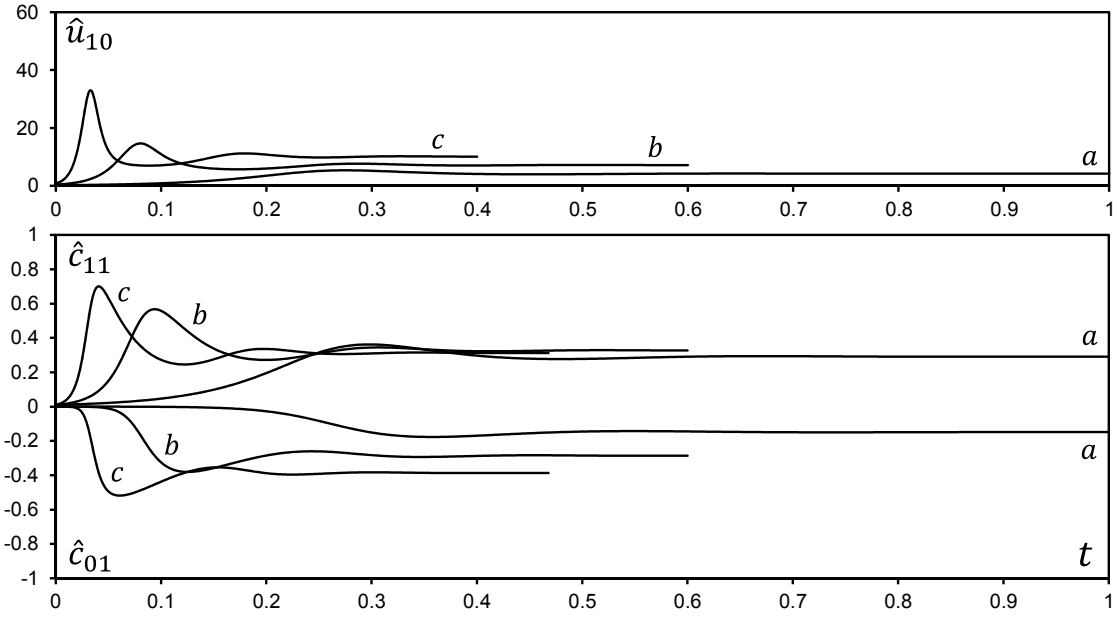

Figure 2.4. Evolution of the mode amplitudes $\hat{c}_{01}$, $\hat{c}_{11}$ and $\hat{u}_{10}(t)$ from initial fluctuation to the stationary state at $\beta = 12$ and *(a)* $Rs_m = 5000$, *(b)* $Rs_m = 10\,000$, *(c)* $Rs_m = 20\,000$.

The calculated time-dependent evolution of the selected mode amplitudes from the arbitrary fluctuation $\hat{c}_{11} = 0.01$ eventually result in a stationary state, although some initial oscillations are possible at higher magnetosolutal Rayleigh numbers (Figure 2.4). The system (2.57)-(2.59) can also be easily solved for the stationary values of the concentration amplitudes

$$\hat{C}_{11} = \frac{\pi}{k}\sqrt{-d_0\varepsilon_{11}^{-1}\hat{C}_{01}C_0\sqrt{\frac{Rs_\infty^{crit}}{Rs_m}}}\,, \quad \hat{C}_{01} = -C_0\left(1-\sqrt{\frac{Rs_\infty^{crit}}{Rs_m}}\right) \tag{2.60}$$

with $k = \sqrt{\pi^2 + k_x^2}$ and the factor $\varepsilon_{11} = 0.5d_H(k_x, \pi)$.

The calculations of the eventual stationary convective motions and the corresponding advective deformations of a single period of the photoabsorptive concentration grating are shown in Figure 2.5. The alternating peristaltic narrowing and stretching of the concentration profile along the direction of the parallel field can be observed above the threshold of the magnetoconvective instability. It results in the gradual formation of a secondary grating perpendicular to the original one.

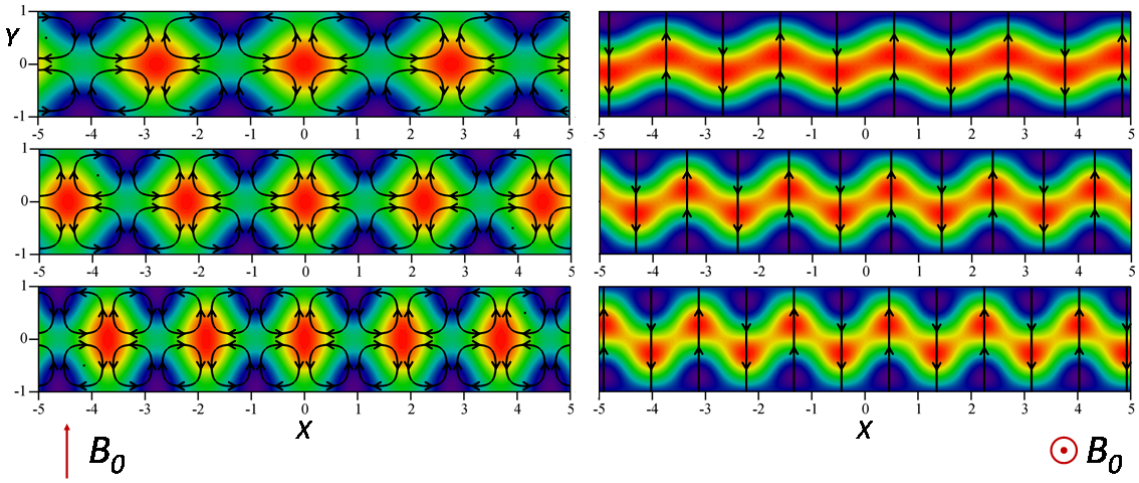

Figure 2.5. Stationary convective deformation of the initially uniform concentration front at $\beta = 12$: left – in parallel applied magnetic field and $Rs_m = 1000$, $Rs_m = 2000$, $Rs_m = 5000$ (from top to bottom); right - in perpendicular magnetic field and $Rs_m = 5000$, $Rs_m = 10\,000$, $Rs_m = 20\,000$ (from top to bottom); concentration contours and convective streamlines.

In turn, the calculated stationary convective currents and the associated perturbations of the photoabsorptive grating correspond to the progressive undulatory bending of the concentration stripes in the configuration of the perpendicular applied field. In both cases the

decrease of the longitudinal period of the perturbations, i.e. the interfringe of the emerging secondary grating, and the scale of the convective motions, becomes noticeable with the increase of the magnetic Rayleigh number.

Making use of the obtained stationary amplitudes of the perturbation modes (2.53)-(2.54) and (2.60) as the initial conditions and substituting the stationary diffusive base state by the appropriate transient base state (2.16), the models (2.48)-(2.51) and (2.57)-(2.59) also describe the relaxation of the periodic photoabsorptive microstructure in the corresponding configuration of the external magnetic field (Figure 2.6).

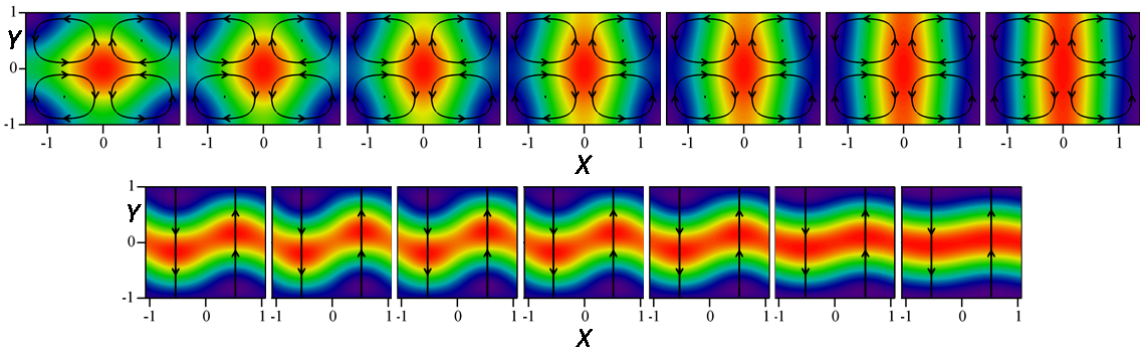

Figure 2.6. Convective-diffusive relaxation of the element of photoabsorptive grating: top – in parallel applied magnetic field with $Rs_m = 1000$, bottom – in perpendicular magnetic field with $Rs_m = 5000$ at $t = 0.0, 0.025, 0.05, 0.075, 0.1, 0.15, 0.2$ (from left to right); concentration contours and convective streamlines.

In parallel field the primary grating rapidly vanishes in the course of the relaxation process, followed by the gradual disappearance of the remaining secondary grating formed by the advective phenomena. The relaxation rate of the concentration modes possessing variations in parallel direction is enhanced by the magnetic interactions through the process of *magnetodiffusion* [53]. Consequently, by comparing the expressions (2.46) and (2.47), it becomes apparent that the mode $\hat{c}_{10}$ is the single perturbation mode not affected by the magnetic effects and it determines the regular regime of the relaxation process but solely in the longitudinal direction. In turn, the anisotropy of the magnetic diffusion disappears in the perpendicular configuration of the external field and the induced grating retains its approximate shape in the course of the relaxation stage.

2.2.4. Enhancement of mass transport

Both stages of the FRS process – the formation and relaxation of the extended photoabsorptive microstructures – serve the purpose of determining the effective transport

coefficients. The intensification of the total mass transfer along the direction of the induced photoabsorptive modulation can be described by an effective coefficient of magnetodiffusion defined as the relaxation rate of the first parallel mode of the concentration grating, which determines the regular regime of the relaxation process in the parallel direction

$$\delta_{eff}(t) = -\frac{1}{\pi^2 J(t)}\frac{\partial J}{\partial t}, \qquad J(t) = |c(t) + \hat{c}_{01}(t)| \tag{2.61}$$

In turn, the magnetic Soret coefficient is determined by the stationary state and can be defined in the following form

$$\sigma_{eff} = \frac{J}{J_0}, \tag{2.62}$$

where J_0 is calculated without the account for magnetoadvection and is equal to C_0.

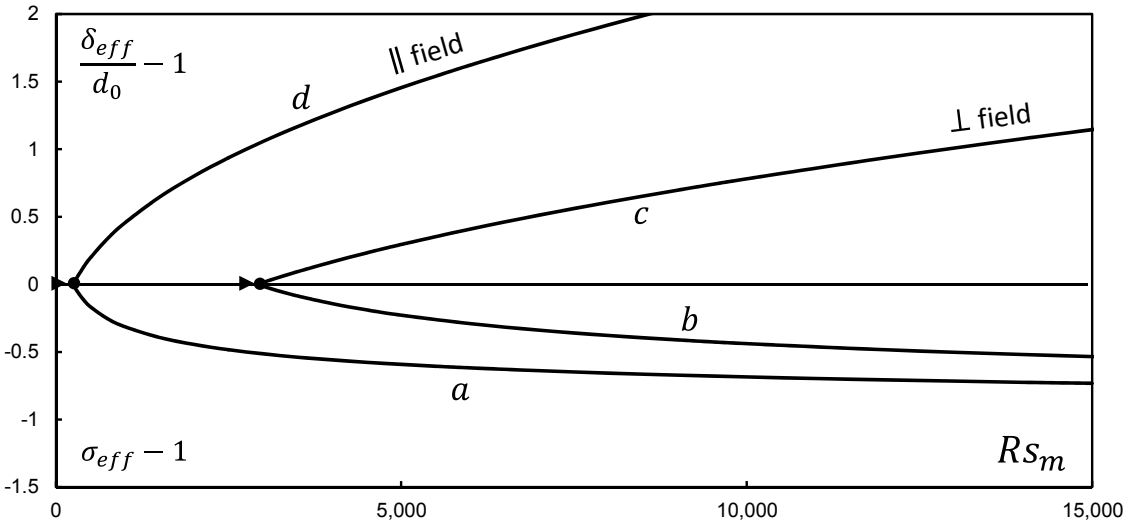

Figure 2.7. Influence of the symmetry-breaking microconvection on the calculated mass transport coefficients: magnetic Soret coefficient - *(a), (b)* and initial magnetic diffusion coefficient - *(d)*, *(c)* in parallel and perpendicular configuration of applied magnetic field, $\beta = 12$.

Both the quantities (2.61) and (2.62) can be calculated from the 4-mode model (2.48)-(2.51) (Figure 2.7). The value of the magnetic Soret coefficient can also be obtained from the analytical expressions (2.53)-(2.54) and (2.60) without difficulty. From (2.53) and (2.60) it follows that both $\hat{C}_{10}$ and $\hat{C}_{11}$ have to be positive, while $\hat{C}_{01}$ is negative in either situation and so is $\hat{C}_{12}$ in the parallel configuration of the external magnetic field. Consequently, the emergence of symmetry breaking magnetic microconvection leads to the decrease of the effective coefficient of magnetic thermodiffusion in both configurations of the applied

magnetic field. In turn, the magnetoconvective intensification of the mass transport along the direction of the optical modulation enhances the effective coefficient of magnetodiffusion.

From the expressions (2.53), (2.60), (2.61) and (2.62) it is apparent that above the threshold of instability there exists an obvious limit on the advective attenuation of the magnetic Soret coefficient $0 < \sigma_{eff} < 1$, with 0 corresponding to the perfect mixing of the non-homogeneities of ferroparticle concentration and 1 – to the vanishing of convective currents.

The increase of the effective coefficient of magnetodiffusion δ_{eff} and the corresponding decrease of the coefficient of magnetic thermodiffusion σ_{eff} with the increasing of the magnetosolutal Rayleigh number is consistent with the character of the dependence of these quantities on the intensity of the applied magnetic field in parallel configuration (Figure 1.1) although the underlying mechanisms of these phenomena are considerably different – the magnetophoretic mass transport in the former situation and magnetoadvective in the latter. The distinctive feature of the emergence of magnetoconvection through symmetry breaking is the presence of the threshold, which becomes more apparent in narrow layers. The critical thresholds (2.35) and (2.36) of the corresponding perturbations depend on the friction factor β and thus on the inverse square of the thickness of the ferrofluid layer. The reducing of the gap of the layer generally leads to higher magnetoconvective stability of the photoabsorptive grating. In turn, the intensity of magnetoconvection is lower and the subsequent dependence of the calculated mass transport coefficients on the magnetic Rayleigh number is much weaker in thin layers. Consequently, it may be difficult to isolate the threshold and thus ascertain the convective symmetry breaking in experimental observations of the formation and relaxation of photoabsorptive microstructures. Thus far, the presence of the threshold has not been affirmed by systematic experimental research.

Extended microstructures

3.1. Formation

In the previous section the microconvective instability in thin ferrofluid layers under the action of the applied lateral magnetic field was considered. The thickness of the layer is defined only in terms of the aspect ratio l of the element of photoabsorptive microstructure and if l is small (i.e. the thickness of the layer is much smaller than the interfringe of the photoabsorptive grating) then the 2D microconvection may emerge through the development of the convective instability.

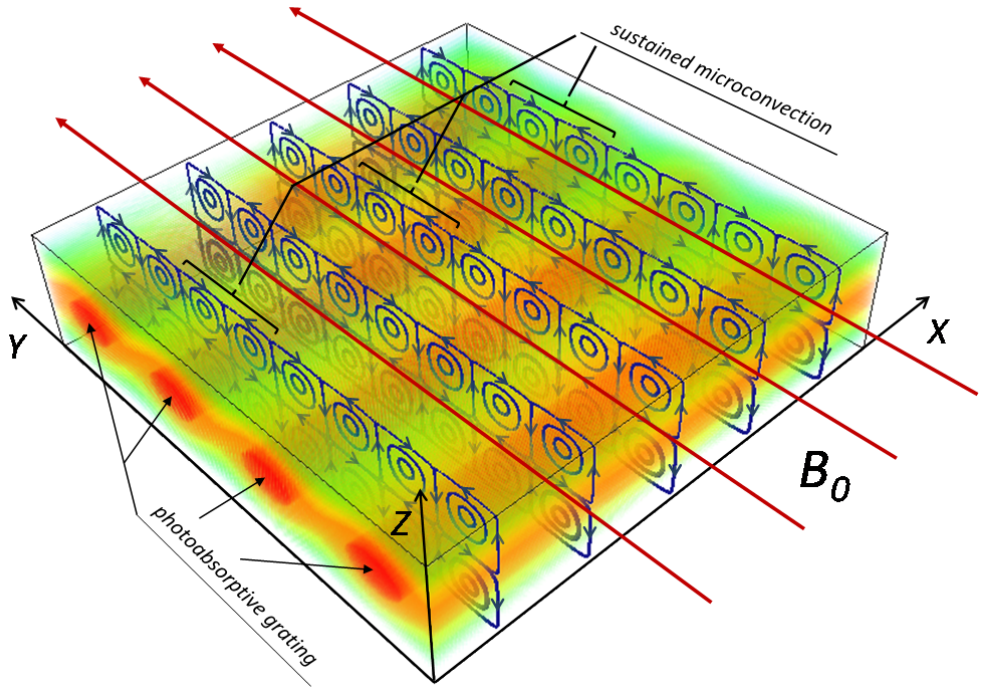

Figure 3.1. Definition of the problem: the concentration maxima of the optically induced concentration grating within the ferrofluid layer under the action of the applied uniform magnetic field. The transversal convective currents are incited by the magnetic forces.

The discarding of the transversal direction destroys important aspects of the method of creation of the photoabsorptive concentration microstructures. The formation of the stationary thermal grating inevitably involves the appearance of the transversal gradients as a consequence of dissipation of thermal energy through the transversal boundary and the formation of the corresponding concentration gradients - due to the thermophoresis. The two-

dimensional approximation is than an abstraction, which may arguably be the closer to reality the smaller is $l \to 0$ and, correspondingly, the larger is the dimensionless factor $\beta \to \infty$. This is not always quite accurate, though.

There is possible, however, a completely different type of microconvection in such system (Figure 3.1), which may be referred to as the parasitic microconvection and is distinguished from the previously described microconvective instability by the absence of a distinct threshold. The use of the term *parasitic* in reference to this kind of microconvection implies that it is something unwanted or may even be a nuisance, but it has appeared historically in the course of the discussions concerning the unexpected results of the FRS experiments and the considerable influence of the magnetic field on the mass transport in photoabsorptive microstructures. This type of the magnetic microconvection is driven exactly by the interactions of the transversal gradients of the concentration and demagnetizing field and will be described in the subsequent sections.

3.1.1. Transversal boundary

For the proper description of the transversal boundary and its influence of the transport processes within the photoabsorptive microstructures the formulation of the corresponding physical and mathematical boundary conditions is necessary for all involved fields. The condition for the temperature field has to account for the diffusion of heat through the sidewall and the convenient form has been previously discussed (2.6).

In turn, the boundary condition for the concentration field is imposed on the drift flux of the ferroparticles $\boldsymbol{J}_c$ (1.24) and the appropriate form is the impermeability condition

$$\boldsymbol{n} \cdot \boldsymbol{J}_c = 0 \tag{3.1}$$

which restricts the penetration of the solid phase through the boundary; $\boldsymbol{n}$ in this case is the surface normal vector

In some situations the deposition of the dispersed phase has been observed on the solid surfaces. This process usually takes place in high gradient magnetic fields and its intensity is described by the concentration Biot number Bi_c [1]. In fact, the non-vanishing slip flux on the boundary can create significant buoyant force in the boundary layer near the solid wall and by itself induce convective motion [89]. Here it is assumed that the near-wall gradients of the demagnetizing field are not large and there is no need to consider the deposition of the ferroparticles. The condition (3.1) is then reasonable.

The conditions for the demagnetizing field perturbation are not intuitive and require additional treatment to formulate the magnetic open boundary condition for the layer. Considering the interface between the ferrofluid and some non-magnetic medium the continuity conditions are obtained from the Maxwell's equations (1.11)-(1.12) in integral form

$$\left[\boldsymbol{n}\cdot\boldsymbol{B}^{in}=\boldsymbol{n}\cdot\boldsymbol{B}^{out}\right]_{\partial S} \tag{3.2}$$

The scalar potential ψ describing the magnetic field (1.25) within the layer should be modified to account for the presence of the interface. This can be done by introducing an additional auxiliary potential φ, which is decomposed into the purely internal φ_{int} and external parts φ_{ext}. Then the boundary condition (3.2) is written in the equivalent potential formulation

$$\left[\frac{\partial}{\partial\boldsymbol{n}}\psi=\boldsymbol{n}\cdot\boldsymbol{M}\right]_{\partial S} \quad \text{and} \quad \left[\frac{\partial}{\partial\boldsymbol{n}}\varphi_{int}=\frac{\partial}{\partial\boldsymbol{n}}\varphi_{ext}\right]_{\partial S} \tag{3.3}$$

with $\boldsymbol{M}$ – the magnetization vector (1.27).

The continuity of the total scalar potential requires an additional condition on the interface

$$[\psi+\varphi_{int}=\varphi_{ext}]_{\partial S} \tag{3.4}$$

In fact, it is more convenient to absorb the internal auxiliary potential φ_{int} into ψ.

The external auxiliary potential φ_{ext} is defined only in the free space outside the ferrofluid layer and then is a harmonic function, because the magnetization is negligible there. From (1.39)

$$\Delta\psi=\tilde{\alpha}_c\boldsymbol{h}\boldsymbol{\nabla}c \quad \text{and} \quad \Delta\varphi_{ext}=0 \tag{3.5}$$

with boundary conditions on the surface of the layer

$$\left[\frac{\partial}{\partial\boldsymbol{n}}\psi=\tilde{\alpha}_c(\boldsymbol{n}\cdot\boldsymbol{h})c+\frac{\partial}{\partial\boldsymbol{n}}\varphi_{ext}\right]_{\partial S},\ \ [\psi=\varphi_{ext}]_{\partial S} \tag{3.6}$$

It should also be required that φ_{ext} vanishes at infinite distance from the surface of the layer.

The treatment presented above is sufficient if only one boundary is present, but in fact the layer is bounded by two sidewalls and two corresponding interfaces. The mutual influence of the opposite boundaries can be accounted for, but estimations show that it is rather small for reasonable thickness of the ferrofluid layer.

3.1.2. Stationary diffusive state

In the previous sections the processes of the formation and relaxation of the flat periodic microstructures in thin ferrofluid layers have been considered under the influence of the applied homogeneous magnetic field in the parallel and perpendicular configurations (Section 2.2). Clearly, such orientations of the external field are not the only possible ones. In fact, there are many possible orientations of the external magnetic field, which can be decomposed into the three main components perpendicular among themselves. Making use of the notation adopted in [53], the first is the parallel field, which causes the direct increase of the effective magnetic diffusion coefficient due to the magnetophoretic contributions. This situation has been studied most extensively in the conditions of the experiment [53]-[62].

The other possible orientation is the longitudinal field, in which case the magnetic field and the exciting thermal gradient are orthogonal but still lie within the plane of the ferrofluid layer. In fact, no additional treatment is necessary for this situation and the distributions of the field perturbations are simply obtained from the ones described for the parallel field by setting the magnetophoretic number $\mathcal{M}_{ph} = 0$, because the magnetic force vanishes in the approximation of non-interacting ferroparticles (see also [53] for details).

The third is the perpendicular orientation of the magnetic field with the field lines perpendicular to the sidewalls of the layer. Apart from interparticle interactions, which are most significant in very concentrated ferrocolloids, the model based on the equilibrium of the slip-fluxes predicts that the process of diffusion in the parallel direction is uninfluenced by the magnetic field in the perpendicular and longitudinal orientations. On the other hand, in thick ferrofluid layers the assumption of transversal homogeneity of the concentration field does not hold. In fact the jump of the ferrofluid magnetization on the transversal sidewalls of the layer can cause significant transversal magnetic field gradients and the corresponding magnetic force.

The stationary diffusive state of the induced photoabsorptive microstructure is determined by the equilibrium of the concentration flux $\boldsymbol{J}_c = \boldsymbol{\nabla} c - \mathcal{M}_{ph} \boldsymbol{\nabla} H + s_m \boldsymbol{\nabla} T$ driven by the optically induced thermal gradient

$$\boldsymbol{\nabla} \cdot \boldsymbol{J}_c = 0 \tag{3.7}$$

For the moment the secondary photoabsorption will be neglected $r_c \to 0$ and the temperature field described by equation (2.5) then decouples from the concentration distribution. The solution to the temperature equation under these circumstances is already known (2.7)-(2.9).

The profiles of the demagnetizing field are in turn described by the equations (3.5) within and outside the ferrofluid layer.

The boundary conditions on the sidewalls of the layer follow from their impermeability to the flux of the ferroparticles (3.1) and the continuity of the normal and tangential components of the magnetic field (3.6).

Under the assumption of the linear dependence of the ferrofluid magnetization on the concentration of the magnetic phase (in the limit of dilute ferrocolloid and non-interacting magnetic particles) the longitudinal projection of the imposed field does not influence the phoretic motion of the ferroparticles due to the translational symmetry of the concentration perturbation. For the arbitrary orientation of the external field this direction can be neglected.

Then the normal vector in the direction of the applied magnetic field can be decomposed discarding the longitudinal coordinate - $\boldsymbol{h} = \left(0; h_y; h_z\right)$. The component of the demagnetizing field along the direction of the external field can be expressed making use of the scalar potential formulation

$$H = -\left(h_y \frac{\partial}{\partial y} + h_z \frac{\partial}{\partial z}\right)\psi \tag{3.8}$$

The distributions of all fields (c, T, ψ) in the parallel direction are considered up to the first Fourier mode

$$X = X_0 + X_+ e^{i\pi y} + X_- e^{-i\pi y} \tag{3.9}$$

and it is convenient to introduce auxiliary expressions for the components of the fields

$$X_{\substack{p \\ m}} = X_+ \pm X_- \tag{3.10}$$

The equation for the external potential φ_{ext} is solved in the free space outside the ferrofluid layer and the solution is a suitable harmonic function according to (3.5). Additional conditions for the proper external potential require for it to vanish at infinite distance from the surface of the ferrofluid layer, so it is readily expressed under the adopted decomposition

$$\varphi_{ext} = \left(\Phi_+ e^{i\pi y} + \Phi_- e^{-i\pi y}\right)\begin{cases} e^{-\pi z}, & z \geq 0 \\ e^{+\pi z}, & z < 0 \end{cases} \tag{3.11}$$

with unknown coefficients $\Phi_\pm$, which are unimportant, and can be excluded from the set of equations and boundary conditions.

The equations (3.7) and (3.5) are projected onto the selected ansatz (3.9)-(3.10) and are more compactly written in matrix form

$$\left(d_z\mathbf{E}\frac{\partial^2}{\partial z^2}-\pi^2 d_y\mathbf{R_1}+2i\pi d_{yz}\mathbf{R_2}\frac{\partial}{\partial z}\right)\mathbf{C}=\frac{1}{2}\pi^2 s_m\mathbf{S} \tag{3.12}$$

$$\left(\mathbf{E}\frac{\partial^2}{\partial z^2}-\pi^2\mathbf{R_1}\right)\mathbf{\Psi}=\tilde{\alpha}_c\left(h_z\mathbf{E}\frac{\partial}{\partial z}+i\pi h_y\mathbf{R_2}\right)\mathbf{C} \tag{3.13}$$

with the transversal boundary conditions (3.1) and (3.6)

$$\frac{\partial}{\partial z}\left[\mathbf{EC}+s_m\mathbf{ST}+\mathcal{M}_{ph}\left(h_z\mathbf{E}\frac{\partial}{\partial z}+\pi h_y\mathbf{R_2}\right)\mathbf{\Psi}\right]=0 \tag{3.14}$$

$$\left(\frac{\partial}{\partial z}+\pi\mathbf{R_1}\right)\mathbf{\Psi}=\tilde{\alpha}_c h_z\mathbf{C} \tag{3.15}$$

Some auxiliary coefficients have been introduced for convenience

$$\mathbf{R_1}=\begin{bmatrix}1&0&0\\0&0&0\\0&0&1\end{bmatrix},\ \mathbf{R_2}=\begin{bmatrix}0&0&1\\0&0&0\\1&0&0\end{bmatrix},\ \mathbf{X}=\begin{bmatrix}X_p\\X_0\\X_m\end{bmatrix},\ \mathbf{S}=\begin{bmatrix}1\\1\\0\end{bmatrix},\ \mathbf{T}=\begin{bmatrix}T_1\\T_0\\0\end{bmatrix}$$

with $\mathbf{X}$ – the vectors of expansion coefficients for concentration, temperature and magnetic potential, and

$$d_y=1+\tilde{\alpha}_c\mathcal{M}_{ph}h_y^2\quad d_z=1+\tilde{\alpha}_c\mathcal{M}_{ph}h_z^2\quad d_{yz}=\tilde{\alpha}_c\mathcal{M}_{ph}h_y h_z \tag{3.16}$$

The expressions for d_y and d_z have the form of the dimensionless coefficients of magnetodiffusion (1.35) along the corresponding direction. Clearly, the application of the external magnetic field introduces the anisotropy of the gradient diffusion within the layer of the ferrocolloid.

By the form of the equations (3.12)-(3.13) the distributions of the concentration and demagnetizing field perturbations are decoupled and the magnetic contributions are introduced into the coefficients. The coupling remains only in the transversal boundary conditions (3.14). In consequence, the influence of the transversal boundary is crucial for the correct description of the photoabsorptive processes in ferrofluid layers and the models accounting only for the bulk interactions have very limited applicability.

Keeping in mind that the imposed temperature field is symmetric across the mid-plane of the layer, it follows from the equation (3.12) and the symmetry of the boundary conditions that the profiles C_p and Ψ_m also possess the same symmetry, but C_m and Ψ_p are antisymmetric.

Eliminating the cross-terms from (3.12) a characteristic equation for the determination of the roots and formation of the general solution is obtained

$$f^4 - 2\pi^2 \frac{d_y d_z - 2d_{yz}}{d_z^2} f^2 + \pi^4 \frac{d_y^2}{d_z^2} = 0 \tag{3.17}$$

The solution to this biquadratic equation yields the required roots $f_{1,2} = \pm r_1$ and $f_{3,4} = \pm r_2$

$$r_{\frac{1}{2}} = \frac{\pi}{d_z} \sqrt{d_y d_z - 2d_{yz} \pm 2\sqrt{D}} \tag{3.18}$$

with the corresponding discriminant

$$D = d_{yz}^2 - d_y d_z d_{yz} \tag{3.19}$$

Taking into account the symmetry of the fields the expressions for the auxiliary mode amplitudes are obtained for the concentration field

$$C_m(z) = 2i\pi d_{yz} \sum_i Y_i \frac{r_i \sinh(r_i z)}{\pi^2 - d_z r_i^2} \tag{3.20}$$

$$C_p(z) = \sum_i Y_i \cosh(r_i z) - \frac{1}{2} \frac{s_m}{d_y} \tag{3.21}$$

and the internal scalar potential

$$\Psi_m(z) = Y_m \cosh(\pi z) + \tilde{\alpha}_c i\pi \left[\sum_i Y_i \frac{\cosh(r_i z)}{r_i^2 - \pi^2} \left(h_y + 2 \frac{r_i^2 d_{yz}}{\pi^2 - d_z r_i^2} h_z \right) + \frac{1}{2} \frac{s_m}{d_y} \frac{h_y}{\pi^2} \right] \tag{3.22}$$

$$\Psi_p(z) = Y_p \sinh(\pi z) + \tilde{\alpha}_c \sum_i Y_i \frac{r_i \sinh(r_i z)}{r_i^2 - \pi^2} \left(h_z - 2 \frac{\pi^2 d_{yz}}{\pi^2 - d_z r_i^2} h_y \right) \tag{3.23}$$

and zero order contributions

$$C_0(z) = \frac{1}{4} \pi^2 \frac{s_m}{d_z} \left(z^2 - \frac{1}{3} l^2 \right) \tag{3.24}$$

$$\Psi_0(z) = \frac{1}{12} \tilde{\alpha}_c \pi^2 h_z \frac{s_m}{d_z} (z^3 - l^2 z) \tag{3.25}$$

with $i = 1, 2$.

The unknown coefficients $Y_{i,m,p}$ must be determined from the boundary conditions (3.14)-(3.15) and are not given here for the general case. The proper modes $X_\pm$ can in turn be obtained from the auxiliary ones by simple relations $X_\pm = \frac{1}{2}(X_p \pm X_m)$. The solution within a single period of the grating is plotted in Figure 3.2 for some arbitrary orientations of the external field.

Evidently, the antisymmetric terms appear in the profiles of the concentration and the demagnetizing field perturbations if the imposed external field possesses both parallel and

perpendicular components. While such situations are sometimes studied experimentally [68], the parallel and the perpendicular orientations of the external field are the ones more frequently considered [53]-[62]. These are the two main configurations, which are symmetric across the mid-plain of the layer and are also more illustrative of the general case.

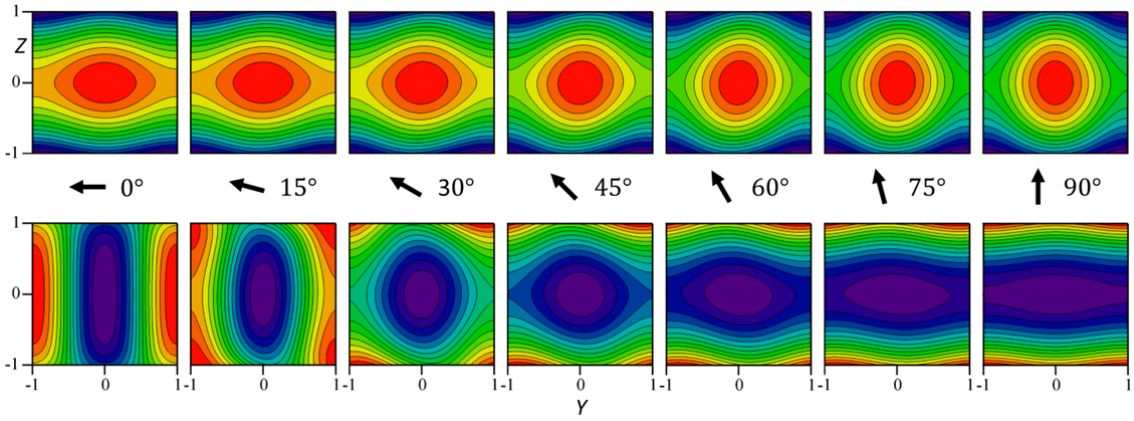

Figure 3.2. Distributions of the concentration (top) and the demagnetizing field (bottom) perturbations within the element of the photoabsorptive grating at different orientations of the external field (0° - parallel configuration, 90° - perpendicular configuration).

The solution and coefficients of (3.20)-(3.25) for the symmetric configurations of the external magnetic field can be expressed up to the leading mode of the thermal grating, bearing in mind the symmetry of the fields

$$c(y,z) = C_0(z) + C_1(z)\cos(\pi y) \tag{3.26}$$

$$H(y,z) = H_0(z) + H_1(z)\cos(\pi y) \tag{3.27}$$

with corresponding mode amplitudes

$$C_0(z) = \frac{1}{4}\frac{\pi^2}{d_z} s_m \left(z^2 - \frac{1}{3}l^2\right) \tag{3.28}$$

$$C_1(z) = \frac{s_m}{2}\left[\frac{1}{d_z g_r}\left(Bi\frac{g_0}{f_0} - \frac{d_y - d_z}{d_y}\pi\right)\cosh(r_0 z) - \frac{1}{d_y}\right] \tag{3.29}$$

$$H_1(z) = \frac{1}{\mathcal{M}_{ph}}\left\{C_1(z) + \frac{s_m}{2}\left[1 - \frac{Bi}{f_0}\cosh(\pi z)\right]\right\} \tag{3.30}$$

where only the single exponent $r_0 = \pi\sqrt{\frac{d_y}{d_z}}$ is retained from (3.18) and

$$g_{0_r} = \frac{\pi}{r_0}\sinh(\pi l) + \pi\cosh(\pi l)\,, \quad f_0 = \pi\sinh(\pi l) + Bi\cdot\cosh(\pi l)$$

In turn, the mode $H_0(z) = -\tilde{\alpha}_c C_0(z)$ is present in (3.27) only in the case of the perpendicular orientation of the external field, otherwise it vanishes for the parallel configuration.

Noting that the relation $c - \mathcal{M}_{ph} H + s_m T = const$ holds true, however, it is more appropriate to express (3.30) explicitly to avoid the ambiguity associated with relating the magnetic field to temperature, because H should depend only on the concentration distribution.

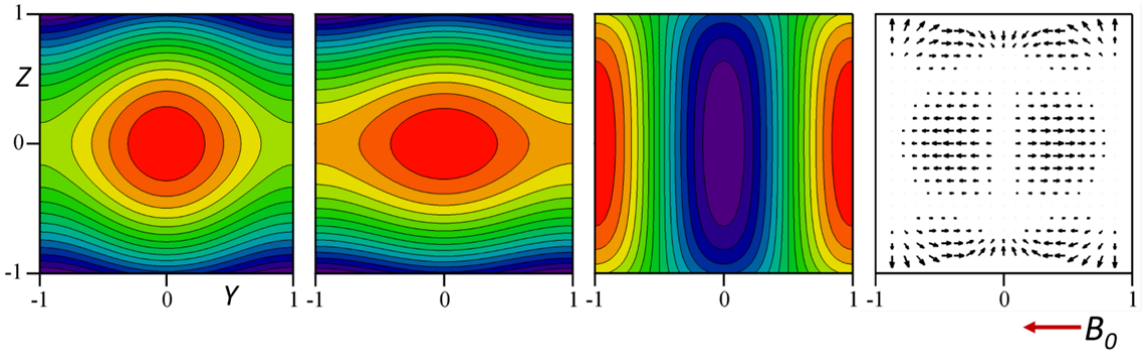

Figure 3.3. Photoabsorptive distributions of temperature, concentration, primary component of demagnetizing field and magnetic force perturbations (from left to right) in the parallel configuration of the external field.

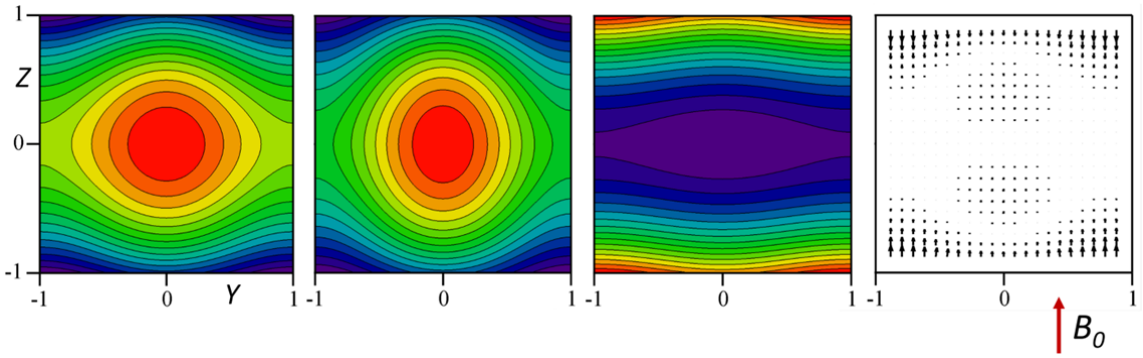

Figure 3.4. Photoabsorptive distributions of temperature, concentration, primary component of demagnetizing field and magnetic force perturbations (from left to right) in the perpendicular configuration of the external field.

In the parallel configuration of the applied field (Figure 3.3) the photoabsorptive concentration profile is slightly elongated in the direction of the applied field comparing to the profile of the temperature field due to the magnetophoretic contributions and the effective anisotropy of the magnetic diffusion coefficient. The perturbation of the magnetic field is rather uniform across the thickness of the layer, but the induced magnetic force, created by the combination of the gradient of the demagnetizing field and the irregularity of concentration, is

not. In fact, it is clear that the configuration of the magnetic force promotes transversal circulation composed of four convective rolls for each period of the grating.

For the perpendicular orientation of the external field (Figure 3.4) the distribution of concentration is once again extended in the direction of the applied field, which now corresponds to the transversal coordinate. While the configuration of the magnetic field seems similar to the case of the laterally applied external field (Figure 3.3), in the former situation it is mainly determined by the discontinuity of the magnetization on the transversal boundaries in contrast to the bulk contributions in the latter case. The jump in magnetization on the sidewalls of the layer causes the appearance of strong magnetic field gradients in the vicinity of the boundary and the corresponding considerable magnetic forces.

Increasing the aspect ratio of the induced grating, i.e., under the adopted normalization, decreasing the thickness of the layer, the main features of the magnetic force configuration remain relatively unchanged. The magnetic force is so irregular that it is doubtful that the reduction of dimension by means of averaging employed in the previous section can give meaningful results if the aspect ratio is not extreme, which it rarely is in the conditions of the experiment. This substantiates the necessity to consider the third dimension in the investigation of the photoinduced microstructures in order to obtain even qualitative correspondence with the experimental results.

3.1.3. Secondary photoabsorption

The absorption of the incident optical intensity within the ferrofluid layer consists of two parts. The first is the initial absorption by the unperturbed distribution of the ferroparticles, the second contribution comes from the accumulation of the nanoparticles due to the established temperature gradient and Soret effect. If the photoinduced concentration perturbation Δc becomes comparable with the initial concentration c_0 then the absorption of incident intensity is increased and the temperature equation becomes coupled to the concentration equation through the coupling parameter r_c (2.5). If the parameter r_c becomes significant, the temperature equation cannot be decoupled and must be solve in conjunction with the concentration balance equation (3.7). The method of solution is similar as in the previous section and will not be discussed in detail.

With the allowance for the secondary photoabsorption the problem (3.7), (3.5) and (2.5) yields the solution to the characteristic equation after the separation of the spatial variables (3.26)-(3.27)

$$r_{\frac{1}{2}} = \frac{r_0}{\sqrt{2}}\sqrt{1+\frac{s_m r_c}{d_y} \pm \sqrt{D}}, \qquad D = 1+\frac{1}{2}\left(\frac{s_m r_c}{d_y}\right)^2 \tag{3.31}$$

Taking into account the symmetry of the fields across the midplane of the layer and the boundary conditions (2.6), (3.1), (3.6) the modes of the concentration distribution for the symmetric configurations can be expressed

$$C_0(z) = \sum_i \frac{a_i}{p_i}\cosh(r_i z) - \frac{1}{r_c}, \qquad C_1(z) = 2\sum_i a_i \cosh(r_i z) \tag{3.32}$$

The coefficients are determined from the appropriate boundary conditions

$$a_i = \pm\frac{l}{r_c}\frac{1}{b_i}\frac{1}{\frac{1}{b_1 p_1}\frac{\sinh(r_1 l)}{r_1} - \frac{1}{b_2 p_2}\frac{\sinh(r_2 l)}{r_2}}, \quad b_i = g_i(d_z - d_i) + \frac{g_0}{f_0} f_i d_i, \quad p_i = \frac{2d_z}{s_m r_c}\frac{r_i^2}{\pi^2} - 1, \quad d_i = d_z\frac{r_i^2 - r_0^2}{r_i^2 - \pi^2}$$

with $i = 1, 2$ and

$$f_i = r_i \sinh(r_i l) + Bi \cdot \cosh(r_i l) \text{ and } g_i = r_i \sinh(r_i l) + \pi \cosh(r_i l)$$

The temperature modes can then be expressed

$$T_0(z) = \frac{d_z}{s_m}\sum_i \frac{a_i}{p_i}\left[\frac{f_i}{Bi} - \cosh(r_i z)\right] \tag{3.33}$$

$$T_1(z) = \frac{2}{s_m}\sum_i a_i d_i \left[\frac{f_i}{f_0} cosh(\pi z) - \cosh(r_i z)\right] \tag{3.34}$$

and the demagnetizing field

$$H_1(z) = \frac{1}{\mathcal{M}_{ph}}\left\{C_1(z) + 2\sum_i a_i\, d_i \left[\frac{f_i}{f_0} cosh(\pi z) - \cosh(r_i z)\right]\right\} \tag{3.35}$$

As previously, the mode $H_0(z) = -\tilde{\alpha}_c C_0(z)$ is present in (3.27) only in the case of the perpendicular orientation of the external field and vanishes for the parallel configuration.

Increasing the value of the coupling parameter r_c the concentration grating becomes sharper (Figure 3.5). The intensity of the demagnetizing field increases within the layer and is attenuated outside. From the physical point of view higher values of the coupling parameter r_c mean enhanced absorption of incident intensity due to the migration of the nanoparticles into the heated region, which in turn further increases the production of heat and the mass flux until countered by the diffusion and the magnetophoresis. The temperature distribution then becomes slightly elongated in the direction of the applied field due to the secondary photoabsorption.

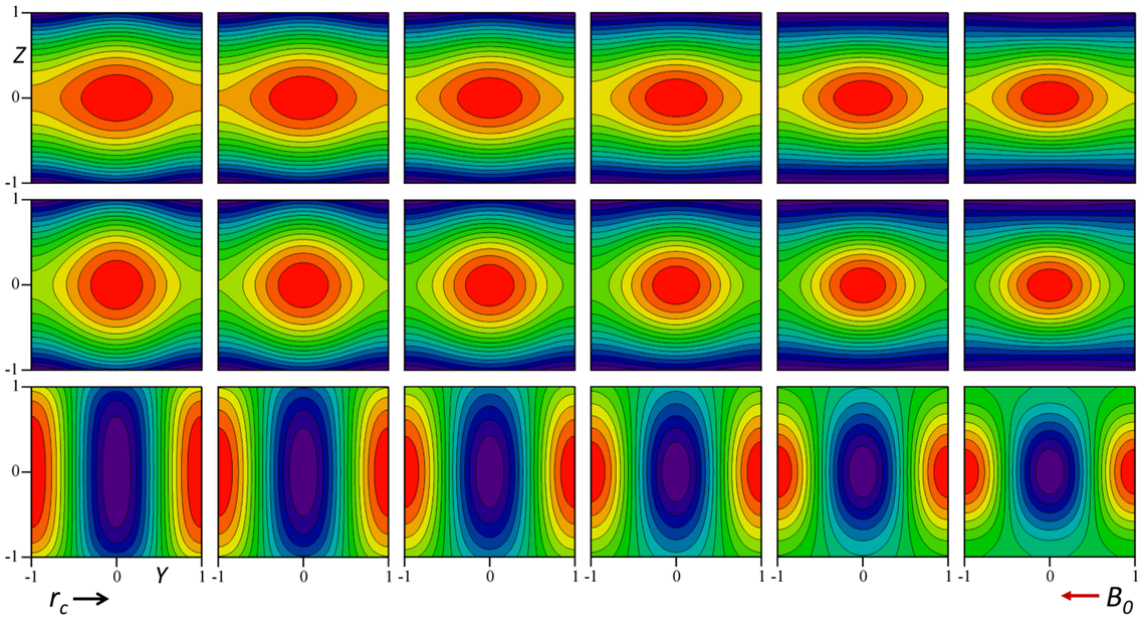

Figure 3.5. Secondary photoabsorption: distributions of temperature (top), concentration (middle), demagnetizing field (bottom) in the parallel configuration of the external field at $r_c = 0.0, 0.1, 0.2, 0.3, 0.4, 0.5$ (from left to right).

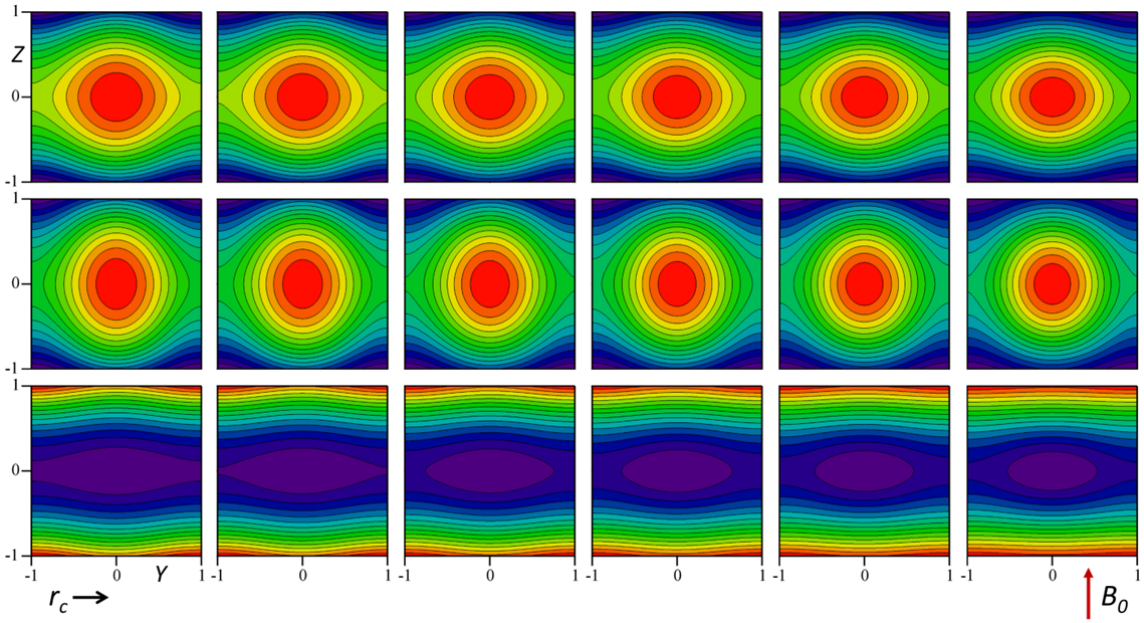

Figure 3.6. Secondary photoabsorption: distributions of temperature (top), concentration (middle), demagnetizing field (bottom) in the perpendicular configuration of the external field at $r_c = 0.0, 0.1, 0.2, 0.3, 0.4, 0.5$ (from left to right).

Still, at reasonable values of the coupling parameter r_c the influence of the secondary absorption on the stationary state is rather small.

3.1.4. Diffusive relaxation

In the absence of microconvection the relaxation of the photoabsorptive structures upon the switching off of the optical pumping is governed by the diffusion and the magnetophoresis in the self magnetic field of the ferrocolloid. The characteristic time of the relaxation of the induced concentration structures is estimated by the diffusion timescale $\frac{L^2}{D}$, while the characteristic thermal scale is expressed through the thermal diffusivity of the colloid $\frac{L^2}{\kappa}$. The dimensionless Lewis number is expressed as the ratio of these scales $Le = \frac{D}{\kappa}$. It is generally very small in typical ferrocolloids, so the relaxation of temperature after the turning off of the pumping beams is almost instantaneous in comparison with the characteristic time for the relaxation of concentration structures. Bearing in mind the different timescales for temperature and concentration, it is possible to formulate the set of equations describing the process of diffusive relaxation of the photoabsorptive concentration microstructures. From (1.37)

$$\frac{\partial}{\partial t} c = \Delta\left(c - \mathcal{M}_{ph} H\right) \tag{3.36}$$

with the boundary conditions for concentration and demagnetizing field on the upper sidewall of the layer expressed by (3.1) and (3.6)

$$\left[\frac{\partial}{\partial z}\left(c - \mathcal{M}_{ph} H\right) = 0\right]_{z=l} \tag{3.37}$$

$$\left[\frac{\partial}{\partial z}\psi = \tilde{\alpha}_c h_z c + \frac{\partial}{\partial z}\varphi_{ext}\right]_{z=l}, \left[\psi = \varphi_{ext}\right]_{z=l} \tag{3.38}$$

and the initial conditions are determined either by (3.28)-(3.29) or (3.32).

The solution of the system (3.36)-(3.38) can be carried out by the method of Laplace transformation, which is generally most suitable for the solving of the initial value problems of this kind. Separating the spatial variables in the following way

$$c(y, z, t) = C_0(z, t) + C_1(z, t)\cos(\pi y) \tag{3.39}$$

the set of dynamic equations for the mode amplitudes is obtained. The relaxation problem for the zero-order concentration mode becomes

$$\frac{\partial C_0}{\partial t} = d_z \frac{\partial^2 C_0}{\partial z^2} \tag{3.40}$$

making use of the relation $H_0(z, t) = -\tilde{\alpha}_c C_0(z, t)$, which is valid in the perpendicular configuration of the applied field. Otherwise, in the case of the parallel orientation of the

external field, the zero parallel mode of the demagnetizing field vanishes owing to the initial conditions. On the sidewall of the layer $C_0(z,t)$ obeys the homogeneous Neumann boundary condition $\left[\frac{\partial C_0}{\partial z}=0\right]_{z=l}$ at all times and the temporal and spatial variables can be separated in a simple manner yielding the eigenvalue problem. The solution is then obtained without difficulty as decomposition into Fourier modes

$$C_0(z,t)=\sum_{n=1}^{\infty} c_n \cos\left(\frac{\pi n z}{l}\right) e^{-d_z\left(\frac{\pi n}{l}\right)^2 t} \tag{3.41}$$

with the coefficients c_n determined from the zero-order parallel mode of the initial concentration profile $C_0^{init}(z)$.

$$c_n=\frac{1}{l}\int_{-l}^{l} C_0^{init}(z)\cos\left(\frac{\pi n z}{l}\right)dz \tag{3.42}$$

At the same time the coefficient c_0 disappears due to the conservation of the ferroparticles.

For the initial distribution (3.32) the coefficients of the series (3.41) become

$$c_n=2\frac{(-1)^n}{l}\sum_i \frac{a_i}{p_i} r_i \frac{\sinh(r_i l)}{r_i^2+\left(\frac{\pi n}{l}\right)^2} \tag{3.43}$$

with the appropriate values of the coefficients.

In the decoupled case of negligible secondary photoabsorption $r_c \to 0$ the coefficients are expressed from the relation (3.28) and have simple form

$$c_n=(-1)^n\frac{\pi^2 s_m}{d_z\left(\frac{\pi n}{l}\right)^2} \tag{3.44}$$

The projected equations for the first parallel modes are in turn expressed

$$\frac{\partial C_1}{\partial t}=\left[d_z\frac{\partial^2}{\partial z^2}-d_y\pi^2\right]C_1(z,t) \tag{3.45}$$

$$\left[\frac{\partial^2}{\partial z^2}-\pi^2\right]\Psi_1(z,t)=\tilde{\alpha}_c\left(h_z\frac{\partial}{\partial z}-\pi h_y\right)C_1(z,t) \tag{3.46}$$

where Ψ_1 is the corresponding mode of the internal scalar potential ψ. The boundary conditions after excluding the external potential φ_{ext}

$$\left[\frac{\partial}{\partial z}\left\{C_1+\mathcal{M}_{ph}\left(h_z\frac{\partial}{\partial z}+\pi h_y\right)\Psi_1\right\}=0\right]_{z=l},\ \left[\left(\frac{\partial}{\partial z}+\pi\right)\Psi_1=\tilde{\alpha}_c h_z C_1\right]_{z=l} \tag{3.47}$$

For the purpose of obtaining the solution a one-way Laplace transformation

$$\hat{f}(z,s) = \mathcal{L}\{f(z,t)\} = \int_0^\infty e^{-st} f(z,t)dt \tag{3.48}$$

is applied to the problem (3.45)-(3.47). Equation (3.45) becomes

$$\left[d_z \frac{\partial^2}{\partial z^2} - d_y \pi^2\right] \hat{C}_1(z,s) - s\hat{C}_1(z,s) + C_1^{init}(z) = 0 \tag{3.49}$$

where the time derivative has been transformed by making use of the integration by parts and $C_1^{init}(z)$ is the initial profile of the first parallel concentration mode. The form of the equation (3.46) remains unchanged in the *s*-domain and the same applies to the boundary conditions (3.47).

The transformed equations are linear with constant coefficients and can be solved without difficulty, taking into account the symmetry of the fields. For concentration

$$\hat{C}_1(z,s) = X_1(s)\cosh(r_s z) + \frac{1}{r_s}\left(x_1 \int C_1^{init} x_2 dz - x_2 \int C_1^{init} x_1 dz\right) \tag{3.50}$$

with the fundamental set of solutions $x_1(z,s) = \cosh(r_s z)$ and $x_2(z,s) = \sinh(r_s z)$ and the exponent $r_s(s) = \sqrt{\frac{d_y\pi^2+s}{d_z}}$.

The following form of the first initial parallel mode is assumed (3.32)

$$C_1^{init}(z) = 2\sum_i a_i \cosh(r_i z) \tag{3.51}$$

Then the first parallel mode of the perturbation in the *s*-domain becomes

$$\hat{C}_1(z,s) = X_1(s)\cosh(r_s z) - \frac{2}{d_z}\sum_i \frac{a_i}{r_i^2 - r_s^2}\cosh(r_i z) \tag{3.52}$$

Satisfying the boundary conditions (3.47) the *s*-dependant coefficient X_1 is expressed

$$X_1 = \frac{\Phi(s)}{\Psi(s)} \tag{3.53}$$

with

$$\Phi(s) = 2(r_s^2 - \pi^2)\sum_i \frac{a_i\left[\tilde{s}_i r_i \sinh(r_i l) + \frac{d_y - d_z}{d_z}\pi^3 \sinh(\pi l)\frac{g_i}{g_0}\right]}{(r_i^2 - \pi^2)(r_i^2 - r_s^2)} \tag{3.54}$$

$$\Psi(s) = s r_s \sinh(r_s l) + (d_y - d_z)\pi^3 \sinh(\pi l)\frac{g_s}{g_0} \tag{3.55}$$

with $g_s = r_s \sinh(r_s l) + \pi\cosh(r_s l)$ and $\tilde{s}_i = r_i^2 - r_0^2$.

Once obtained, the solution in the s-domain must be converted to the time domain. For that purpose the inverse problem of finding the function $f(z,t)$ by its image $\hat{f}(z,s)$ must be solved. The inverse transformation is expressed in general form by the integral

$$f(z,t) = \mathcal{L}^{-1}\{\hat{f}(z,s)\} = \frac{1}{2\pi i}\int_{\sigma-i\infty}^{\sigma+i\infty} e^{st}\,\hat{f}(z,s)ds \tag{3.56}$$

which is known as the Bromwich integral, the Riemann-Mellin formula or the Fourier-Mellin integral. The integration is performed along the vertical line in complex space from $\sigma - i\infty$ to $\sigma + i\infty$ in such a way so that all the singularities of $\hat{f}(z,s)$ are on the left side of the integration path ensuring the convergence of the improper integral (3.56).

It was shown that if the image function $\hat{f}(z,s)$ can be represented as a ratio $\hat{f}(z,s) = \frac{\Phi(s)}{\Psi(s)}$ of two integral functions (i.e. functions, which are analytic over the whole complex plane) $\Phi(s)$ and $\Psi(s)$, then the inverse transformation can be expressed as a functional series

$$f(z,t) = \sum_{n=1}^{\infty} \frac{\Phi(s_n)}{\Psi'(s_n)} e^{s_n t} \tag{3.57}$$

The summation is performed over the roots s_n of the denominator $\Psi(s)$. The series (3.57) is known in the literature as the Vaschenko-Zakharchenko or Heaviside expansion. It is assumed that the roots s_n are simple and $\Psi(s)$ does not have a trivial root $\mathrm{s} = 0$.

The expansion (3.57) is used to obtain the inverse transformation of (3.52). Formally the numerator (3.54) is not integral and has two simple poles at $s = d_z\tilde{s}_i$ so the expansion is not applicable. On the other hand, it is more convenient to use the form (3.54) rather than introduce the denominator of $\Phi(s)$ into $\Psi(s)$ (thus obtaining $\widetilde{\Phi}(s)$ and $\widetilde{\Psi}(s)$). Indeed taking into account that

$$\frac{\widetilde{\Phi}(\tilde{s}_i)}{\widetilde{\Psi}'(\tilde{s}_i)} = -2a_i \tag{3.58}$$

so that the second term in (3.52) cancels out from the resulting expansion. The terms corresponding to the poles $s = \tilde{s}_i$ also vanish from the expansion of the mode H_1 of the demagnetizing field.

It is now necessary to analyze the other roots of $\Psi(s)$. A special case is the pole $s = \left(d_z - d_y\right)\pi^2$, which can be either positive or negative depending on the configuration of the external field. Still, the term contributing to this pole cancels from the resulting expansion because it is at the same time the root of $\Phi(s)$ and the ambiguity with regard to its sign is thus resolved.

The rest of the poles are obtained from the transcendental relation

$$\coth(r_s l) + \frac{r_s}{\pi}\left[1 + \frac{s g_0}{(d_y - d_z)\pi^3 \sinh(\pi l)}\right] = 0 \tag{3.59}$$

This expression yields another pole $s = (d_z - d_y)\pi^2$, which is simultaneously the root of $\Phi(s)$ and so this term is cancelled from the resulting decomposition. For the parallel configuration of the applied field the expression (3.59) possesses additional root s_0, for which r_s is real. The pole s_0 can be determined numerically.

The rest of the poles can be obtained under the condition $s < -d_y\pi^2$ and then r_s lies on the imaginary axis. For this case it is convenient to introduce the imaginary part $x = \Im\{r_s\}$, then $s_n = -(d_z x_n^2 + d_y\pi^2)$ and the relation (3.59) becomes

$$\cot(xl) - \frac{x}{\pi}\left[1 - \frac{(d_z x_n^2 + d_y\pi^2) g_0}{(d_y - d_z)\pi^3 \sinh(\pi l)}\right] = 0 \tag{3.60}$$

which has infinite number of roots x_n with $n = 1,2 \ldots$

The transcendental relations (3.59) and (3.60) can be solved numerically for the purpose of obtaining the necessary poles. All roots are real and negative ensuring the monotonous relaxation. The first parallel modes of the concentration perturbation can then be transformed back to the time domain

$$C_1(z,t) = \sum_{n=0}^{\infty} \frac{\Phi(s_n)}{\Psi'(s_n)} \cosh[r_s(s_n) z]\, e^{s_n t} \tag{3.61}$$

For the decoupled case $r_c \to 0$ the initial shape of first lateral mode $C_1^{init}(z)$ corresponds to the assumed form (3.51) with $r_1 = r_0$ and $r_2 = 0$. The poles remain in place and are still determined from the relations (3.59) and (3.60) since the denominator $\Psi(s)$ does not depend on the coefficient of secondary absorption. The nominator $\Phi(s)$ in turn becomes

$$\Phi(s) = \frac{\pi s_m}{2 d_z} \sinh(\pi l)\left[\frac{(d_y - d_z)\pi^3}{(d_y\pi^2 + s) g_0} - \frac{Bi}{f_0}\right]\left[1 + \frac{(d_y - d_z)\pi^2}{s}\right] \tag{3.62}$$

The form of the relation for the concentration mode in the time domain also remains the same (3.61).

The relaxation stage of the FRS experiment is a dynamic process governed by the complex interaction of the concentration and the demagnetizing field perturbations. The magnetophoretic contributions in the self magnetic field of the ferrocolloid determine the

intensification of the relaxation process in the direction along the applied field so that the advancement of the concentration profile is faster in that direction.

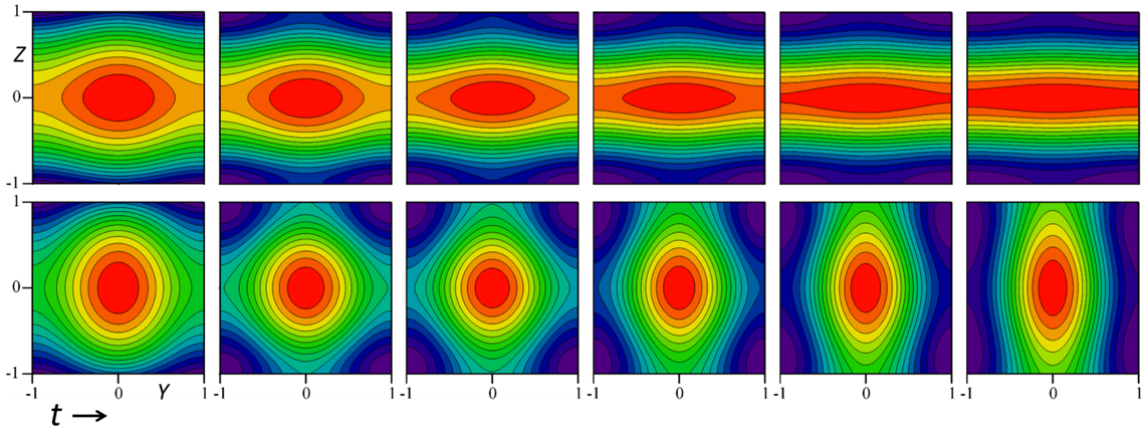

Figure 3.7. Relaxation progress of concentration microstructures: distributions of concentration at $t = 0.0,\ 0.02,\ 0.05,\ 0.1,\ 0.15,\ 0.2$ (from left to right) in the parallel (top) and perpendicular (bottom) configurations of the applied field.

The spatial distributions of the involved fields ensure the nonhomogeneity of the effective transport coefficients and their anisotropy everywhere within the ferrofluid layer. On the other hand, the effective concentration diffusion coefficient is deduced from the rate of relaxation of the diffraction signal of a probing laser beam from the photoinduced grating in the conditions of the experiment. It was determined that the intensity of the first diffraction maximum depends solely on the periodic variation of the concentration field [93] rather than the zero order contribution $C_0(z,t)$. It should depend, however, on the transversal profile of the parallel modes. So, some form of averaging in the transversal direction has to be employed for the purpose of obtaining the effective transport coefficients characterizing the diffusion in the self magnetic field, which would correlate with the parameters calculated from the measurable quantities. Without partaking in the discussion on the most suitable form of averaging for comparison with the experimental measurements, the effective lateral relaxation rate is introduced in the following form, consistent with (2.61)

$$\delta_{eff}(t) = -\frac{1}{\pi^2 J(t)}\frac{\partial J}{\partial t}, \qquad J(t) = \sqrt{\int_{-l}^{l} C_1^2(z,t)dz} \tag{3.63}$$

with the calculated signal $J(t)$ expressed as an L^2-norm of the first parallel mode of the concentration field perturbation.

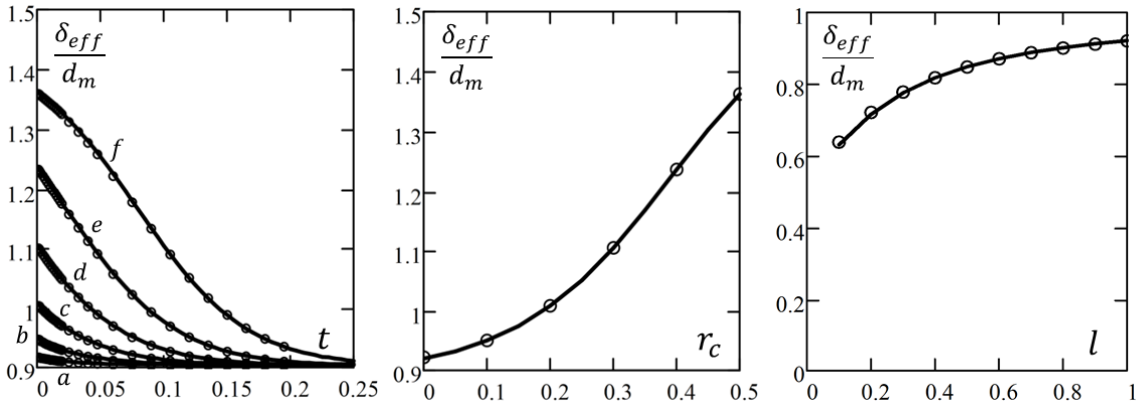

Figure 3.8. Diffusive relaxation of the concentration microstructures in parallel applied field: left - dependence of the effective parallel diffusion coefficient δ_{eff} on time (symbols – numerical simulations, lines – model (3.63)); middle – influence of the secondary absorption on the initial relaxation rate (symbols – numerical simulations, lines – model (3.63)); right – dependence of the initial diffusion coefficient on the thickness of the layer (symbols – model (3.63), lines – thin layer approximation).

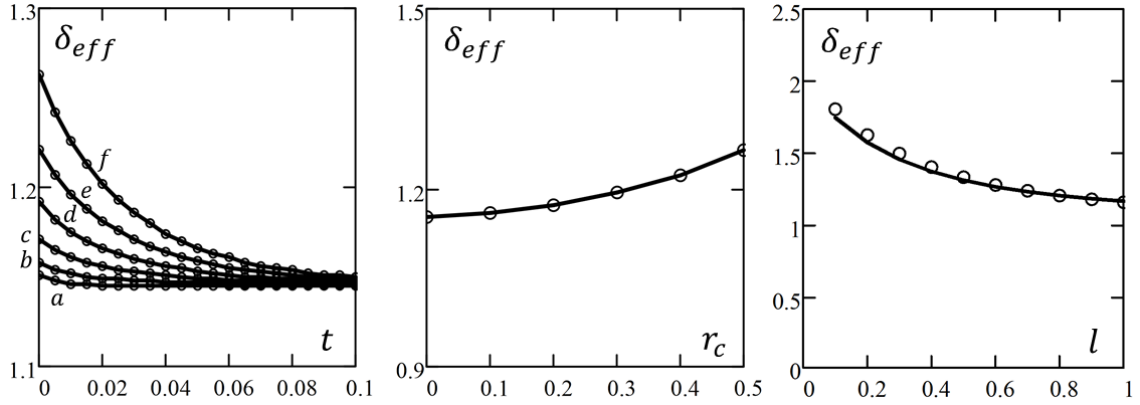

Figure 3.9. Diffusive relaxation of the concentration microstructures in perpendicular applied field: left - dependence of the effective lateral diffusion coefficient δ_{eff} on time (symbols – numerical simulations, lines – model (3.63)); middle – influence of the secondary absorption on the initial relaxation rate (symbols – numerical simulations, lines – model (3.63)); right – dependence of the initial diffusion coefficient on the thickness of the layer (symbols – model (3.63), lines – thin layer approximation).

The calculations of the effective relaxation rates show its initial dependence on the coupling between the thermal and concentration perturbations for both parallel (Figure 3.8) and perpendicular (Figure 3.9) configurations of the applied field. The value of δ_{eff} increases with

the increasing of the coupling parameter r_c, so this effect is significant at higher intensities of the optical pumping and larger induced concentration differences. The dependence is stronger in the parallel orientation of the applied magnetic field and the increase of δ_{eff} is more significant for this configuration. As the relaxation process progresses the effective relaxation rate approaches its value in the uncoupled case evidencing that the account of the secondary absorption appreciably influences exactly the transversal profile of the concentration distribution, leading to enhanced depletion of the ferroparticles from near the boundary regions.

In turn, the presence of the transversal boundary of the layer, which is impermeable to the flux of the ferroparticles, also influences the course of the relaxation process in the parallel direction. Decreasing the thickness of the ferrofluid layer the effective relaxation rate can be decreased or increased accordingly in the parallel or perpendicular configuration of the external magnetic field due to the influence of the magnetic interactions. The experimentally measured diffusion coefficient can then be considerably different from its physical value if the measurement is performed in a very narrow layer and the appropriate correction is not applied.

It is interesting to compare this coefficient (3.63) calculated with full account for the transversal phoretic mass transport and the corresponding diffusion coefficient d_0 (2.20) introduced in the framework of the thin layer approximation. The comparison shows almost perfect correspondence for both the parallel (Figure 3.8, right) and perpendicular (Figure 3.9, right) configurations of the applied field even for layers, which can no longer be considered "thin", i.e. the thickness $2l$ is comparable with the interfringe of the grating. In compliance with the discussed properties of the factors f_H (2.18), in the parallel field configuration the effective lateral diffusion coefficient δ_{eff} approaches its bulk value d_m in infinitely thick layers and tends to unity in narrow layers. In turn, in perpendicular field the corresponding limits are exactly reversed. In this regard – the gap averaged amplitude of the concentration grating and its relaxation dynamics can be accurately predicted by the simplified model if the formation of the grating is accomplished by just the phoretic effects, but this assumption may not always be correct.

3.1.5. Photoabsorptive microconvection

The considering of the transversal direction and the calculations of the diffusive base state evidence that the phoretic effects may not be the sole contributing factor to the formation of the stationary photoabsorptive microstructures. Usually, the description of the convective motions involves some intuitive assumptions about its general configuration. This *ansatz*

generally permits to reduce the symmetry of the problem and simplify its solution. The photoabsorptive gratings possess many symmetries and the most obvious choice is to primarily consider the motions within the plane of the layer. Nevertheless, the previously discussed two-dimensional flows belonging to this type of convective motion in fact violate the longitudinal symmetry of the photoabsorptive gratings and so can only emerge through the mechanism of the convective instability.

Alternatively, considering of the transversal direction reveals that the complex interactions of the gradients of concentration and demagnetizing field induced in a thick layer of ferrofluid through photoabsorption and thermodiffucion cause the appearance of the non-potential configuration of the magnetic force and may promote parasitic transversal microconvection. This configuration of convective motion is contained within the profile plane of the grating and obeys all of its symmetries. Thus, it is not the consequence of the exchange of stabilities but is rather the inherent property of the interactions of the photoabsorptive microstructures with the applied magnetic field. The determination of the role of the transversal convective flows in the formation of the photoabsorptive gratings requires the solution of the nonlinear convective-diffusive problem in the profile plane of the grating and will be carried out in this section.

The set of governing equations describing the stationary microconvection possesses non-linearity both in the concentration and the momentum balance equation. For the parallel configuration of the applied magnetic field, from (1.36)-(1.39)

$$-\boldsymbol{\nabla} P + \Delta \boldsymbol{U} + R s_m C \boldsymbol{\nabla} H = 0 \tag{3.64}$$

$$\Delta\left(C - \mathcal{M}_{ph} H + s_m T\right) - \boldsymbol{U}\boldsymbol{\nabla} C = 0 \tag{3.65}$$

$$\Delta \Psi = \tilde{\alpha}_c \frac{\partial C}{\partial y} \tag{3.66}$$

The equation (3.5) for the perturbation of the external potential Φ_{ext} is also added to the system and should be solved in the free space outside of the layer

$$\Delta \Phi_{ext} = 0 \tag{3.67}$$

The boundary conditions on the transversal sidewalls of the layer consist of the impermeability condition (3.1) for the concentration field

$$\left[\frac{\partial}{\partial \boldsymbol{n}}\left(C - \mathcal{M}_{ph} H + s_m T\right) = 0\right]_{\partial S} \tag{3.68}$$

and the continuity condition (3.6) for the distributions of the internal and the external magnetic scalar potentials

$$\left[\frac{\partial}{\partial \boldsymbol{n}}\Psi = \frac{\partial}{\partial \boldsymbol{n}}\Phi_{ext}\right]_{\partial S}, \quad [\Psi = \Phi_{ext}]_{\partial S} \tag{3.69}$$

The hydrodynamic no-slip boundary condition for the velocity field is also imposed on the sidewall of the layer

$$[\boldsymbol{U} = 0]_{\partial S} \tag{3.70}$$

All fields are also assumed periodic in the parallel direction with the imposed period of the photoabsorptive grating.

The solution will be considered up to the first mode in the parallel direction, the approximation which may be valid only in the regime of weak nonlinearity at low values of the magnetic Rayleigh number

$$C(y,z) = C_0(z) + C_1(z)\cos(\pi y) \quad \text{and} \quad H(y,z) = H_1(z)\cos(\pi y) \tag{3.71}$$

where the mode $H_0(z)$ of the demagnetizing field vanishes owing to the equation (3.66).

With $\boldsymbol{U} = V\mathbf{e_y} + W\mathbf{e_z}$ the parallel and perpendicular velocity components are similarly decomposed

$$V(y,z) = V(z)\sin(\pi y), \quad W(y,z) = W(z)\cos(\pi y) \tag{3.72}$$

In the following analysis it is assumed that the convective flows possess all the symmetries of the diffusive base state, which creates them. It is then convenient to express the influence of the stationary convective fluxes on the profiles of the concentration and demagnetizing field as perturbations $\tilde{C}$ and $\widetilde{H}$ of the diffusive distributions of the corresponding fields calculated without the account for microconvection (3.28)-(3.30)

$$C_{0,1} = C_{0,1}^{dif}(z) + \tilde{C}_{0,1}(z) \quad \text{and} \quad H_1 = H_1^{dif}(z) + \widetilde{H}_1(z) \tag{3.73}$$

where H^{dif} is the configuration of the demagnetizing field corresponding to the diffusive distribution of concentration C^{dif} (3.28)-(3.29).

The temperature distribution is decoupled from the concentration field assuming negligible secondary photoabsorption. In turn, taking into account that the intensity of convective motions is comparable to the characteristic diffusive mobility of the ferroparticles, the vast difference between the thermal and concentration diffusivities characterized by the Lewis number Le, which is rather small in ferrofluids, assures that the temperature field remains

unperturbed by the magnetically induced microconvective currents. The established distribution of temperature has been expressed under these circumstances (2.7)-(2.9).

From the continuity condition $\boldsymbol{\nabla} \cdot \boldsymbol{U} = 0$ the relation between the hydrodynamic modes is obtained

$$V(z) = -\frac{1}{\pi}\frac{\partial W}{\partial z} \tag{3.74}$$

Taking into account that the pressure for incompressible flows is not an independent dynamic variable, but is rather a kinematic constraint necessary for ensuring the condition of the divergence-free velocity field, it can be excluded by taking the *curl* of the Stokes equation (3.64)

$$\Delta\boldsymbol{\omega} + Rs_m \boldsymbol{\nabla} \times [C\boldsymbol{\nabla}H] = 0 \tag{3.75}$$

and making use of the vorticity vector as $\boldsymbol{\omega} = \boldsymbol{\nabla} \times \boldsymbol{U}$, which has only the longitudinal *x*-component and is perpendicular to the profile plane *y*-*z* of the grating. The amplitude ω_1 of the first parallel mode of the vorticity is then expressed

$$\omega_1(z) = \frac{1}{\pi}\left(\frac{\partial^2}{\partial z^2} - \pi^2\right) W(z) \tag{3.76}$$

The projected equations for the mode amplitudes are obtained from the set of governing equations (3.65)-(3.66) and (3.75) after some transformations

$$\frac{\partial^2}{\partial z^2}\tilde{C}_0 = \frac{1}{2}\frac{\partial}{\partial z}\left[W(z)\left(C_1^{dif} + \tilde{C}_1\right)\right] \tag{3.77}$$

$$\left(\frac{\partial^2}{\partial z^2} - d_m\pi^2\right)\tilde{C}_1 - W(z)\frac{\partial}{\partial z}\left(C_0^{dif} + \tilde{C}_0\right) = 0 \tag{3.78}$$

$$\left(\frac{\partial^2}{\partial z^2} - \pi^2\right)\tilde{H}_1 = \tilde{\alpha}_c\pi^2\tilde{C}_1(z) \tag{3.79}$$

and the equation for the hydrodynamic mode

$$\left[\frac{\partial^2}{\partial z^2} - \pi^2\right]^2 W = -\pi^2 Rs_m\left[H_1^{dif}(z) + \tilde{H}_1(z)\right]\frac{\partial}{\partial z}\left(C_0^{dif} + \tilde{C}_0\right) \tag{3.80}$$

Due to its large thermal diffusivity the temperature field is unperturbed by the microconvection on the diffusive scale and vanishes from the equations for the perturbation mode amplitudes owing to the employed form of the field perturbations (3.73).

From the relation (3.80) it becomes apparent that the microconvective structures in the parallel configuration of the applied magnetic field are formed by the interaction of the first

parallel mode of the induced demagnetizing field and the transversal gradient of the zero-order concentration mode. The first mode of the internal magnetic field is determined exclusively by the first concentration mode, so it can be said that the magnetically driven convection emerging within the concentration microstructures under this orientation of the external field is the result of the interaction between the two concentration modes. Still, this is a matter of interpretation of the mass transport process.

In order to proceed with the solution it is mathematically convenient to introduce the auxiliary field $\xi = C - \mathcal{M}_{ph}H$ with the expressions for the perturbation modes following from the definition

$$\xi_0(z) = \tilde{C}_0(z) \text{ and } \xi_1(z) = \tilde{C}_1(z) - \mathcal{M}_{ph}\tilde{H}_1(z) \tag{3.81}$$

The equations for the mode amplitudes then become

$$\frac{\partial^2}{\partial z^2}\xi_0 = \frac{1}{2}\frac{\partial}{\partial z}\left[W(z)\left(C_1^{dif} + \mathcal{M}_{ph}\tilde{H}_1 + \xi_1\right)\right] \tag{3.82}$$

$$\left(\frac{\partial^2}{\partial z^2} - \pi^2\right)\xi_1 - W(z)\frac{\partial}{\partial z}\left(C_0^{dif} + \xi_0\right) = 0 \tag{3.83}$$

$$\left(\frac{\partial^2}{\partial z^2} - d_m\pi^2\right)\tilde{H}_1 = \tilde{\alpha}_c\pi^2\xi_1(z) \tag{3.84}$$

$$\left(\frac{\partial^2}{\partial z^2} - \pi^2\right)^2 W = -\pi^2 Rs_m\left[H_1^{dif}(z) + \tilde{H}_1(z)\right]\frac{\partial}{\partial z}\left(C_0^{dif} + \xi_0\right) \tag{3.85}$$

and the concentration boundary conditions (3.68) are greatly simplified taking the form of the homogeneous Neumann type condition

$$\left[\frac{\partial}{\partial z}\xi_0 = 0\right]_{z=l},\ \left[\frac{\partial}{\partial z}\xi_1 = 0\right]_{z=l} \tag{3.86}$$

The hydrodynamic boundary condition (3.70) in turn yields the boundary condition for the hydrodynamic mode amplitude

$$\left[\frac{\partial W}{\partial z} = W = 0\right]_{z=l} \tag{3.87}$$

The external potential Φ_{ext} is solved for in the free space according to the equation (3.67) and excluded from the continuity conditions (3.69) for the magnetic scalar potential under the condition of the attenuation at infinity $\Phi_{ext} \sim e^{-\pi z}$ on the upper half-plane yielding the boundary condition for the demagnetizing field amplitude

$$\left[\frac{\partial}{\partial z}\widetilde{H}_1 + \pi\widetilde{H}_1(z) = 0\right]_{z=l} \tag{3.88}$$

The equation (3.84) is linear with constant coefficients and can be solved without difficulty obtaining the solution for arbitrary function $\xi_1(z)$

$$\widetilde{H}_1(z) = Xf_1(z) - \frac{\tilde{\alpha}_c\pi^2}{r_0}\left[f_1(z)\int_0^z \xi_1 f_2 dz - f_2(z)\int_0^z \xi_1 f_1 dz\right] \tag{3.89}$$

where the fundamental solutions are $f_1(z) = \cosh(r_0 z)$ and $f_2(z) = \sinh(r_0 z)$ and only the term, which is symmetric across the midplane of the layer, has been retained. The lower limit of integration in (3.89) has also been chosen from the symmetry considerations. The exponent is $r_0 = \pi\sqrt{d_m}$.

After satisfying the boundary condition (3.88) the constant X is expressed as

$$X = \frac{\tilde{\alpha}_c\pi^2}{r_0}\int_0^l \xi_1(z)\left[f_2(z) - \frac{r_0 f_1(l) + \pi f_2(l)}{r_0 f_2(l) + \pi f_1(l)} f_1(z)\right] dz \tag{3.90}$$

Considering the boundary condition (3.86) the first parallel mode of the auxiliary field $\xi_1(z)$ can be expanded in symmetric Fourier series across the transversal direction

$$\xi_1(z) = \sum_{n=0}^{\infty} \hat{\xi}_{1,n} \cos\left(\frac{\pi n z}{l}\right) \tag{3.91}$$

The expansion obviously by definition satisfies the imposed homogeneous Neumann boundary condition on the sidewall of the layer.

Expressing the coefficient (3.90) and the first parallel mode of the magnetic field (3.89) in terms of the coefficients of the expansion (3.91) yields

$$\widetilde{H}_1(z) = -\tilde{\alpha}_c \sum_{n=0}^{\infty} \hat{\xi}_{1,n} f_n(z) \tag{3.92}$$

with the set of functions f_n

$$f_n(z) = \frac{\pi^2}{r_0^2 + \left(\frac{\pi n}{l}\right)^2}\left[(-1)^{n+1}\frac{\pi}{g_0}\cosh(r_0 z) + \cos\left(\frac{\pi n z}{l}\right)\right] \tag{3.93}$$

The expression (3.92) has the form of an expansion in an infinite series in terms of functions $f_n(z)$, which are obviously non-orthogonal and are not normalized. Obtaining the coefficients of such expansions is the basis of the employed Galerkin method.

Now $\xi_0(z)$ can be expressed from the equation (3.82) by twice repeated integration

$$\xi_0(z) = \frac{1}{2}\int_0^z W(z)\left(C_1^{dif} + \xi_1 + \mathcal{M}_{ph}\widetilde{H}_1\right)dz - Y \tag{3.94}$$

taking into account that the constant of integration after performing the first integration is zero due to the symmetry of $\xi_0(z)$ across the midplane of the layer. The second constant is expressed as

$$Y = \frac{1}{2l}\int_{-l}^{+l} \xi_0(z)dz \tag{3.95}$$

which conveys the condition of the conservation of the amount of ferroparticles within the layer and formally along with (3.94) constitutes a double integral, but can be reduced to a single integral through integration by parts

$$Y = \frac{1}{2l}\int_0^l (l-z)W(z)\left(C_1^{dif} + \xi_1 + \mathcal{M}_{ph}\widetilde{H}_1\right)dz \tag{3.96}$$

Considering the homogeneous boundary condition (3.86) it is possible to expand $\xi_0(z)$ into the even Fourier series

$$\xi_0(z) = \sum_{n=1}^{\infty} \hat{\xi}_{0,n} \cos\left(\frac{\pi n z}{l}\right) \tag{3.97}$$

The expansion (3.97) does not possess a zero-order term since it is expressed by the relation (3.95) and cancels out.

To obtain the solution of the convective problem it is necessary to express the velocity mode $W(z)$ in some way. Formally, the equation (3.85) is linear with constant coefficients and its solution can be obtained by standard method. For example, bearing in mind the symmetry of the fields

$$W(z) = W_2\,\mathrm{w}_2(z) + W_4\,\mathrm{w}_4(z) + \frac{1}{2}Rs_m \sum_i \mathrm{w}_\mathrm{i}(z)\int_0^z \mathrm{F}(\tau)\,\mathrm{x}_\mathrm{i}(\tau)\,d\tau \tag{3.98}$$

where $\mathrm{w}_\mathrm{i}(z) = \{\cosh(\pi z), z\cosh(\pi z), \sinh(\pi z), z\sinh(\pi z)\}$ is a vector of fundamental solutions, $\mathrm{F}(z) = \left[H_1^{dif}(z) + \widetilde{H}_1(z)\right]\frac{\partial}{\partial z}\left(C_0^{dif} + \xi_0\right)$ is the distribution of the magnetic force density and $\mathrm{x}_\mathrm{i}(z)$ is expressed as

$$\mathrm{x}_\mathrm{i}(z) = \left\{\mathrm{w}_2(z) - \frac{1}{\pi}\mathrm{w}_3(z) \quad -\mathrm{w}_1(z) \quad -\mathrm{w}_4(z) + \frac{1}{\pi}\mathrm{w}_1(z) \quad \mathrm{w}_3(z)\right\}$$

Making use of the expansions (3.92) and (3.97) it is not difficult to express (3.98) in terms of the expansion coefficients, however it presents a non-trivial task to actually satisfy the

boundary conditions (3.87) in this manner, because both coefficients of integration would depend on all the coefficients of the expansions. Additionally, the expression itself is too cumbersome and complicated to use. Instead, it is more convenient expand the hydrodynamic mode into a series of orthonormal antisymmetric functions $S_n(z)$

$$W(z) = \sum_{n=1}^{\infty} \widehat{w}_n S_n(z) \tag{3.99}$$

These antisymmetric Chandrasekhar functions $S_n(z)$ [95] form a complete set for antisymmetric functions on the interval under consideration and are defined by the expression

$$S_n(z) = \frac{1}{\sqrt{2}}\left[\frac{\sinh\left(\frac{\mu_n z}{l}\right)}{\sinh(\mu_n)} - \frac{\sin\left(\frac{\mu_n z}{l}\right)}{\sin(\mu_n)}\right] \tag{3.100}$$

where all characteristic values μ_n are obtained from the transcendental relation

$$\coth(\mu) - \cot(\mu) = 0 \tag{3.101}$$

The convenient property of the Chandrasekhar functions is that they satisfy the hydrodynamic boundary conditions (3.87) and promote rapid convergence of the series (3.99) for typical flows.

Using the expansions (3.91), (3.92), (3.97) and (3.99) the equation for the coefficients $\hat{\xi}_{0,n}$ is obtained from (3.94)

$$\hat{\xi}_{0,n} = \frac{1}{2}\left[\sum_{k=1}^{\infty}\sum_{l=0}^{\infty} \hat{\xi}_{1,l}\widehat{w}_k\left(\mathrm{K}_{k,l}^{n} - \tilde{\alpha}_c \Lambda_{k,l}^{n}\right) + \sum_{k=1}^{\infty} \widehat{w}_k L_{n,k}\right] \tag{3.102}$$

with the coefficients in matrix form

$$\mathrm{K}_{k,m}^{n} = \mathcal{F}_k^n\left\{\cos\left(\frac{\pi m z}{l}\right)\right\}, \quad \Lambda_{k,m}^{n} = \mathcal{F}_k^n\{f_m(z)\}, \quad L_{n,k} = \mathcal{F}_k^n\{C_1(z)\} \tag{3.103}$$

The functional $\mathcal{F}_k^n\{f(z)\}$ is defined as a double integral

$$\mathcal{F}_k^n\{f(z)\} = \frac{1}{l}\int_{-l}^{+l}\int_{0}^{z} S_k(\tau)\, f(\tau) \cos\left(\frac{\pi n z}{l}\right) d\tau\, dz \tag{3.104}$$

The expression (3.104) is not convenient because the evaluation of multiple integrals is numerically complicated. It can be simplified by the integration by parts, so after some transformations it becomes

$$\mathcal{F}_k^n\{f(z)\} = 2\int_{0}^{l} S_k(z) f(z)\left[\delta_{n,0} - \frac{z}{l}\operatorname{sinc}\left(\frac{\pi n z}{l}\right)\right] dz \tag{3.105}$$

where the *sinc* function has been used for the purpose of preserving the general form (3.105) for the zero-order coefficients as well and $\delta_{n,0}$ is the Kronecker's delta.

Projecting the equation (3.83) by making use of the expansions (3.91), (3.97) and (3.99) the equation for the first parallel mode of the auxiliary field is obtained

$$D_{n,n}\hat{\xi}_{1,n} - \sum_{k=1}^{\infty}\sum_{m=1}^{\infty}\hat{\xi}_{0,m}\widehat{w}_k \mathrm{G}_{k,m}^{n} + \sum_{k=1}^{\infty}\widehat{w}_k M_{n,k} = 0 \tag{3.106}$$

with the diagonal coefficients

$$D_{n,n} = \left[1 + \delta_{n,0}\right]\left[\left(\frac{\pi n}{l}\right)^2 + \pi^2\right] \tag{3.107}$$

and the cross-coefficients

$$\mathrm{G}_{k,m}^{n} = \frac{2}{l}\frac{\pi m}{l}\int_0^l S_k(z)\sin\left(\frac{\pi m z}{l}\right)\cos\left(\frac{\pi n z}{l}\right)dz \tag{3.108}$$

$$M_{n,k} = \frac{2}{l}\int_0^l S_k(z)\frac{\partial C_0^{dif}}{\partial z}\cos\left(\frac{\pi n z}{l}\right)dz \tag{3.109}$$

Finally, from (3.85)

$$\begin{aligned}\widehat{w}_n X_{n,n} - 2\pi^2 \sum_{k=1}^{\infty}\widehat{w}_k N_{n,k}^{w} \\ - \pi^2 Rs_m\left[\tilde{\alpha}_c\left(\sum_{k=0}^{\infty}\hat{\xi}_{1,n}N_{n,k}^{1} - \sum_{k=0}^{\infty}\sum_{m=1}^{\infty}\hat{\xi}_{1,k}\hat{\xi}_{0,m}\Omega_{k,m}^{n}\right) + \sum_{k=1}^{\infty}\hat{\xi}_{0,k}N_{n,k}^{0}\right] \\ = -\pi^2 Rs_m F_n\end{aligned} \tag{3.110}$$

with the coefficients

$$X_{n,n} = \left(\frac{\mu_n}{l}\right)^4 + \pi^4 \tag{3.111}$$

$$N_{n,k}^{w} = \frac{2}{l}\int_0^l S_k''(z)\, S_n(z)dz \tag{3.112}$$

$$N_{n,k}^{0} = \frac{2}{l}\frac{\pi k}{l}\int_0^l H_1^{dif}(z)S_n(z)\sin\left(\frac{\pi k z}{l}\right)dz \tag{3.113}$$

$$N_{n,k}^{1} = \frac{2}{l}\int_0^l \frac{\partial C_0^{dif}}{\partial z}f_k(z)\, S_n(z)dz \tag{3.114}$$

$$\Omega_{k,m}^{n} = \frac{2}{l}\frac{\pi m}{l}\int_0^l f_k(z)\sin\left(\frac{\pi m z}{l}\right)S_n(z)dz \tag{3.115}$$

$$F_n = \frac{2}{l}\int_0^l H_1^{dif}(z)\frac{\partial C_0^{dif}}{\partial z}S_n(z)dz \tag{3.116}$$

It is convenient to rewrite the equations (3.102), (3.106) and (3.110) in matrix form, making use of the properties of the quadratic forms, since that is the order of the nonlinearity in the equations

$$\hat{\xi}_0 - \frac{1}{2}\sum_{n=1}^{\infty}\left[\hat{w}^T(\mathrm{K}^n - \tilde{\alpha}_c\Lambda^n)\,\hat{\xi}_1\right]E^{\langle n\rangle} - \frac{1}{2}L\hat{w} = 0 \tag{3.117}$$

$$D\hat{\xi}_1 - \sum_{n=0}^{\infty}\left(\hat{w}^T\mathrm{G}^n\,\hat{\xi}_0\right)E^{\langle n\rangle} + M\hat{w} = 0 \tag{3.118}$$

$$(X - 2\pi^2 N^w)\hat{w} - \pi^2 Rs_m\left\{\tilde{\alpha}_c\left[N^1\hat{\xi}_1 - \sum_{n=1}^{\infty}\left(\hat{\xi}_1^T\Omega^n\,\hat{\xi}_0\right)E^{\langle n\rangle}\right] + N^0\hat{\xi}_0 + F\right\} = 0 \tag{3.119}$$

where E is the identity matrix and $^{\langle n\rangle}$ denotes the n-th column of the matrix.

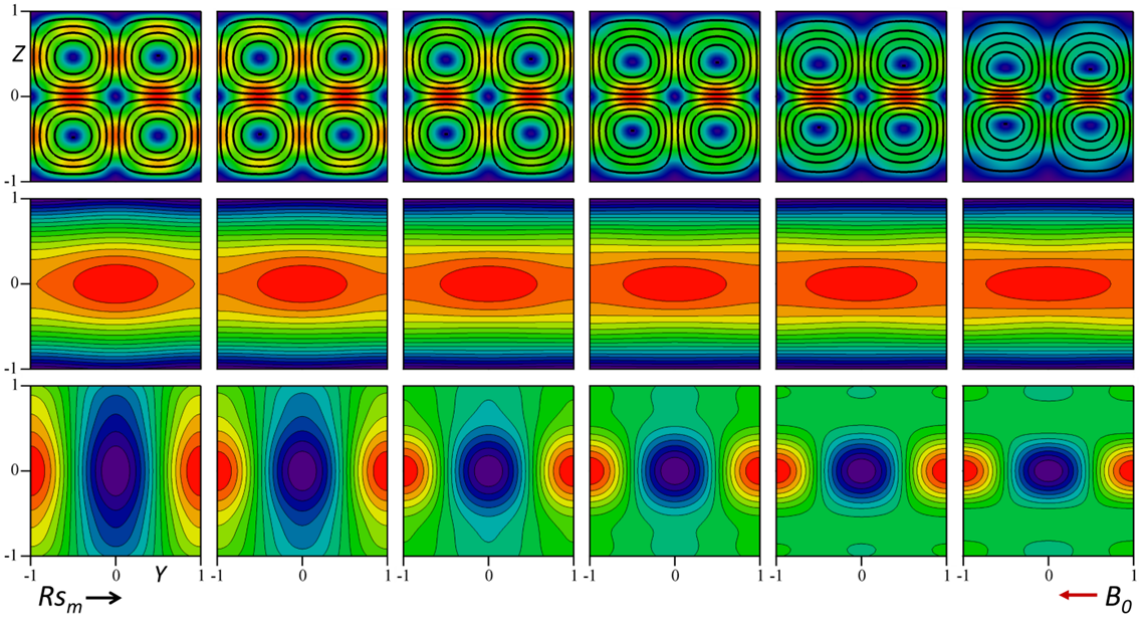

Figure 3.10 Solution of the stationary convection problem in parallel external field: from top to bottom – streamlines of the velocity field (color denotes magnitude of velocity), distributions of the concentration and demagnetizing field for the selected values of the magnetic Rayleigh number $Rs_m = 100, 200, 500, 1000, 2000, 5000$ (left to right).

The set of nonlinear matrix equations (3.117)-(3.119) can be solved by a number of numerical methods, for example the multidimensional Newton-Raphson method, with the desired number of the contributing modes and the required precision. Some obtained solutions are plotted on Figure 3.10 for the selected values of the magnetosolutal Rayleigh number Rs_m.

The configuration of the calculated microconvective motions consists of a coordinated system of four convective rolls forming around each element of the grating, with the axes of the rolls oriented along the extent of the grating in the longitudinal direction. The transversal microconvective currents are sufficiently intense to cause significant deformation of the stationary distribution of the concentration field. The direction of the advective flux corresponds to that of the magnetodiffusive effect, stretching the photoabsorptive concentration microstructure in the direction of the external field. The corresponding decrease of the amplitude of the regular concentration perturbation would cause the considerable attenuation of the visibility of the photoabsorptive grating in the conditions of the experiment. In turn, increasing the value of the magnetosolutal Rayleigh number, the convective rolls undergo deformation along the transversal direction and the regions of most intensive convective motion are localized in the midplane of the layer on the edges of the grating element.

While the intensity of the magnetic microconvection does indeed depend on the thickness of the layer, i.e. the aspect ratio of the photoabsorptive concentration microstructures, the magnetic force in the case of the parallel orientation of the externally applied magnetic field is mainly directed along the same coordinate. It is then possible to conclude that the normalization of the dimensional quantities by the half-period of the layer rather than its thickness seems more suitable under this configuration of the external field. In fact, the proper definition of the solutal Rayleigh number in photoabsorptive gratings has been a matter of debate.

Consequently, in the parallel configuration of the applied magnetic field the parasitic microconvection affects primarily the parallel variation of the ferroparticle concentration and demagnetizing field and not the transversal gradients. This supposition allows obtaining interesting results with some further simplifications. Returning once again to the set of equations (3.117)-(3.119), the solution is considered only up to the first transversal mode. Assuming that the zero-order parallel mode $\hat{\xi}_0$ of the auxiliary field constituting purely transversal variation has negligible role in the driving of the convective motion it is decoupled and the resulting system of algebraic equations is thus linearized. After some transformations the amplitude of a single hydrodynamic mode can then be expressed in explicit form

$$\widehat{w}_1 = \frac{-\pi^2 Rs_m F_1}{X_{11} - 2\pi^2 N_{11}^w + \tilde{\alpha}_c \pi^2 Rs_m \left[N_{10}^1 \frac{M_{01}}{D_{00}} + N_{11}^1 \frac{M_{11}}{D_{11}} \right]} \tag{3.120}$$

The integral coefficients in (3.120) depend only on the stationary diffusive state of the photoabsorptive grating, determined by the equilibrium of thermophoretic and magnetodiffusive fluxes, and can be calculated without difficulty according to the relations (3.107), (3.109), (3.111)-(3.116).

In turn, the amplitudes of the first parallel mode of the auxiliary field $\hat{\xi}_1$ are obtained in simple form

$$\hat{\xi}_{1,0} = -\frac{M_{01}}{D_{00}}\widehat{w}_1, \qquad \hat{\xi}_{1,1} = -\frac{M_{11}}{D_{11}}\widehat{w}_1 \tag{3.121}$$

The expression (3.120) characterizes the intensity of the convective motions and it is compared to the solution of the full spectral model. The calculated amplitudes of the transversal velocity $W(z)$ (3.99) are plotted on Figure 3.11.

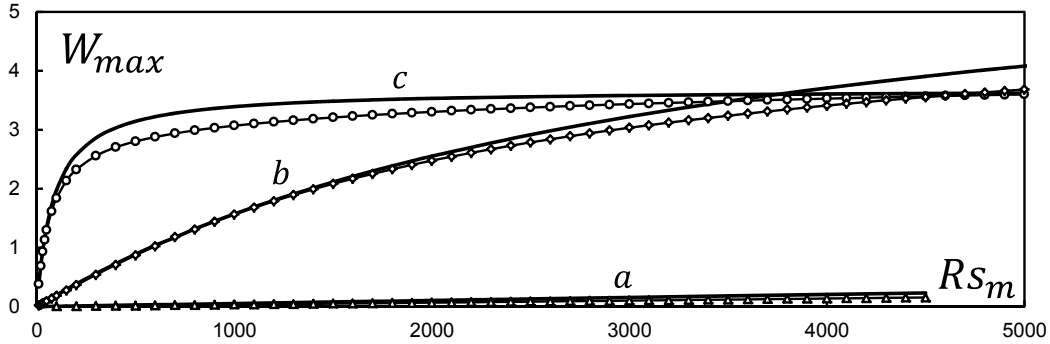

Figure 3.11 Calculated amplitude of the transversal velocity, results of the spectral model (3.117)-(3.119) (symbols) and simplified expression (3.120) (lines) for ferrofluid layers with different thickness: *(a)* $l = 0.25$, *(b)* $l = 0.5$, *(c)* $l = 1.0$.

Reasonable correspondence of the simplified analytical expression (3.120) with the numerical calculations has been obtained across an important range of the magnetosolutal Rayleigh numbers, which justifies the adopted assumptions about the mechanisms of the photoabsorptive magnetoconvection.

3.1.6. Normal field

The comparison with the numerical simulations by finite volume method integration of the full system of equations (3.64)-(3.66) demonstrates that the spectral model based on the leading mode approximation is quite sufficient in the important range of the magnetic Rayleigh numbers for the parallel configuration of the applied field, since the internal microconvection is driven by the bulk forces induced within the volume of the ferrofluid layer. It, however, would not present acceptable correspondence for the perpendicular

orientation of the external field, as in this case the discontinuity of the concentration field on the transversal sidewalls of the layer causes the corresponding jump of the magnetization and the appearance of strong gradients of the demagnetizing field perturbation in the vicinity of the boundary. The magnetic force then includes significant, in some cases defining, boundary contributions, which affect the corresponding configuration of the stationary microconvective flow. So, it is necessary to take into accounts additional lateral modes and construct a full spectral model for the purpose of solving the stationary convective-diffusive problem and determining the distributions of the perturbations of concentration, velocity and the magnetic field.

The approach, which has been used for constructing the truncated model (3.117)-(3.119) can be generalized in a straightforward way. The expansion of the auxiliary field now includes additional contributions along the parallel direction

$$\xi(y,z) = \sum_{n=0}^{\infty}\sum_{m=0}^{\infty} \hat{\xi}_{mn} \cos\left(\frac{\pi m z}{l}\right) \cos(\pi n y) \tag{3.122}$$

where the coefficient $\hat{\xi}_{00}$ should be omitted due to the imposed condition of the conservation of the ferroparticles in the bulk of the layer.

The perturbation $\widetilde{H}$ of the demagnetizing field is in turn determined exclusively by the advective perturbation of the concentration field and is formally expanded in a functional series

$$\widetilde{H}(y,z) = -\tilde{\alpha}_c \sum_{n=0}^{\infty}\sum_{m=0}^{\infty} \hat{\xi}_{mn} f_{mn}(z) \cos(\pi n y) \tag{3.123}$$

where the contribution of the leading parallel mode is now preserved. The form of the functions $f_{mn}(z)$ is not important at the moment - it depends on the configuration of the externally applied field and will be determined later.

Finally, the single longitudinal component of the vorticity vector can be expressed similarly to (3.76) from its definition and the continuity condition of the divergence-free velocity field

$$\omega(y,z) = \sum_{n=1}^{\infty} \frac{1}{\pi n}\left[\frac{\partial^2}{\partial z^2} - (\pi n)^2\right] W_n(z) \sin(\pi n y) \tag{3.124}$$

with the amplitudes of the parallel modes expressed through the Chandrasekhar functions with appropriate transversal symmetry

$$W_n(z) = \sum_{m=1}^{\infty} \widehat{w}_{mn} S_m(z) \tag{3.125}$$

Projecting the governing equations onto the expansions and making use of the matrix formulation yields the system of nonlinear algebraic equations in the form

$$Tr\left\{X_{mn}^{\xi}\hat{\xi} + L_{mn}^{\xi}\widehat{w}\right\} + \sum_{k=0}^{\infty}\sum_{l=0}^{\infty}\left[\left(\widehat{w}^{\langle k\rangle}\right)^{T} \mathrm{G}_{kl}^{mn}\, \hat{\xi}^{\langle l\rangle}\right] = 0 \tag{3.126}$$

$$Tr\{X_{mn}^{w}\widehat{w}\} + Rs_m\left\{F_{mn} - Tr\{L_{mn}^{w}\hat{\xi}\} + \tilde{\alpha}_c \sum_{k=0}^{\infty}\sum_{l=0}^{\infty}\left[\left(\hat{\xi}^{\langle k\rangle}\right)^{T} \Omega_{kl}^{mn}\, \hat{\xi}^{\langle l\rangle}\right]\right\} = 0 \tag{3.127}$$

with Tr – matrix trace operator.

The diagonal coefficients are determined according to the relations

$$X_{mn,ij}^{\xi} = \delta_{i,n}\delta_{j,m}\left(1+\delta_{0,n}\right)\left(1+\delta_{0,m}\right)\left[\left(\frac{\pi m}{l}\right)^2 + (\pi n)^2\right] \tag{3.128}$$

$$X_{mn,ij}^{w} = \left(1-\delta_{0,n}\right)\delta_{i,n}\frac{1}{\pi n}\left\{\left[\left(\frac{\mu_m}{l}\right)^4 + (\pi n)^4\right]\delta_{j,m} - 2(\pi n)^2\frac{1}{l}\int_{-l}^{+l} S_m(z)S_j''(z)dz\right\} \tag{3.129}$$

For convenience, making use of the functionals

$$\mathcal{F}_{mn}^{\xi}\{f(z)\} = \frac{1}{l}\int_{-1}^{+1}\int_{-l}^{+l} f(z)\cos\left(\frac{\pi m z}{l}\right)\cos(\pi n y)\, dz\, dy \tag{3.130}$$

$$\mathcal{F}_{mn}^{w}\{f(z)\} = \frac{1}{l}\int_{-1}^{+1}\int_{-l}^{+l} f(z)S_m(z)\sin(\pi n y)\, dz\, dy \tag{3.131}$$

The rest of the coefficients are defined as

$$L_{mn,ij}^{\xi} = \Lambda_{\,mn,ij}^{\xi,1} - \Lambda_{\,mn,ij}^{\xi,2} \tag{3.132}$$

$$L_{mn,ij}^{w} = \Lambda_{\,mn,ij}^{w,1} + \Lambda_{\,mn,ij}^{w,2} + \tilde{\alpha}_c\left[\mathrm{K}_{\,mn,ij}^{w,1} + \mathrm{K}_{\,mn,ij}^{w,2}\right] \tag{3.133}$$

and the quadratic forms

$$\mathrm{G}_{kl,ij}^{mn} = \mathrm{A}_{kl,ij}^{mn} + \mathrm{B}_{kl,ij}^{mn}, \quad \Omega_{kl,ij}^{mn} = \mathrm{M}_{kl,ij}^{mn} - \mathrm{N}_{kl,ij}^{mn} \tag{3.134}$$

with

$$\Lambda_{\,mn,ij}^{\xi,1} = \mathcal{F}_{mn}^{\xi}\left\{\frac{\partial C^{dif}}{\partial z}S_j(z)\cos(\pi i y)\right\}, \qquad \Lambda_{\,mn,ij}^{\xi,2} = \mathcal{F}_{mn}^{\xi}\left\{\frac{1}{\pi i}\frac{\partial C^{dif}}{\partial y}\frac{\partial S_j}{\partial z}\sin(\pi i y)\right\} \tag{3.135}$$

$$\Lambda_{\,mn,ij}^{w,1} = \mathcal{F}_{mn}^{w}\left\{(\pi i)p_{ji}(z)\frac{\partial H^{dif}}{\partial z}\sin(\pi i y)\right\}, \ \Lambda_{\,mn,ij}^{w,2} = \mathcal{F}_{mn}^{w}\left\{\frac{\partial p_{ji}}{\partial z}\frac{\partial H^{dif}}{\partial y}\cos(\pi i y)\right\} \tag{3.136}$$

$$\mathrm{K}_{\,mn,ij}^{w,1} = \mathcal{F}_{mn}^{w}\left\{(\pi i)f_{ji}(z)\frac{\partial C^{dif}}{\partial z}\sin(\pi i y)\right\}, \ \mathrm{K}_{\,mn,ij}^{w,2} = \mathcal{F}_{mn}^{w}\left\{\frac{\partial f_{ji}}{\partial z}\frac{\partial C^{dif}}{\partial y}\cos(\pi i y)\right\} \tag{3.137}$$

$$\mathrm{A}_{kl,ij}^{mn} = \mathcal{F}_{mn}^{\xi}\left\{\frac{\partial p_{jl}}{\partial z}S_i(z)\cos(\pi k y)\cos(\pi l y)\right\} \tag{3.138}$$

$$\mathrm{B}_{kl,ij}^{mn} = \mathcal{F}_{mn}^{\xi}\left\{\frac{\pi l}{\pi k} p_{jl}(z)\frac{\partial s_i}{\partial z}\sin(\pi k y)\sin(\pi l y)\right\} \tag{3.139}$$

$$\mathrm{M}_{kl,ij}^{mn} = \mathcal{F}_{mn}^{w}\left\{(\pi k) p_{ik}(z)\frac{\partial f_{jl}}{\partial z}\sin(\pi k y)\cos(\pi l y)\right\} \tag{3.140}$$

$$\mathrm{N}_{kl,ij}^{mn} = \mathcal{F}_{mn}^{w}\left\{(\pi l)\frac{\partial p_{ik}}{\partial z} f_{jl}(z)\cos(\pi k y)\sin(\pi l y)\right\} \tag{3.141}$$

Finally, the unperturbed magnetic force

$$F_{mn} = \mathcal{F}_{mn}^{w}\{F_0(y,z)\} \quad \text{with} \quad F_0(y,z) = \frac{\partial C^{dif}}{\partial y}\frac{\partial H^{dif}}{\partial z} - \frac{\partial C^{dif}}{\partial z}\frac{\partial H^{dif}}{\partial y} \tag{3.142}$$

The calculated convective patterns (Figure 3.12) are generally similar to the ones found for the parallel configuration of the applied magnetic field (Figure 3.10), taking into account that the direction of the convective currents is reversed.

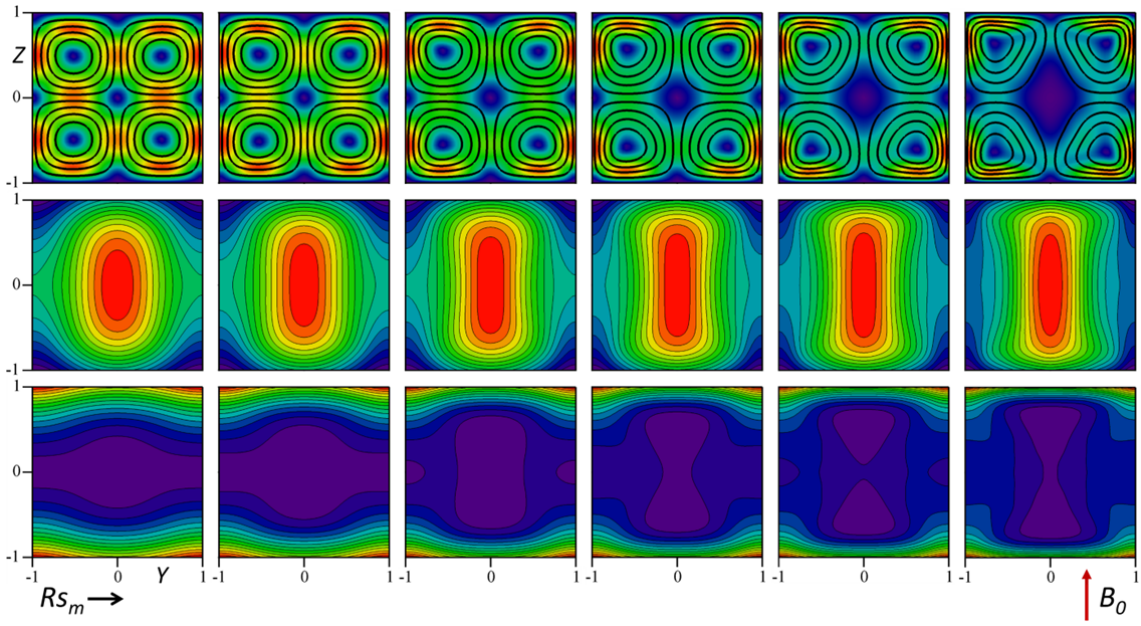

Figure 3.12 Solution of the stationary convection problem in perpendicular external field: from top to bottom – streamlines of the velocity field (color denotes magnitude of velocity), distributions of the concentration and demagnetizing field for the selected values of the magnetic Rayleigh number $Rs_m = 100, 200, 500, 1000, 2000, 5000$ (left to right).

In this configuration the induced advective fluxes also enhance the mass transport within the element of the grating along the direction of the applied field (this time the transversal direction), the effect, which can be interpreted phenomenologically in terms of the effective magnetodiffusion as the increase of the magnetic diffusion coefficient or correspondingly as the decrease of the effective magnetic Soret coefficient. In turn, within the plane of the layer,

i.e. the only plane, which can be observed in real measurements, the direction of the advective mass transport is actually opposite to that of the magnetodiffusive fluxes and the effective Soret coefficient should increase along the parallel direction. Consequently, the visibility of the photoabsorptive grating would be improved by the presence of magnetoconvection as compared with the diffusive base state.

At higher values of the magnetosolutal Rayleigh number the convective rolls experience deformation and the most intensive convective motions are concentrated primarily near the boundaries of the layer in between the elements of the concentration grating. In turn, a region of stagnation develops within the core of the grating element and the intensification of mass transport begins to saturate. In this regard the difference in the resulting convective patterns reflects the distinction in the origin of the magnetic force as compared with the parallel orientation of the applied field.

3.1.7. Determination of transport coefficients

Magnetically driven microconvection emerging within the photoabsorptive concentration microstructures under the action of the external magnetic field can significantly influence the stationary shape of the concentration gratings under certain conditions, but can as well affect their relaxation behavior. In contrast to the laterally connecting circulation which would take place within the plane of the ferrofluid layer as a consequence of the microconvective instability of the flat periodic concentration front (Section 2.2), the transversal parasitic microconvection emerges subtly without a threshold and does not break the mirror or translational symmetry of the grating as the undulation and peristaltic modes may do in the supercritical regime above the threshold of the instability. Consequently, it is technically complicated to distinguish the principal manifestation of this type of microconvection in the concentration gratings under the action of the magnetic field as opposed to regular magnetodiffusion or magnetic thermodiffusion by the qualitative differences of the transport processes. In this respect, the hydrodynamic microstructures can be considered integral constituents of the photoabsorptive convective-diffusive magnetic microstructures. Thus, there remains the possibility to draw the quantitative distinction in the stationary regime or the dynamics of the relaxation process. For this purpose, a suitable simplified relaxation model can be formulated along the lines of Section 2.2.3 for the parallel configuration of the externally applied field, considering the principal mechanisms of the convective-diffusive relaxation of concentration.

The relaxation of the induced photoabsorptive concentration perturbation driven by the magnetodiffusion and magnetoconvection after the switching off of the pumping laser beams and the consequent immediate relaxation of the thermal modulation is described by the dynamic equation (1.37)

$$\frac{\partial C}{\partial t} = \Delta\left(C - \mathcal{M}_{ph}H\right) - \boldsymbol{U}\boldsymbol{\nabla}C \tag{3.143}$$

From the general considerations it is apparent that the microconvective fluxes attempt to destroy the perturbation that drives them. From (3.98) and the stationary profiles (Figure 3.10) it becomes clear that the zero order lateral concentration mode remains virtually unchanged and the principal parallel mode is significantly attenuated by the advective transport in the stationary regime. It is then convenient to consider only the magnetoconvective relaxation of the first parallel modes and assume that the zero-order modes are subjected exclusively to the diffusive relaxation. For this purpose the time-dependent concentration field and demagnetizing field are expressed as the perturbations $\tilde{C}$ and $\widetilde{H}$ of the diffusive base state (3.39)

$$C(y,z,t) = C_0^{dif}(z,t) + \left[C_1^{dif}(z,t) + \tilde{C}_1(z,t)\right]\cos(\pi y) \tag{3.144}$$

$$H(y,z,t) = \left[H_1^{dif}(z,t) + \widetilde{H}_1(z,t)\right]\cos(\pi y) \tag{3.145}$$

where H_1^{dif} – is the first parallel mode of the demagnetizing field, corresponding to (3.39)

In turn, a single parallel mode is retained from the time dependent velocity field $\boldsymbol{U}$ with components

$$U_y(y,z,t) = V(z,t)\sin(\pi y) \tag{3.146}$$

$$U_z(y,z,t) = W(z,t)\cos(\pi y) \tag{3.147}$$

The transversal profile of the parallel component U_y of velocity is expressed from the continuity condition in accordance with (3.74) and the no-slip boundary conditions (3.87) remain on the sidewall of the layer. The transversal velocity mode $W(z,t)$ is approximated by the first term of the expansion (3.99) in antisymmetric Chandrasekhar functions and the spatial and temporal variables are separated in the form

$$W(z,t) = \widehat{w}_1(t)S_1(z) \tag{3.148}$$

Considering the nonlinear term of (3.143) in the same way as previously in Section 2.2.3, it is reasonable to retain only the most significant transversal modes of the principal parallel mode

of the auxiliary field $\xi_1(z,t) = \tilde{C}_1 - \mathcal{M}_{ph}\tilde{H}_1$ perturbation, which are the zero-order and the second-order modes

$$\xi_1(z,t) = \hat{\xi}_{1,0}(t) + \hat{\xi}_{1,2}(t)\cos\left(\frac{2\pi z}{l}\right) \tag{3.149}$$

with the corresponding time-dependent amplitudes $\hat{\xi}_{1,0}$ and $\hat{\xi}_{1,2}$.

From the employed expansions for the transversal profiles of the first parallel modes of the auxiliary field (3.149) and the demagnetizing field perturbations (3.92), the definition of the auxiliary field allows obtaining the periodic part of the concentration perturbation with account for the adopted truncation of the modes

$$\tilde{C}_1(z,t) = \hat{\xi}_{1,0}(t)p_0(z) + \hat{\xi}_{1,2}(t)p_2(z) \tag{3.150}$$

where the form of the expansion functions $p_n(z)$ is expressed as

$$p_n(z) = \cos\left(\frac{\pi n z}{l}\right) - (d_m - 1)f_n(z) \tag{3.151}$$

with $f_n(z)$ defined by (3.93)

Making use of the chosen ansatz (3.148)-(3.150), the concentration balance equation (3.143) is projected onto the selected modes. Taking into account that the contribution of the non-diagonal elements on the LHS is much less than that of the diagonal elements and can be neglected in comparison

$$B_0\frac{\partial\hat{\xi}_{1,0}}{\partial t} = -\pi^2\hat{\xi}_{1,0}(t) - \widehat{w}_1(t)G_0(t) \tag{3.152}$$

$$B_2\frac{\partial\hat{\xi}_{1,2}}{\partial t} = -\left[\left(\frac{2\pi}{l}\right)^2 + \pi^2\right]\hat{\xi}_{1,2}(t) - \widehat{w}_1(t)G_2(t) \tag{3.153}$$

with the coefficients

$$B_n = \frac{1}{(1+\delta_{n,0})}\frac{1}{l}\int_{-l}^{+l} p_n(z)\cos\left(\frac{\pi n z}{l}\right)dz \tag{3.154}$$

$$G_n(t) = \frac{1}{(1+\delta_{n,0})}\frac{1}{l}\int_{-l}^{+l}\frac{\partial}{\partial z}\left[C_0^{dif}(z,t)\right]S_1(z)\cos\left(\frac{\pi n z}{l}\right)dz \tag{3.155}$$

and the expression for the hydrodynamic mode is obtained from (3.119) after some simplifications

$$\widehat{w}_1(t) = -\frac{\pi^2 Rs_m}{X_{11} - 2\pi^2 N_{11}^w}\left\{F_1(t) - \tilde{\alpha}_c\left[\hat{\xi}_{1,0}(t)N_{10}^1(t) + \hat{\xi}_{1,2}(t)N_{12}^1(t)\right]\right\} \tag{3.156}$$

The coefficients of (3.156) are determined from the relations (3.111)-(3.116) but are now time-dependent since the base state is diffusively relaxing.

The Lorenz-type system (3.152)-(3.156) can be integrated numerically after applying the appropriate initial conditions for the selected modes. The values of $\hat{\xi}_{1,0}$ and $\hat{\xi}_{1,2}$ at the initial time are obtained from the solution of the stationary system (3.117)-(3.119). In turn, the hydrodynamic mode w_{11} does not possess a dynamic equation and so does not require an initial condition.

The effective transport coefficients can be introduced phenomenologically to account for the influence of the magnetic microconvection on the photoabsorptive phoretic transport.

The effective coefficient of magnetic diffusion can be defined as the relaxation rate of the primary parallel concentration mode

$$\delta_{eff}(t) = -\frac{1}{\pi^2 J(t)}\frac{\partial J}{\partial t}, \qquad J(t) = \sqrt{\int_{-l}^{l}\left[\int_{-1}^{1} C(y,z,t)\cos(\pi y)\,dy\right]^2 dz} \tag{3.157}$$

and is consistent with the similar definitions (2.61) and (3.63).

The dynamics of the calculated signals $J(t)$ can be determined from the simplified model (3.152)-(3.156) by appropriate time stepping and from numerical simulations by finite volume integration of the full system of equations.

In turn, the effective Soret coefficient can be determined from the stationary state of the grating as

$$\sigma_{eff} = \frac{J}{J_0} \tag{3.158}$$

where the calculated signals J_0 and J - are the L^2-norms (3.157) of the primary parallel concentration mode determined accordingly for the purely diffusive (3.26) and convective-diffusive formation of the grating.

The convective stationary state is obtained from numerical calculations according to the spectral model (3.117)-(3.119) for the parallel and (3.126)-(3.127) for the perpendicular configuration of the applied magnetic field. In the case of the parallel orientation of the external field a good estimate of the effective Soret coefficient can be obtained making use of the analytical expression (3.121).

The calculated values of the effective transport coefficients are plotted in Figure 3.13. The effective parallel relaxation rate is plotted in relation to the corresponding coefficient of magnetodiffusion d_0 (2.20) calculated in the framework of thin layer approximation under the conditions of purely phoretic formation and relaxation of the grating. For parallel orientation of the applied magnetic field d_0 is close to d_m (Figure 3.8), otherwise it approaches 1 for the perpendicular configuration (Figure 3.9).

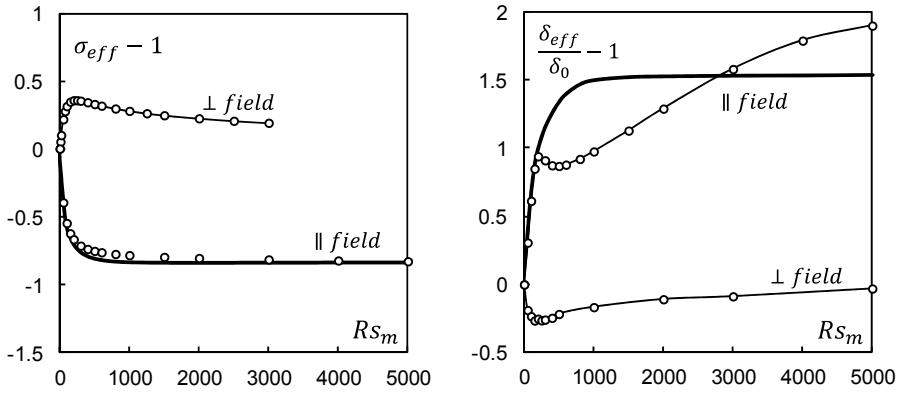

Figure 3.13 Influence of microconvection on the effective transport coefficients: dependence of the Soret coefficient (left) and relaxation rate (right) on the magnetosolutal Rayleigh number for different orientations of the applied field: symbols – numerical calculations, bold lines – corresponding simplified models (3.121) and (3.152)-(3.156).

The decrease of the effective Soret coefficient in the parallel field configuration and the increase for the perpendicular orientation of the external field is the direct consequence of the magnetoconvective fluxes attempting to erase the concentration grating in the former case and accentuate it in the latter one. The same conclusion applies to the effective diffusion coefficient. Unfortunately the simplified Lorenz-type model predicts the saturation of the relaxation rate, which does not take place according to the more detailed numerical simulations. Otherwise, it gives an acceptable approximation for the effective diffusion coefficient in the parallel configuration of the external field within an important range of the values of the magnetic Rayleigh number.

The intensification of magnetodiffusion in the parallel direction and a slight decrease of the effective diffusion coefficient in the perpendicular configuration conform to the predictions of the phoretic theory with account for the interparticle interactions (Figure 1.1, right). In this regard the influence of microconvection is also very similar, which makes the separation of

the two effects in real observations a complicated task. Further increasing the magnetosolutal Rayleigh number, the effective diffusion coefficient exceeds the coefficient of magnetodiffusion many times while the effective Soret coefficient determined from the calculated convective-diffusive stationary state experiences saturation with respect to the control parameter rather quickly.

3.2. Stability

3.2.1. Definition of the problem

The formation of magnetic microconvection within the photoabsorptive microstructures in ferrofluid layers and the shape of the emerging convective microstructures is still a matter of debate. In fact, some observed effects attributed to the influence of the magnetoconvection can under some circumstances be explained by complex magnetic interactions within the ferrocolloid [68]-[71]. There is then an obvious necessity for any prospective model of the photoabsorptive magnetoconvection to discern the peculiarities of the microconvective transport and suggest the possibility to qualitatively identify its presence in real observations.

The form of the transversal parasitic microconvection suggested in the previous section allows neither to ascertain its influence on the photoabsorptive concentration grating nor even to determine its existence in the conditions of the experiment. The influence of the advective fluxes partially coincides with the expected direction of the phoretic transport, complicating the unambiguous identification of the source of the quantitative discrepancies. Also, the convective microstructure consisting of a coordinated system of convective rolls with axes parallel to the axis of translational symmetry of the grating possesses the same symmetry in the parallel and longitudinal directions, impeding direct observation. The consequent inability of the proposed model to suggest an acceptable criterion for the identification of the magnetic microconvection in extended systems is not satisfactory; the convective motion is in all senses "invisible" [70].

Recognizing that the formation of the magnetoconvection is an inherent feature of the photoabsorptive ferroparticle concentration microstructures rather than the property of their convective stability, the notion of the convective-diffusive microstructures appears in a natural way. Unavoidably, the issue of the hydrodynamic stability of these formations is brought up as well. Clearly, the compliance with the formulated system of hydrodynamic equations does not necessarily imply the physical realisability of the convective regime unless it is stable to perturbations [90].

The establishing of the hydrodynamic instability inevitably leads to the breaking of the spatial or temporal symmetries of the convective pattern. If the destabilization of the photoabsorptive microstructure can be detected in real conditions, the parameters of the critical perturbation may yield important information on its internal structure and the current transport regime. The consideration of the stability of the convective-diffusive microstructures is then essential both

to determine the feasibility of the existence of the magnetic microconvection and to identify its presence in real observations.

The secondary stability and evolution of the photoabsorptive convective-diffusive microstructures is governed by the system of equations (1.36)-(1.39). At the present for the sake of generality it is convenient to refrain from discussing the configuration of the external field and the exact form of the corresponding distribution of the induced demagnetizing field. The consideration of the linear stability problem of the extended stationary microstructure will be carried out for the purpose of determining the critical parameters of the threshold. Applying infinitesimal perturbations $\tilde{c}$, $\tilde{h}$ and $\tilde{\boldsymbol{u}}$ to the stationary profiles C, H and $\boldsymbol{U}$

$$c = C(y,z) + \tilde{c}(x,y,z) \tag{3.159}$$

$$H = H(y,z) + \tilde{h}(x,y,z) \tag{3.160}$$

$$\boldsymbol{u} = \boldsymbol{U}(y,z) + \tilde{\boldsymbol{u}}(x,y,z) \tag{3.161}$$

a set of linearized equations is obtained

$$-\boldsymbol{\nabla} p + \Delta\tilde{\boldsymbol{u}} + Rs_m\left(\tilde{c}\boldsymbol{\nabla}H + C\boldsymbol{\nabla}\tilde{h}\right) = 0 \tag{3.162}$$

$$\boldsymbol{\nabla}\cdot\tilde{\boldsymbol{u}} = 0 \tag{3.163}$$

$$\frac{\partial\tilde{c}}{\partial t} + \boldsymbol{U}\boldsymbol{\nabla}\tilde{c} + \tilde{\boldsymbol{u}}\boldsymbol{\nabla}C = \Delta\left(\tilde{c} - \mathcal{M}_{ph}\tilde{h}\right) \tag{3.164}$$

The most general form of $\tilde{\boldsymbol{u}}$, which satisfies the continuity condition (3.163) is

$$\tilde{\boldsymbol{u}} = \boldsymbol{\nabla}\times\boldsymbol{\nabla}\times(\Phi\mathbf{e_z}) + \boldsymbol{\nabla}\times(\Psi\mathbf{e_z}) \tag{3.165}$$

The three vector components of $\tilde{\boldsymbol{u}}$ have been replaced by two scalar potentials Ψ and Φ. The relation (3.165) is usually referred to as the plane poloidal-toroidal decomposition and is frequently used for the analysis of three-dimensional problems. The form (3.165) is valid only assuming that no integral cross-flow is present in the system. If such flow exists, the expression must be modified to include the mean flow as well. This is not necessary for the present case.

Making use of the hydrodynamic scalar potentials Ψ and Φ the components of the hydrodynamic perturbation $\tilde{\boldsymbol{u}} = u_x\mathbf{e_x} + u_y\mathbf{e_y} + u_z\mathbf{e_z}$ of the velocity field can be expressed

$$u_x = \frac{\partial\Psi}{\partial y} + \frac{\partial^2\Phi}{\partial z\,\partial x}, \quad u_y = -\frac{\partial\Psi}{\partial x} + \frac{\partial^2\Phi}{\partial z\,\partial y} \tag{3.166}$$

$$u_z = -\Delta_\perp\Phi \tag{3.167}$$

where $\Delta_\perp = \frac{\partial^2}{\partial x^2} + \frac{\partial^2}{\partial y^2}$ is the transverse Laplacian.

The equations for the potentials Ψ and Φ are obtained correspondingly by taking the single and double *curl* of (3.162) and projecting the result on the transversal axis $\mathbf{e_z}$. After some transformations

$$\Delta\Delta_\perp\Psi - Rs_m\left[\nabla\times\left(\tilde{c}\boldsymbol{\nabla}H + C\boldsymbol{\nabla}\tilde{h}\right)\right]_z = 0 \tag{3.168}$$

$$\Delta\Delta\Delta_\perp\Phi + Rs_m\left[\nabla\times\nabla\times\left(\tilde{c}\boldsymbol{\nabla}H + C\boldsymbol{\nabla}\tilde{h}\right)\right]_z = 0 \tag{3.169}$$

with

$$\left[\nabla\times\left(\tilde{c}\boldsymbol{\nabla}H + C\boldsymbol{\nabla}\tilde{h}\right)\right]_z = \frac{\partial H}{\partial y}\frac{\partial\tilde{c}}{\partial x} - \frac{\partial C}{\partial y}\frac{\partial\tilde{h}}{\partial x} \tag{3.170}$$

$$\left[\nabla\times\nabla\times\left(\tilde{c}\boldsymbol{\nabla}H + C\boldsymbol{\nabla}\tilde{h}\right)\right]_z =$$

$$\left[\frac{\partial C}{\partial z}\Delta_\perp + \frac{\partial^2 C}{\partial z\,\partial y}\frac{\partial}{\partial y} - \frac{\partial}{\partial y}\left(\frac{\partial C}{\partial y}\frac{\partial}{\partial z}\right)\right]\tilde{h} - \left[\frac{\partial H}{\partial z}\Delta_\perp + \frac{\partial^2 H}{\partial z\,\partial y}\frac{\partial}{\partial y} - \frac{\partial}{\partial y}\left(\frac{\partial H}{\partial y}\frac{\partial}{\partial z}\right)\right]\tilde{c} \tag{3.171}$$

Subsequently, in the linear regime of exponential amplification of the infinitesimal perturbations $\tilde{c}$, $\tilde{h}$ and $\tilde{\boldsymbol{u}}$ the time dependence of their amplitudes is separated as $\sim e^{\omega t}$ with ω - the growth increment. Assuming that the exchange of stabilities takes place at the threshold $\omega = 0$ and introducing the auxiliary field $\tilde{\xi} = \tilde{c} - \mathcal{M}_{ph}\tilde{h}$, the equation (3.164) becomes

$$\Delta\tilde{\xi} - \boldsymbol{U}\boldsymbol{\nabla}\left(\tilde{\xi} + \mathcal{M}_{ph}\tilde{h}\right) - \tilde{\boldsymbol{u}}\boldsymbol{\nabla}C = 0 \tag{3.172}$$

The boundary conditions for the hydrodynamic potentials on the sidewall of the layer follow from the imposed no-slip condition $[\tilde{\boldsymbol{u}} = 0]_{\pm l}$ on the velocity perturbation. Bearing this in mind, the required boundary conditions are obtained from (3.166)-(3.167)

$$[\Phi = 0]_{\pm l}, \quad \left[\frac{\partial\Phi}{\partial \mathrm{z}} = 0\right]_{\pm l} \tag{3.173}$$

$$[\Psi = 0]_{\pm l} \tag{3.174}$$

In turn, the boundary condition for the perturbation of the auxiliary field $\tilde{\xi}$ is the homogeneous Neumann condition

$$\left[\frac{\partial\tilde{\xi}}{\partial \mathrm{z}} = 0\right]_{\pm l} \tag{3.175}$$

The set of linear equations (3.168)-(3.169) and (3.172) with the boundary conditions (3.173)-(3.175) will yield the dispersion relation and eventually the critical parameters of the threshold of the instability. For the purpose of obtaining the critical threshold the Galerkin method can be applied and the fields are expanded in appropriate functional series with account for their symmetry.

In the following it is assumed that the most dangerous direction is the longitudinal direction and the symmetry breaking may take place exclusively along the extent of the grating, destroying the longitudinal translational symmetry, while the symmetry across the midplane of the layer and the periodicity in the parallel direction is preserved. This assumption is in agreement with the corresponding numerical simulations of the evolution of the grating. In that case the auxiliary field is expressed with account to the boundary condition (3.175) as

$$\tilde{\xi}(x,y,z) = \sum_{n=0}^{\infty}\sum_{m=0}^{\infty} \hat{\xi}_{mn} \cos\left(\frac{\pi m z}{l}\right) \cos(\pi n y) \sin(k_x x) \tag{3.176}$$

with k_x - the longitudinal wave number of the emerging unstable perturbation.

The perturbation of the demagnetizing field is in turn expressed in series of arbitrary functions $f_{mn}(z)$ along the transversal directions

$$\tilde{h}(x,y,z) = -\tilde{\alpha}_c \sum_{n=0}^{\infty}\sum_{m=0}^{\infty} \hat{\xi}_{mn} f_{mn}(z) \cos(\pi n y) \sin(k_x x) \tag{3.177}$$

The necessary form of $f_{mn}(z)$ depends on the configuration of the external field and will be discussed separately.

For convenience, the perturbation of concentration is also formally expanded in series of $p_{mn}(z)$

$$\tilde{c}(x,y,z) = \tilde{\xi} + \mathcal{M}_{ph}\tilde{h} = \sum_{n=0}^{\infty}\sum_{m=0}^{\infty} \hat{\xi}_{mn} p_{mn}(z) \cos(\pi n y) \cos(k_x x) \tag{3.178}$$

with $p_{mn}(z)$ expressed as

$$p_{mn}(z) = \cos\left(\frac{\pi m z}{l}\right) - (d_m - 1) f_{mn}(z) \tag{3.179}$$

The hydrodynamic potential Φ is expanded in antisymmetric Chandrasekhar functions $S_m(z)$

$$\Phi(x,y,z) = \sum_{n=0}^{\infty}\sum_{m=1}^{\infty} \hat{\phi}_{mn} S_m(z) \cos(\pi n y) \sin(k_x x) \tag{3.180}$$

In turn, the potential Ψ retains the symmetry across the midplane of the layer. Considering the boundary condition (3.174) it is expressed in the following form

$$\Psi(x,y,z) = \sum_{n=1}^{\infty}\sum_{m=0}^{\infty} \hat{\psi}_{mn} \cos\left[\frac{\pi(2m+1)z}{2l}\right] \sin(\pi n y) \cos(k_x x) \tag{3.181}$$

Making use of the expansions (3.176)-(3.181) and projecting the set of equations (3.168)-(3.169) and (3.172) a system of linear equations is obtained in matrix form

$$\hat{\phi}_{mn} D^{\phi}_{mn} - \sum_{k=1}^{\infty} \hat{\phi}_{kn} \mathrm{A}^{mn}_{k} - Rs_m \sum_{i=0}^{\infty} \sum_{j=0}^{\infty} \hat{\xi}_{ij} \mathrm{M}^{mn}_{ij} = 0 \tag{3.182}$$

$$\hat{\psi}_{mn} D^{\psi}_{mn} - Rs_m \sum_{i=0}^{\infty} \sum_{j=0}^{\infty} \hat{\xi}_{ij} \mathrm{N}^{mn}_{ij} = 0 \tag{3.183}$$

$$\hat{\xi}_{mn} D^{\xi}_{mn} + \sum_{i=0}^{\infty} \sum_{j=0}^{\infty} \left(\hat{\xi}_{ij} \mathrm{B}^{mn}_{ij} + \hat{\phi}_{ij} \mathrm{P}^{mn}_{ij} + \hat{\psi}_{ij} \mathrm{Q}^{mn}_{ij} \right) = 0 \tag{3.184}$$

with diagonal elements D^{ϕ}_{mn}, D^{ψ}_{mn}, D^{ξ}_{mn}, non-diagonal elements A^{mn}_{k}, B^{mn}_{ij} and cross-elements M^{mn}_{ij}, N^{mn}_{ij}, P^{mn}_{ij}, Q^{mn}_{ij}:

$$D^{\phi}_{mn} = (1+\delta_{n0})[(\pi n)^2 + k_x^2] \left\{ \left(\frac{\mu_m}{l} \right)^4 + [(\pi n)^2 + k_x^2]^2 \right\} \tag{3.185}$$

$$D^{\psi}_{mn} = (1-\delta_{n0})[(\pi n)^2 + k_x^2] \left\{ \left[\frac{\pi(2m+1)}{2l} \right]^2 + (\pi n)^2 + k_x^2 \right\} \tag{3.186}$$

$$D^{\xi}_{mn} = (1+\delta_{m0})(1+\delta_{n0}) \left[\left(\frac{\pi m}{l} \right)^2 + (\pi n)^2 + k_x^2 \right] \tag{3.187}$$

non-diagonal elements

$$\mathrm{A}^{mn}_{k} = (1+\delta_{n0})[(\pi n)^2 + k_x^2]^2 \frac{2}{l} \int_{-l}^{+l} S_m(z) S_k''(z) dz \tag{3.188}$$

$$\mathrm{B}^{mn}_{ij} = \frac{1}{l} \int_{-l}^{+l} \int_{-1}^{+1} \left[W \frac{\partial p_{ij}}{\partial z} \cos(\pi j y) - (\pi j) V p_{ij} \sin(\pi j y) \right] \cos\left(\frac{\pi m z}{l} \right) \cos(\pi n y)\, dy dz \tag{3.189}$$

and cross-elements

$$M_{mn} = \left[[(\pi n)^2 + k_x^2] \left(p_{mn} \frac{\partial H}{\partial z} + \tilde{\alpha}_c f_{mn} \frac{\partial C}{\partial z} \right) + \frac{\partial^2 H}{\partial y^2} \frac{\partial p_{mn}}{\partial z} + \tilde{\alpha}_c \frac{\partial^2 C}{\partial y^2} \frac{\partial f_{mn}}{\partial z} \right] \cos(\pi n y) + \tag{3.190}$$

$$+ (\pi n) \frac{\partial}{\partial y} \left[\left(p_{mn} \frac{\partial H}{\partial z} - H \frac{\partial p_{mn}}{\partial z} \right) + \tilde{\alpha}_c \left(f_{mn} \frac{\partial C}{\partial z} - C \frac{\partial f_{mn}}{\partial z} \right) \right] \sin(\pi n y)$$

$$\mathrm{M}^{mn}_{ij} = \frac{1}{l} \int_{-l}^{+l} \int_{-1}^{+1} M_{ij}(y,z) S_m(z) \cos(\pi n y)\, dy dz \tag{3.191}$$

$$\mathrm{N}_{ij}^{mn} = \frac{k_x}{l}\int_{-l}^{+l}\int_{-1}^{+1}\left(p_{ij}\frac{\partial H}{\partial y} + \tilde{\alpha}_c f_{ij}\frac{\partial C}{\partial y}\right)\cos(\pi j y)\cos\left[\frac{\pi(2m+1)z}{2l}\right]\sin(\pi n y)\,dydz \tag{3.192}$$

$$\begin{aligned}\mathrm{P}_{ij}^{mn} = \frac{1}{l}\int_{-l}^{+l}\int_{-1}^{+1}\Big\{&[(\pi j)^2 + k_x^2]\frac{\partial C}{\partial z}S_i\cos(\pi j y) \\ &- (\pi j)\frac{\partial C}{\partial y}\frac{\partial S_i}{\partial z}\sin(\pi j y)\Big\}\cos\left(\frac{\pi m z}{l}\right)\cos(\pi n y)\,dydz\end{aligned} \tag{3.193}$$

$$\mathrm{Q}_{ij}^{mn} = \frac{k_x}{l}\int_{-l}^{+l}\int_{-1}^{+1}\left\{\frac{\partial C}{\partial y}\cos\left[\frac{\pi(2i+1)z}{2l}\right]\sin(\pi j y)\right\}\cos\left(\frac{\pi m z}{l}\right)\cos(\pi n y)\,dydz \tag{3.194}$$

The corresponding integrals (3.188)-(3.194) can be evaluated numerically without principal difficulties. The threshold of the instability and the parameters of the critical perturbation are determined from the dispersion relation, which is obtained by the requirement that the determinant of the linear system (3.182)-(3.184) is equal to zero, permitting the existence of non-trivial solutions.

What remains now is the determination of the form of the expansion functions $f_{mn}(z)$, which depends on the configuration of the applied external field. The equations for the scalar potential of the demagnetizing field perturbation have the form (3.5) with the boundary condition on the transversal sidewalls of the layer (3.6). The external potential $\tilde{\varphi}_{ext}$ in the free space outside the layer is a harmonic function.

Considering the expansion (3.177) and taking into account that the potential $\tilde{\varphi}_{ext}$ vanishes at infinity it is similarly expanded on the upper half-plane

$$\tilde{\varphi}_{ext}(x,y,z) = \sum_{n=-\infty}^{\infty}\hat{\varphi}_n e^{-s_n z}e^{i(\pi n y + k_x x)} \tag{3.195}$$

with $s_n = \sqrt{(\pi n)^2 + k_x^2}$.

The equations for the expansion functions $f_{mn}(z)$ of the demagnetizing field are then obtained from (3.5) making use of the expansions (3.176) and (3.177). The solution of the resulting system of linear differential equations with constant coefficients can be found without difficulty for either of the two principal configurations of the external field and expressed in the form

$$f_{mn}(z) = \frac{1}{d_z}\left[(-1)^{m+1}\beta_{mn}\frac{s_n}{g_n}\cosh(r_n z) + \kappa_{mn}\cos\left(\frac{\pi m z}{l}\right)\right] \tag{3.196}$$

with $r_n = \sqrt{\frac{d_y(\pi n)^2 + k_x^2}{d_z}}$ and $g_n = r_n \sinh(r_n l) + s_n \cosh(r_n l)$, the factor κ_{mn} is $\frac{(\pi n)^2}{r_n^2 + \left(\frac{\pi m}{l}\right)^2}$ for the parallel configuration of the external field and $\frac{\left(\frac{\pi m}{l}\right)^2}{r_n^2 + \left(\frac{\pi m}{l}\right)^2}$ for the perpendicular one. The multiplier β_{mn} equals to κ_{mn} in the former case and $\kappa_{mn} - 1$ in the latter.

Making use of the set of functions (3.196) and forming the determinant of the linear system (3.182)-(3.184) yields the dispersion relation and the critical parameters of the instability can be subsequently determined. Considering the linear magnetoconvective stability of the photoabsorptive formations some terminology of Section 2.2.2 will be used throughout the rest of this section.

3.2.2. Instability in ∥ field

The previous analysis of the linear stability of photoabsorptive gratings induced in thin ferrofluid layers has demonstrated that in the parallel configuration of the external field the most dangerous perturbation corresponds to the peristaltic deformation of the concentration front. The associated convective currents are a coordinated system of vortices located on the fronts of the concentration profile of the grating (Figure 2.5).

In turn, the considering of the transversal profile in ferrofluid layers of finite thickness contributes additional dimension to the shape of the critical perturbation, which was previously reduced by gap averaging. The form of the emerging convective flow now includes transversal currents as well. Still, the calculations show that the critical perturbation of the photoabsorptive grating still retains the symmetries and parallel periodicity of the peristaltic perturbation also in thick layers.

For the case of the parallel field good results have been obtained with expansions up to the leading mode of the initial grating

$$\tilde{\xi}(x, y, z) = \xi_{CR}(z) \sin(k_x x) + \xi_{SQ}(z) \cos(\pi y) \sin(k_x x) \tag{3.197}$$

$$\Phi(x, y, z) = \phi_{CR}(z) \sin(k_x x) + \phi_{SQ}(z) \cos(\pi y) \sin(k_x x) \tag{3.198}$$

$$\Psi(x, y, z) = \psi_{SQ}(z) \sin(\pi y) \cos(k_x x) \tag{3.199}$$

The applied perturbation then consists of two parts – zero order parallel contribution with the index $_{CR}$ and first order periodic term $_{SQ}$. The $_{CR}$ is the periodic crossroll type perturbation corresponding to an emerging longitudinal system of crossrolls with axes perpendicular to the primary system of stationary convective rolls. The infinitesimal

amplitude of the $_{SQ}$ perturbation is related to the amplitude of the crossroll perturbation by the equations (3.182)-(3.184). The second term is then the perturbation of the stationary state by the crossroll perturbation.

For a grating with unit aspect ratio $l = 1$, i.e. the interfringe of the grating is equal to the thickness of the layer, the critical wavenumber of the crossroll perturbation is determined from the calculated neutral curves as $k_{c,p}^{\parallel} \approx 0.5\pi$. This corresponds to the threshold value of the solutal Rayleigh number $Rs_m^{crit} = 1.3 \cdot 10^5$ at which this type of perturbation can begin to grow.

For the same system the previously considered simplified model (Section 2.2.2), which is based on the reduction of the transversal direction by means of gap averaging without the account for the influence of parasitic microconvection, yields the threshold value (2.35) $Rs_{\parallel}^{crit} = 121.7$, i.e. lower by three orders of magnitude. The corresponding longitudinal wavenumber of the critical perturbation then approaches zero $k_{c,p}^{\parallel} \to 0$ – the limit of long wavelengths.

In order to explore the influence of the parasitic microconvection on the stability of the induced concentration gratings in parallel magnetic field and expose the range of applicability of the simplified model, the calculated critical threshold and the longitudinal wavelength of the critical peristaltic perturbation are plotted in Figure 3.14 with respect to the thickness of the ferrofluid layer.

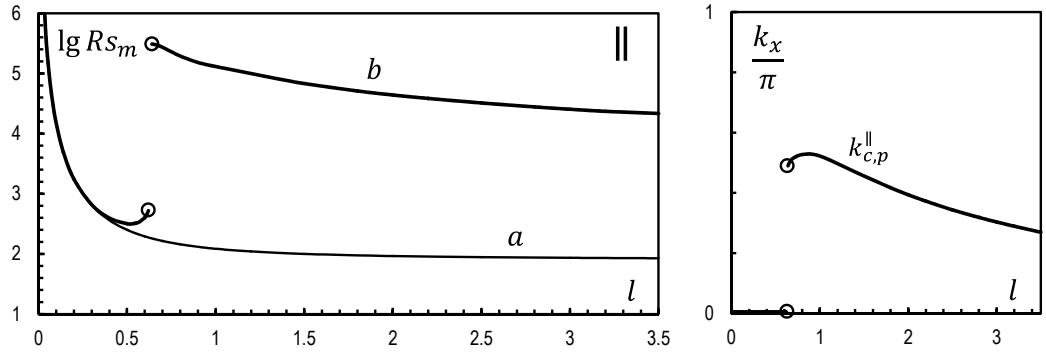

Figure 3.14. Dependence of the calculated critical parameters of the peristaltic perturbation of the photoabsorptive grating in parallel configuration of the applied magnetic field on the thickness of the ferrofluid layer: left - critical threshold Rs_m^{crit}: *(a)* simplified 2D model (Section 2.2.2), *(b)* 3D model; right - critical longitudinal wavenumber $k_{c,p}^{\parallel}$.

The comparison between the simplified plane model of Section 2.2.2 and the present model with account for the transversal direction shows that the former is quite accurate for layers with thickness up to a half of the grating interfringe. Further increasing the thickness of the layer the latter model predicts considerably higher values of the threshold of instability. Consequently, it is apparent that the presence of transversal parasitic microconvection can drastically enhance the stability of the photoabsorptive formations in parallel configuration of the applied magnetic field.

The discontinuous character of the dependence of the critical magnetic Rayleigh number on the thickness of the layer evidences the existence of the regime of efficient mixing. The intensity of stationary magnetic microconvection within the photoabsorptive grating is determined by the equilibrium of the magnetic forces and the shear stresses. Figure 3.14 shows that in narrow layers the parasitic microconvection is completely suppressed by viscous forces. As the thickness of the ferrofluid layer is increased, the latter are decreased and the stationary magnetoadvective currents can begin to homogenize the bulk non-homogeneities of concentration within the photoabsorptive grating to some degree also weakening its contrast. The subsequent decrease of the amplitude of the concentration grating increases the critical threshold (2.35) resulting in enhanced stability.

Further increasing the nominal Rayleigh number and approaching the threshold of the instability (2.35), the threshold rises as well in consequence of the intensification of the advective mixing. Adopting this interpretation, the presence of the discontinuity can be comprehensibly explained – at some well-defined thickness of the ferrofluid layer progressively increasing the value of the nominal Rayleigh number to the threshold of instability results in efficient magnetoadvective mixing causing greater reduction of the amplitude of the concentration grating and thus also elevating the threshold, so that it is always above the nominal Rayleigh number. From some point of view this curious situation resembles one of the famous Zeno's paradoxes.

The thickness of the layer, at which the increasing of the Rayleigh number in this interpreation no longer allows reaching the sequentially elevating threshold of the instability, can be estimated without difficulty. The convectively attenuated amplitude $\langle C_1 \rangle_z$ of the concentration grating can be expressed as

$$\langle C_1 \rangle_z (Rs_m) = \frac{1}{2l} \int_{-l}^{+l} \left[C_1^{dif}(z) + \tilde{C}_1(z) \right] dz \tag{3.200}$$

with $\tilde{C}_1(z)$ obtained from (3.121) as

$$\tilde{C}_1(z) = \left[1 - \tilde{\alpha}_c \mathcal{M}_{ph} f_0(z)\right] \hat{\xi}_{1,0} + \left[\cos\left(\frac{\pi z}{l}\right) - \tilde{\alpha}_c \mathcal{M}_{ph} f_1(z)\right] \hat{\xi}_{1,1} \tag{3.201}$$

where the factors $f_n(z)$ are defined by (3.93) and the amplitudes of the auxiliary field $\hat{\xi}_{1,0}$ and $\hat{\xi}_{1,1}$ depend on Rs_m and then so does also $\tilde{C}_1$.

Now, introducing $\langle C_1 \rangle_z$ into (2.35) instead of C_0 the new threshold $Rs_{\parallel}^{\sim}$ elevated by the magnetoadvective mixing is expressed

$$Rs_{\parallel}^{\sim} = \frac{C_0^2}{\langle C_1 \rangle_z^2} Rs_{\parallel}^{crit} \tag{3.202}$$

The definition (3.202) along with expression (3.200) permits to formulate the equation for the determination of the new threshold

$$P(x) = \langle C_1 \rangle_z(x) - C_0 \sqrt{\frac{1}{x} Rs_{\parallel}^{crit}} = 0 \tag{3.203}$$

Assuming that at certain thickness of the layer l the magnetoadvective mixing is so efficient that the threshold of instability cannot be reached anymore means that the physically relevant solution of (3.203) cannot be obtained. Also, at this point the infinitesimal variation of the nominal Rayleigh number would cause the corresponding infinitesimal change of $Rs_{\parallel}^{\sim}$ meaning that the threshold "runs away" from the increasing Rs_m, imposing an additional condition on the rate of attenuation of the amplitude of the grating

$$\frac{\partial}{\partial x} P(x) = 0 \tag{3.204}$$

The thickness of the layer at which both conditions (3.203) and (3.204) are fulfilled constitutes the jump discontinuity and the corresponding calculations give the value $l_0 = 0.66$ as the location of the discontinuity. The comparison of this result obtained on the grounds of some very simple physical assumptions with the results of the more complicated linear stability analysis presented in Figure 3.14 shows almost perfect correspondence.

The model (3.203) accounting for some influence of parasitic magnetoconvection improves the accuracy of the previous diffusive model (2.35) and well describes the behaviour of the threshold of instability up to the critical aspect ratio l_0. In turn, the dispersion relation based on the spectral model (3.182)-(3.184) should be used for determining the stability of the photoabsorptive gratings in the regime of efficient mixing.

3.2.3. Instability in ⊥ field

The calculations of the perpendicular configuration of the applied magnetic field show that the presence of the transversal parasitic magnetoconvection does not change the character of the convective destabilization of the grating – as predicted by the simplified plane model of Section 2.2.2 the most dangerous perturbation leads to the undulatory deformation of the concentration grating with the associated hydrodynamic perturbation corresponding to shear parallel convective currents of alternating direction (Figure 2.5) and the appropriate symmetries of the critical perturbation are retained with account for the transversal profiles of the fields as well. The calculated neutral curves of the undulatory instability are plotted in Figure 3.15 for some thicknesses of the ferrofluid layer.

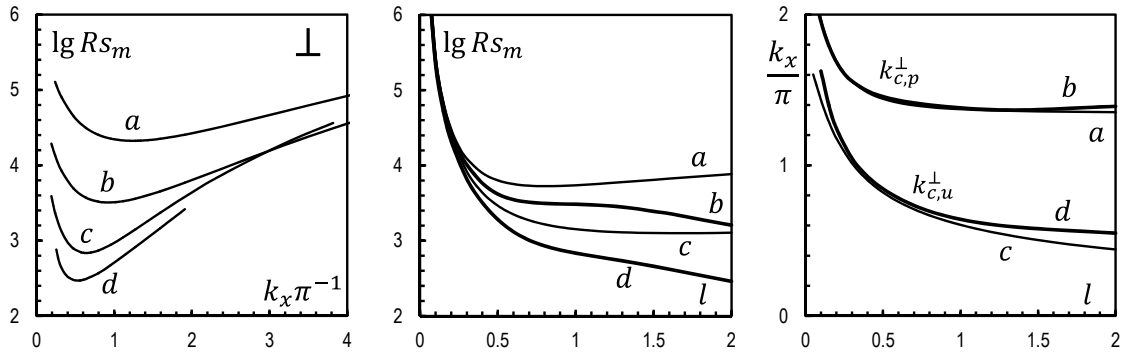

Figure 3.15. Neutral curves of the stability of the photoabsorptive grating in perpendicular magnetic field to undulatory perturbation (left) for layer thickness *(a)* $l = 0.2$, *(a)* $l = 0.4$, *(a)* $l = 1$, *(a)* $l = 2$; middle – dependence of the instability threshold Rs_m^{crit} on the thickness of the layer for peristaltic *(a)*, *(b)* and undulatory *(c)*, *(d)* perturbations: thin lines *(a), (c)* – simplified 2D model (Section 2.2.2) , thick lines *(b), (d)* – 3D model. Right – corresponding critical longitudinal wavenumbers of the perturbations.

For $l = 1$ the calculated critical threshold of the undulatory instability is $Rs_m^{crit} = 683.1$ and the corresponding critical wavenumber of the longitudinal undulations $k_{c,u}^{\perp} \approx 0.65\pi$. In turn, the stability of the grating with respect to the peristaltic perturbation is slightly higher with threshold at $Rs_m \approx 3\,000$ and corresponding wavenumber is twice as large $k_{c,p}^{\perp} \approx 1.4\pi$. For the same situation the plane model of linear stability (Section 2.2.2) slightly overestimates the threshold for the corresponding perturbation - $Rs_m^{crit} = 1420.1$ for the undulatory perturbation and $Rs_m \approx 5\,450$ for the peristaltic one.

Figure 3.15 shows the calculated dependence of the threshold of instability for peristaltic and undulatory perturbations on the thickness l of the ferrofluid layer. The undulatory instability is indeed the most dangerous across the whole considered range of aspect ratios l. The simplified plane model generally overestimates the stability of the grating for both perturbations. In thin layers the correspondence is significantly improved through thus suppressing the influence of the parasitic microconvection. In layers with thickness approximately equal up to half of the interfringe $l \approx 0.5$ the influence of the parasitic microconvection on the stability of the grating is insignificant. The same conclusion seems to apply to the parallel configuration of the external field (Figure 3.14).

Increasing the thickness of the layer the plane model eventually predicts the saturation or even slight elevation (in the case of peristaltic perturbation) of the threshold. In turn, more detailed analysis with account for the transversal direction demonstrates the monotonous decrease of the stability of the grating with the increasing of the layer thickness. On the other hand, the plane model adequately captures the longitudinal wavenumber of the perturbations over the whole range of l and it also decreases monotonically.

From Figure 3.15 becomes apparent that the presence of transversal microconvection reduces the stability of the photoabsorptive gratings in perpendicular configuration of the external field, although this effect is not as substantial as in the previously considered situation of parallel applied field, which showed significant increase of the stability of the grating in the region of efficient mixing. The results of Sections 3.1.5 and 3.1.6 showed that the direction of the parasitic currents is opposite in both situations and, consequently, the region of efficient mixing does not exist in perpendicular field. In thick layers the stability of the grating in perpendicular field is drastically lower than in the case of the parallel field.

3.2.4. Nonlinear regime

The shape of the photoabsorptive grating above the threshold of the instability is obtained by numerical simulations of the equations (1.36)-(1.39) with boundary conditions (3.1), (3.6) and (3.70) in real variables and finite volume formulation. The evolution of the concentration, demagnetizing field and velocity of magnetic microconvection is calculated from the homogeneous initial state, imposing the predetermined stationary distribution of temperature (2.7)-(2.9).

The numerical simulations of the nonlinear regime in real variables and especially the calculations of the bifurcation curves are connected with some difficulties near the point of exchange of stabilities. Clearly, at the onset of the instability the growth rates of the critical perturbations are very low, so in this case the obtaining of the exact stationary state by advancing the dynamic system of equations in time is associated with numerical problems. For this purpose the transient numerical solution is perturbed by the addition of spatially random perturbation to the concentration field with small amplitude $\sim 10^{-3}$ at each global time step.

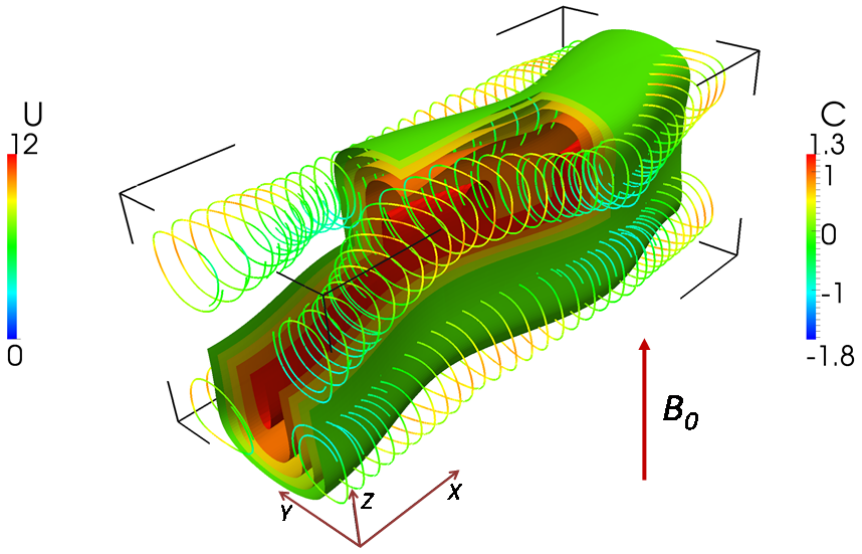

Figure 3.16. Deformation of the convective rolls and bending of the concentration front caused by the development of the undulatory instability in the perpendicular configuration of the external magnetic field at $Rs_m = 1\,000$.

The previous stability analysis has demonstrated that the photoabsorptive gratings are relatively stable in the parallel configuration of the applied magnetic field. In turn, outside the regime of efficient mixing, meaning that the thickness of the ferrofluid layer is smaller than

approximately half of the interfringe, the transversal fluxes are effectively suppressed and the simplified twodimensional model for the gap-averaged quantities well describes the stability of the grating and the course of the convective destabilization. In this regard, it only makes sense to consider the perpendicular configuration of the applied magnetic field.

In perpendicular field the critical perturbation corresponds to the undulatory bending of the concentration front caused by the emerging cross-grating flows of alternating direction (Figure 3.16). The shape of the grating and its progressive deformation in the super-critical regime above the threshold of the instability is characterized by Fourier modes of concentration $C_{01}(t)$, $C_{11}(t)$ and the intensity of convective motions is described by the hydrodynamic mode $U_{10}(t)$, extracted from the concentration and velocity fields $C(x,y,z,t)$ and $\boldsymbol{U}(x,y,z,t)$ calculated in the course of the simulations. The transversal profile of the modes across the gap of the layer is reduced by the RMS averaging in the case of the concentration modes and the gap-averaging for the hydrodynamic mode

$$C_{mn}(t) = \sqrt{\frac{1}{2l}\int_{-l}^{l}[C_{mn}(z,t)]^2}\,, \qquad U_{mn}(t) = \frac{1}{2l}\int_{-l}^{l} U_{mn}(t) \tag{3.205}$$

with

$$C_{01}(z,t) = \frac{k_x}{2\pi}\int_{-1}^{1}\int_{-\frac{\pi}{k_x}}^{+\frac{\pi}{k_x}} C(x,y,z,t)\cos(\pi y)\,dx\,dy \tag{3.206}$$

$$C_{11}(z,t) = \frac{k_x}{\pi}\int_{-1}^{1}\int_{-\frac{\pi}{k_x}}^{+\frac{\pi}{k_x}} C(x,y,z,t)\sin(k_x x)\sin(\pi y)\,dx\,dy \tag{3.207}$$

$$U_{10}(z,t) = \frac{k_x}{2\pi}\int_{-1}^{1}\int_{-\frac{\pi}{k_x}}^{+\frac{\pi}{k_x}} U_y(x,y,z,t)\sin(k_x x)\,dx\,dy \tag{3.208}$$

The selected modes correspond to the primary modes of instability (2.55) and (2.45) in thin layers and such choice of parameters permits convenient comparison of the two situations.

The calculated dynamics of the concentration mode amplitudes and the average velocity magnitude $\overline{U}$ during the formation of the grating at some arbitrary values of the magnetosolutal Rayleigh number above the threshold of the undulatory instability are plotted in Figure 3.17. The destabilization of the photoabsorptive grating is evidenced by the spontaneous decrease of the primary mode amplitude C_{01}, corresponding to the attenuation of the grating contrast, and the simultaneous emergence of the mode C_{11} in the course of the transient numerical simulation after the reaching of the quasi-stationary state.

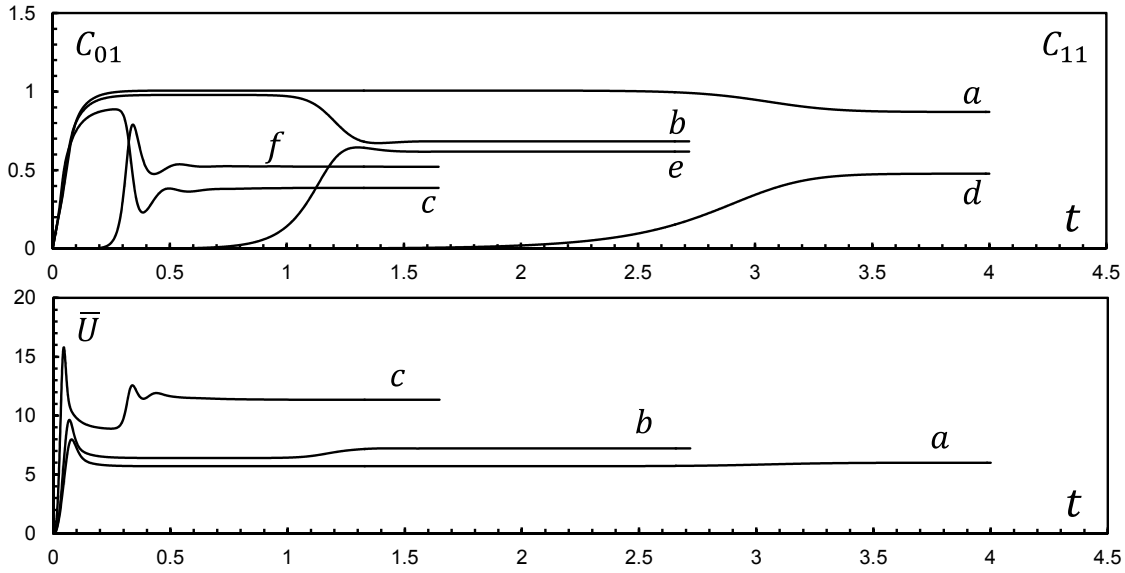

Figure 3.17. Calculated time evolution of the mode amplitudes C_{01}, C_{11} (top) and average velocity magnitude $\overline{U}$ (bottom) in the course of the numerical simulation of the photoabsorptive grating in perpendicular magnetic field: C_{01}, $\overline{U}$ at *(a)* $Rs_m = 1\,000$, *(b)* $Rs_m = 1\,500$, *(c)* $Rs_m = 5\,000$; *(d), (e), (f)* – corresponding dynamics of C_{11}.

The eventual stationary values of the mode amplitudes C_{01}, C_{11} and U_{10} are plotted in Figure 3.19 in relation to the control parameter, defined with respect to the appropriate critical threshold Rs_m^{crit} as

$$r = \frac{Rs_m}{Rs_m^{crit}} - 1 \tag{3.209}$$

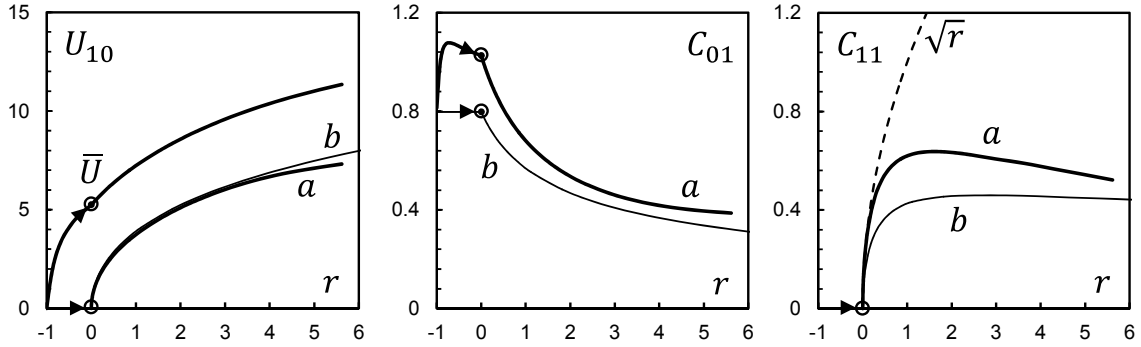

Figure 3.18. Bifurcation curves of the undulatory instability of photoabsorptive grating in the perpendicular configuration of the external field: calculated stationary amplitudes C_{01}, C_{11} and U_{10} – *(a)* numerical simulations, *(b)* – simplified model (2.57)-(2.60).

The bifurcation curves obtained from full numerical simulations are compared with the results of the two-dimensional model based on gap averaging and corresponding mode amplitudes calculated according to the relations (2.60) and (2.57). Both models predict typical supercritical pitchfork-type bifurcations. According to the 2D model the amplitude of the emerging mode C_{11} scales as $\sim[(r+1)^{-0.5}-(r+1)^{-1}]^{0.5}$ with respect to the control parameter r, in turn, the scaling predicted by the simulations is somewhat closer to the normal form $\sim\sqrt{r}$ in the vicinity of the threshold.

The comparison of both models demonstrates that in the perpendicular configuration of the applied magnetic field the presence of the parasitic microconvection can be successfully compensated by gap averaging – the amplitude of the mode U_{10} is almost identical in both cases, although rather intensive convective motion takes place within the elements of the photoabsorptive grating both below and above the threshold of the instability, as evidenced by the results of the numerical simulations and the average velocity magnitude $\bar{U}$. In turn, the influence of the parasitic advective fluxes does not significantly alter the bifurcation behavior as well.

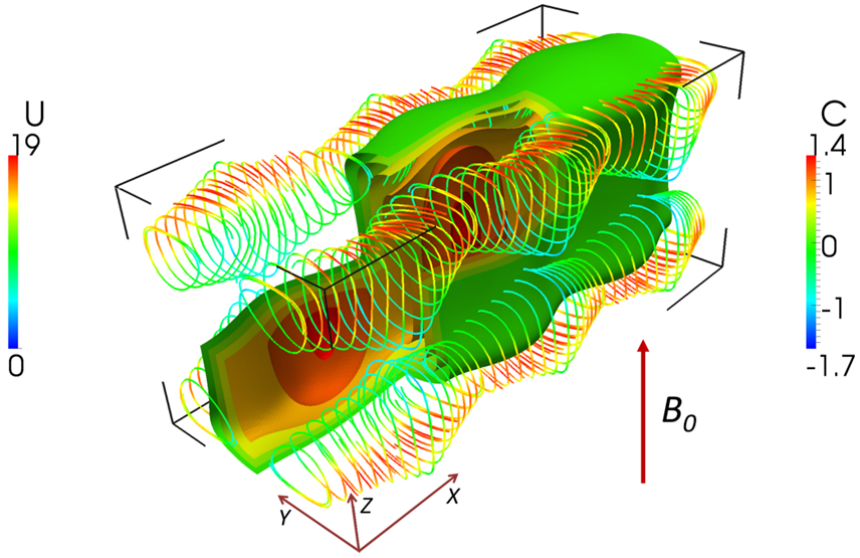

Figure 3.19. Deformation of the convective rolls and the formation of the secondary concentration grating caused by the development of the peristaltic instability in the perpendicular configuration of the external magnetic field at $Rs_m = 3\,750$.

The appearance of the peristaltic stratification of the concentration grating was also observed by numerical simulations of the nonlinear regime. The calculated concentration profiles within a single element of the photoabsorptive grating are plotted in Figure 3.19 for some

arbitrary value of the magnetic Rayleigh numbers reasonably exceeding the threshold of the peristaltic instability.

Further increasing the value of the control parameter above the threshold the convective rolls become considerably deformed and eventually form hydrodynamic structures similar to toroidal convective vortices.

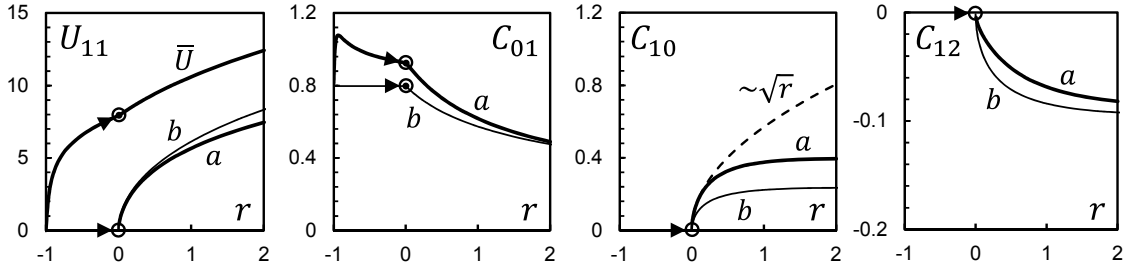

Figure 3.20. Bifurcation curves of the peristaltic instability of photoabsorptive grating in the perpendicular configuration of the external field: calculated stationary amplitudes C_{01}, C_{10}, C_{12} and U_{11} – *(a)* numerical simulations, *(b)* – simplified model (2.52)-(2.54).

The deformation of the grating is characterized with the set of primary modes (2.43)-(2.46) and the bifurcation curves are plotted in Figure 3.20 along with the results of the simplified model (2.52)-(2.54) based on gap-averaging for the same parameters, showing acceptable correspondence. The character of destabilization is generally similar to the case of the undulatory instability and the same principle conclusions apply here as well.

Microstructure grids

The spontaneous symmetry breaking of the photoabsorptive convective-diffusive gratings in the external magnetic field naturally and logically leads to the question of the formation and the stationary form of the non-degenerated bidirectional gratings – microgrids. Such periodic structures can be formed by illuminating a ferrofluid layer through a non-transparent mask with periodically spaced square openings [58] or similarly by simultaneous formation of crossed photoabsorptive gratings [94].

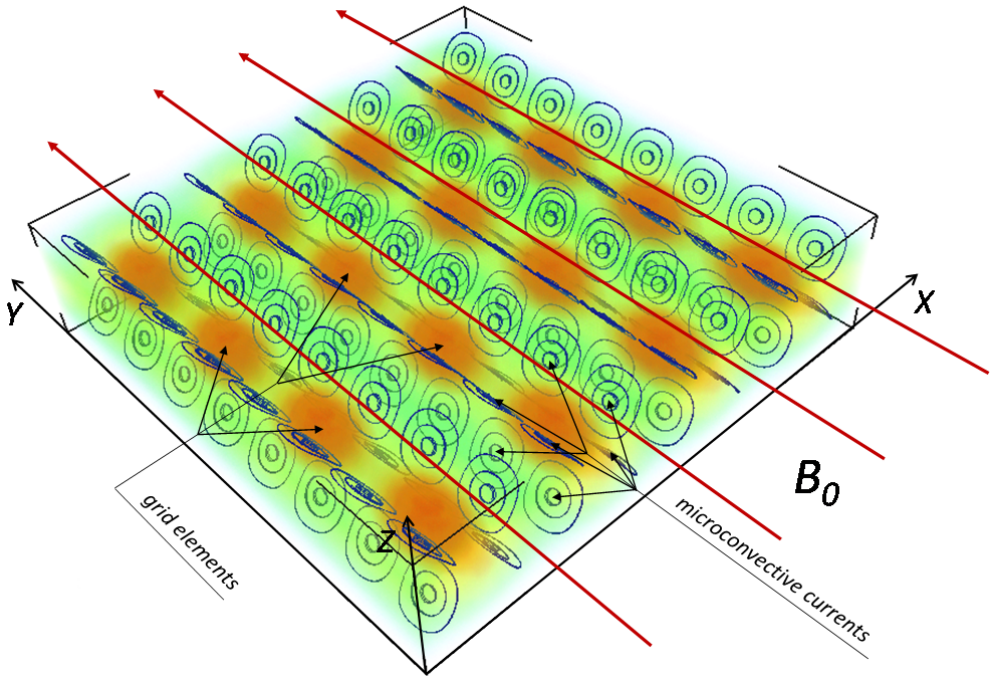

Figure 4.1. Photoabsorptive grids: simulated convective-diffusive microstructures in bidirectional grids under laterally applied magnetic field.

If the opening, through which the ferrofluid layer is illuminated, is perfectly square and the intensity of the incident illumination I_0 is uniform then the transmitted optical intensity is described making use of the rectangular function $\Pi(x)$: $\sim[1 + \Pi(x)][1 + \Pi(y)]$. The process of the formation and relaxation of the concentration grids due to the rectangular heat source in dispersions with anisotropic diffusion has been described [92]. However, the large thermal diffusivity of the temperature field smears the sharp edges of the temperature perturbations and the small diffusivity of the nanoparticles does the same with the induced concentration differences. It seems reasonable, therefore, for the principal description of the basic form of the photoabsorptive magnetoconvection to consider just the primary mode of the heat source:

$\frac{\pi^2}{4}[1+\cos(\pi x)][1+\cos(\pi y)]$, where the coefficient of proportionality, as previously, is obtained from the normalization.

Substituting the assumed form of the heat source into the dimensionless temperature equation (2.5) the temperature distribution within the layer can be determined analytically or numerically. The base state of the bidirectional grid due to the diffusion, Soret effect and magnetophoresis can be obtained without principal difficulties along the same lines as previously for the case of the monodirectional grating, and the role of the microconvection can be described in the spectral approach. It is clear, however, that the magnetic force now possesses all three spatial components, the longitudinal direction is non-degenerated and the flow is fully three-dimensional. The spectral approach then does not offer clear advantages over the numerical methods based on finite volume formulation, which will be employed.

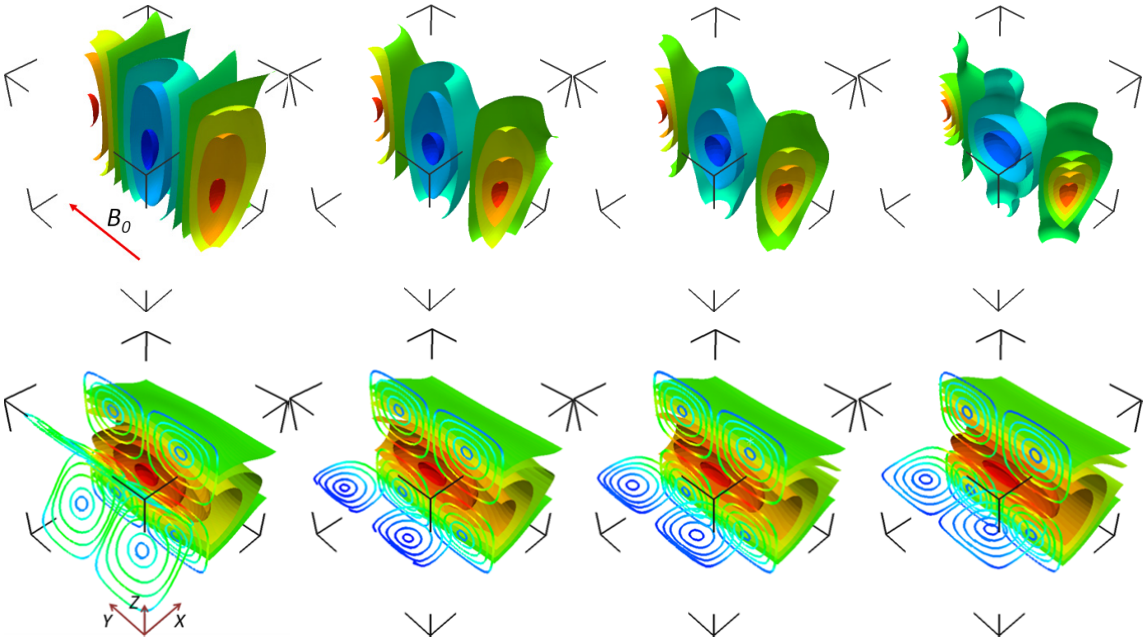

Figure 4.2. Perturbation of the demagnetizing field (top) and the stationary photoabsorptive microstructures (bottom) in bidirectional grids under laterally applied magnetic field (concentration isosurfaces and convective streamlines): *(a)* $Rs_m = 100$, *(b)* $Rs_m = 500$, *(c)* $Rs_m = 1000$, *(d)* $Rs_m = 5000$.

Making use of the calculated temperature distributions the solution of the convective problem can be obtained for different orientations of the applied magnetic field. The direction of the magnetophoretic and magnetoconvective fluxes is determined by the interactions of the photoabsorptive nonhomogeneities of the ferroparticle concentration with the gradients of the primary component of the corresponding demagnetizing field perturbation. If the external

field is applied along the parallel direction, the situation is straightforward – the self magnetic field is weakened within the concentration microstructures due to the influx of the ferroparticles and its maximums are located in-between the neighboring grid elements. The magnetic forces then form a pair of coaxial toroidal vortices around the element with their axes of rotation oriented along the parallel direction (Figure 4.2).

When the external field is perpendicular to the sidewall of the layer the principal component of the demagnetizing field experiences a discontinuity on the sidewall of the layer due to the corresponding jump of magnetization. The magnetic microconvection is then driven by the corresponding near-wall gradients of the demagnetizing field. Still, the resulting magnetoconvective pattern is again a pair of coaxial toroidal vortices with the axis of rotation oriented along the vertical field (Figure 4.3).

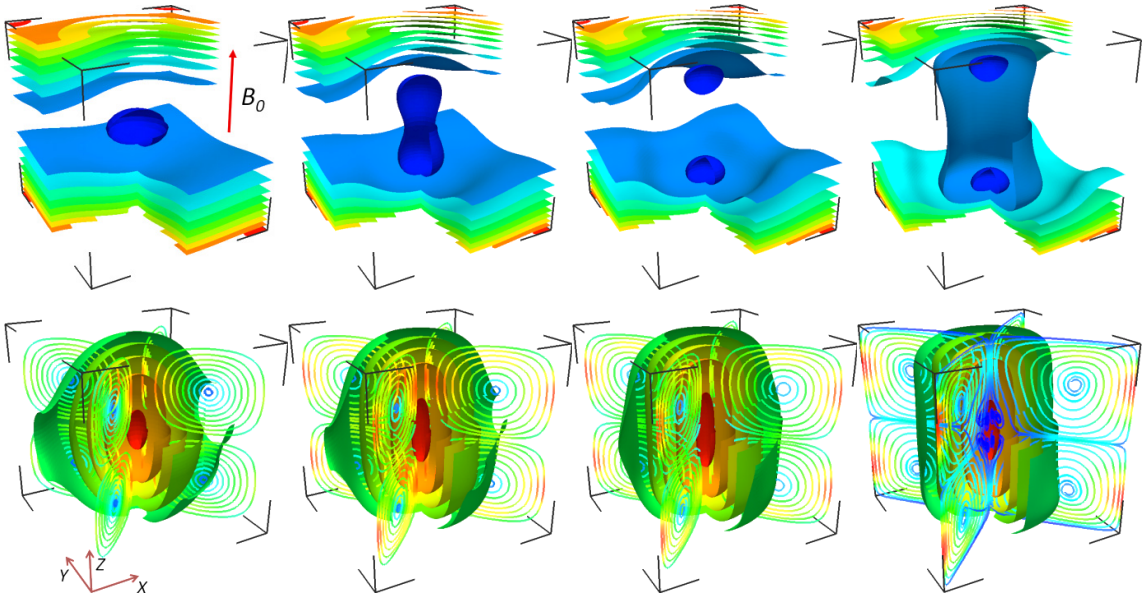

Figure 4.3. Perturbation of the demagnetizing field (top) and the stationary photoabsorptive microstructures (bottom) in bidirectional grids under perpendicularly applied magnetic field (concentration isosurfaces and convective streamlines): *(a)* $Rs_m = 100$, *(b)* $Rs_m = 500$, *(c)* $Rs_m = 1000$, *(d)* $Rs_m = 5000$.

In real conditions the formation of the magnetic microconvection and its structure cannot be observed directly - typical ferrofluids are not transparent and so the internal motions are thus concealed. The role of magnetoconvective transport on the microscale can only be identified by the observations of the peculiarities of evolution of the concentration field, which can be detected by various methods. In turn, in the numerical simulations detailed microscopical information is available about the dynamics and distributions of all fields. This necessitates

the formulation of the observable parameters in order to determine the accordance of the measurements and theoretical predictions.

The integral characteristic (3.157) – the L^2-norm of the first parallel concentration mode - describes the general shape of the extended photoabsorptive concentration microstructure and can be measured in the experiment. Instead, the bidirectional concentration grids in fact possess two preferred orientations – the parallel direction and the longitudinal, so it is reasonable to observe both coordinates

$$J_{\parallel} = \sqrt{\int_{-l}^{l} F_y\{C(x,y,z,t)\}^2 dz} \quad \text{and} \quad J_{\perp} = \sqrt{\int_{-l}^{l} F_x\{C(x,y,z,t)\}^2 dz} \tag{4.1}$$

with functional $F_\tau\{C(x,y)\} = \int_{-1}^{1}\int_{-1}^{1} C(x,y)\cos(\pi\tau)\,dx\,dy$ yielding the primary concentration mode in the corresponding direction.

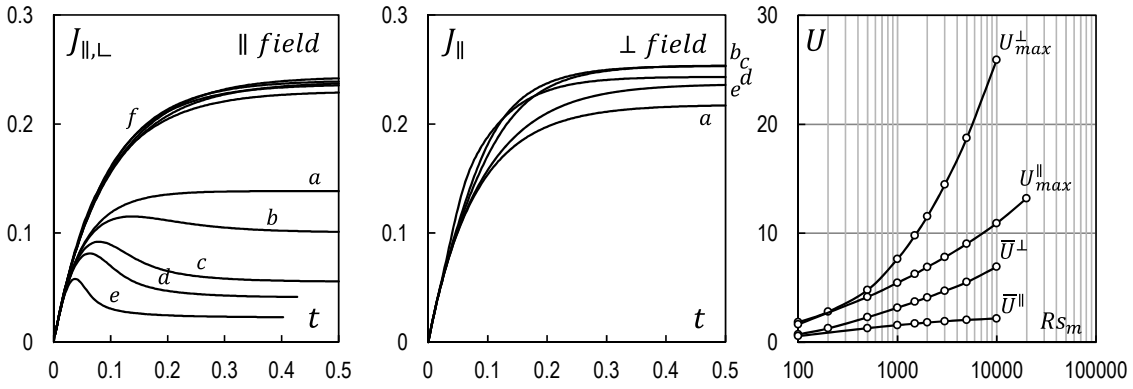

Figure 4.4. Formation of the microstructure grids: left - establishing of the stationary convective-diffusive microstructure in the parallel applied field, calculated signals at *(a)* $Rs_m = 0$, *(b)* $Rs_m = 100$, *(c)* $Rs_m = 500$, *(d)* $Rs_m = 1000$, *(e)* $Rs_m = 5000$ along the direction of the external field and *(f)* in the longitudinal direction; middle - formation of the microstructure in the perpendicular field configuration at *(a)* $Rs_m = 0$, *(b)* $Rs_m = 100, 500, 1000, 5000$; right - dependence of the stationary average and maximum U_{max} convective velocity on the control parameter in the parallel *(a)* $\overline{U}^{\parallel}$, *(c)* $U^{\parallel}_{max}$ and perpendicular *(b)* $\overline{U}^{\perp}$, *(d)* $U^{\perp}_{max}$ configurations.

If the formation of the photoabsorptive grid takes place in the parallel configuration of the applied field, the anisotropy of the magnetic diffusion coefficient introduces the anisotropy of

the measured signals $J_{\parallel,\perp}(t)$ - in the direction of the field the magnitude of the parallel signal is reduced due to the magnetodiffusive contributions to the mass flux (Figure 4.4).

In turn, the microconvective fluxes further homogenize the concentration modulation along the direction of the applied field. Most importantly, the influence of microconvection changes the dynamics of evolution of the photoabsorptive microstructure during the formation stage - after the initially attained maximum the signal $J_{\parallel}$ begins to diminish and gradually reaches its stationary value (Figure 4.4), a characteristic indication of the influence of microconvective transport. In contrast, the dynamics of the longitudinal signal $J_{\perp}$ remains almost unchanged.

In the perpendicular configuration of the external field the anisotropy of $J_{\parallel,\perp}$ vanishes and the evolution of the grid in both directions is identical. In this configuration of the applied field the magnetic forces act mainly in the transversal direction, which is generally unobservable from the experimental point of view. In turn, the character of the dynamics of the measured signals is unaltered by the formation of microconvection within the photoabsorptive structures and even their magnitude is relatively unchanged. Consequently, the presence of microconvection cannot be established by real observations for the vertical orientation of the applied field.

The calculations of the averaged velocity magnitude show saturation with respect to the control parameter in the parallel field configuration (Figure 4.4). The corresponding increase of the maximum velocity points to the localization of the most intensive convective fluxes within the core of the grid element. In the perpendicular configuration the average velocity does not saturate within the considered range of parameters, still the maximum velocity grows more rapidly.

Considering the stability of the bidirectional grids, the calculations in real variables did not show any destabilization of the photoabsorptive convective-diffusive microstructures in the parallel field configuration up to rather large values of the control parameter $Rs_m \sim 10^6$. This conclusion partially correlates with the analysis of the problem of stability of photoabsorptive gratings, which demonstrated that the extended gratings are relatively stable under the action of the parallel field. Nevertheless, the gratings became easily destabilized by the application of perpendicular magnetic field and the same conclusion seems to be valid for the grids.

During the formation of the photoabsorptive grid under the action of the perpendicular field a pair of coaxial toroidal vortices emerges within each element with the axis directed along the applied field (Figure 4.3). Due to the periodicity of the grid in two orthogonal directions – the

parallel and the longitudinal - the vortices are constrained by the presence of the neighboring elements and so do not possess the full toroidal symmetry. Then the symmetry of a single grid element corresponds to the symmetry of the whole periodic array.

If the external magnetic field is applied along the perpendicular direction, then the four planes of reflection describe the initial symmetry of the photoabsorptive convective-diffusive microstructure – the *x*-*z* plane, the *y*-*z* plane and two diagonal planes. In turn, the four rotations by $\frac{\pi}{2}$ about the axis of the paired convective vortices form the rotational symmetry of the element. An additional reflection plane is introduced by the midplane of the layer. Consequently, at moderate values of the magnetosolutal Rayleigh number the associated reflections and rotational symmetries of the grid element constitute the horizontal dihedral group D_{4h}.

Gradually increasing the magnetosolutal Rayleigh number the most intensive convective motions are localized in the space between the neighboring elements of the photoabsorptive grid. At certain value of the control parameter an additional pair of coaxial toroidal vortices emerges within the core of the microstructure (Figure 4.3). Further increase of the Rayleigh number causes the growth of these secondary circulations, which subsequently lead to the eventual loss of stability of the grid element.

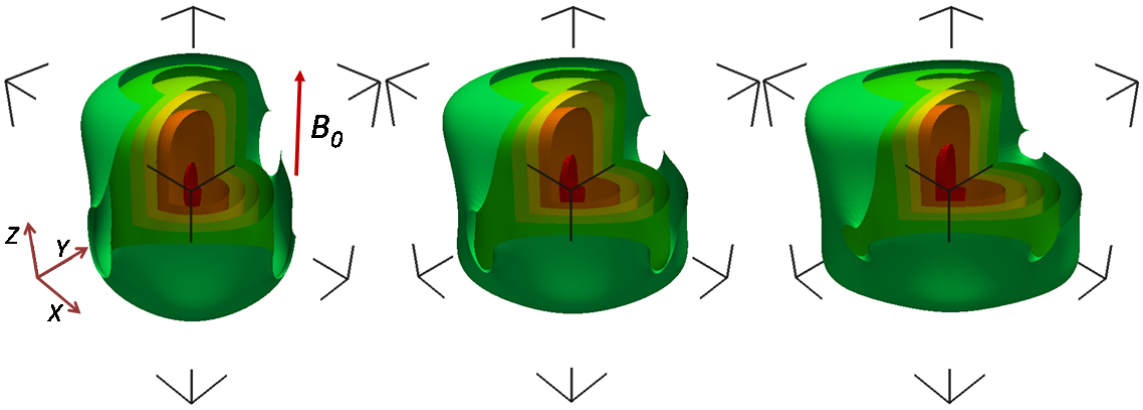

Figure 4.5. Development of the instability: concentration contours within the element of the bidirectional grid at $Rs_m = 3\,000$ (left), $Rs_m = 5\,000$ (middle), $Rs_m = 10\,000$ (right).

The calculations of the evolution of the grid elements show that the peristaltic and undulatory instabilities emerging within the photoabsorptive gratings possess direct counterparts in the bidirectional configuration. Similarly, as the loss of translational symmetry ensues from the destabilization of the extended grating, so the loss of stability of the cuboid group is observed

in the bidirectional system followed by the reduction of the order of the rotational symmetry corresponding to the transition $D_{4h} \rightarrow D_{2h}$.

The emergence of the undulatory instability was accompanied by the appearance of the cross-grating flows and the formation of the similar shear currents takes place in the bidirectional configuration as well, leading to the stretching of the grid element along one of the diagonal directions - by the simultaneous shearing of the element along both of the primary directions of the grid by the advective fluxes (Figure 4.5).

The quantitative description of the destabilization process requires the formulation of the corresponding numerical parameters. The initial symmetries of the grid as well as those of the emerging perturbations and the properties of the equivalent undulatory instability (3.205)-(3.208) in photoabsorptive gratings dictates the corresponding choice of the primary modes for the bidirectional configuration

$$C_{mn}(t) = \sqrt{\frac{1}{2l}\int_{-l}^{l}[C_{mn}(z,t)]^2}\,, \qquad U_{mn}(t) = \frac{1}{2l}\int_{-l}^{l} U_{mn}(t) \tag{4.2}$$

with

$$C_1(z,t) = C_{10} = C_{01} = \frac{1}{2}F_x\{C(x,y,z,t)\} = \frac{1}{2}F_y\{C(x,y,z,t)\} \tag{4.3}$$

$$C_{11}(z,t) = \int_{-1}^{1}\int_{-1}^{+1} C(x,y,z,t)\sin(\pi x)\sin(\pi y)\,dx\,dy \tag{4.4}$$

$$U_1(z,t) = U_{10} = \frac{1}{2}\int_{-1}^{1}\int_{-1}^{+1} U_y(x,y,z,t)\sin(\pi x)\,dx\,dy \tag{4.5}$$

The performed calculations show that the eventual stationary value of the amplitude of the concentration mode $\sim\cos(\pi x)\cos(\pi y)$, which is imposed by the photoabsorptive thermophoretic stratification depends little on the Rayleigh number and well corresponds to the value calculated with respect to the thin layer approximation and just the phoretic mass transport

$$\frac{1}{\sqrt{2l}}\left\|F_{xy}\{C(x,y,z)\}\right\|_2 \approx -\frac{s_m}{d_H(\pi,\pi)}\overline{T}_{11} \quad \text{with} \quad \overline{T}_{11} = \frac{1}{8}\left[1 - \frac{Bi}{f_1}\frac{\sinh(r_1 l)}{r_1 l}\right] \tag{4.6}$$

where $f_1 = r_1\sinh(r_1 l) + Bi\cosh(r_1 l)$ and $r_1 = \pi\sqrt{2}$.

Subsequently, this mode is appreciably influenced neither by the parasitic microconvection, nor by the emerging instability and thus cannot participate in the destabilization of the grid. It is then pointless to consider it any further.

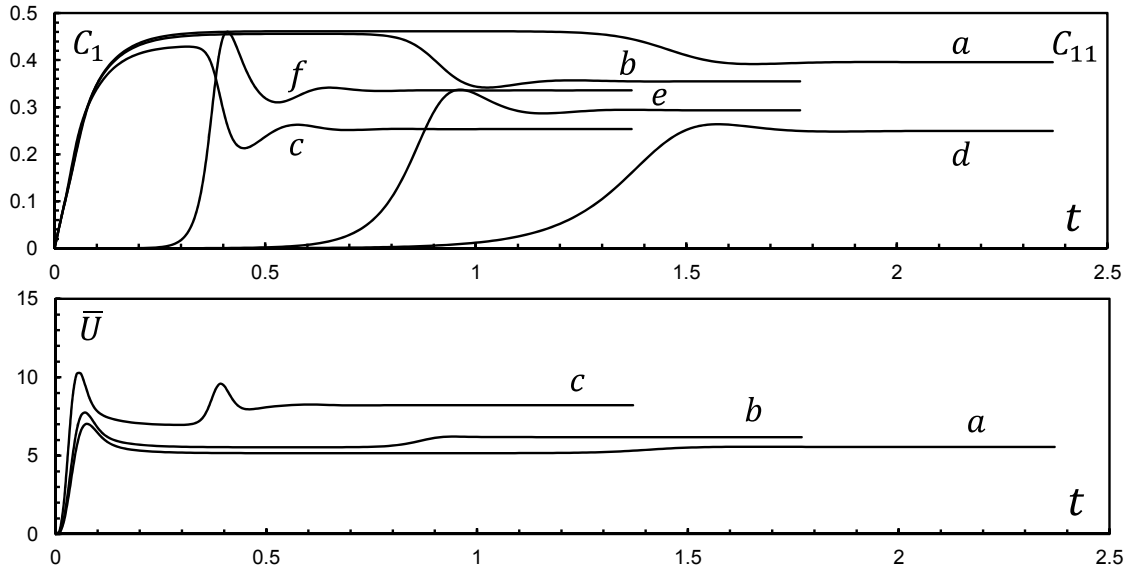

Figure 4.6. Calculated time evolution of the mode amplitudes C_1, C_{11} (top) and average velocity magnitude $\overline{U}$ (bottom) in the course of the numerical simulation of the photoabsorptive grating in perpendicular magnetic field: C_1, $\overline{U}$ at *(a)* $Rs_m = 4\,000$, *(b)* $Rs_m = 5\,000$, *(c)* $Rs_m = 10\,000$; *(d), (e), (f)* – corresponding dynamics of C_{11}.

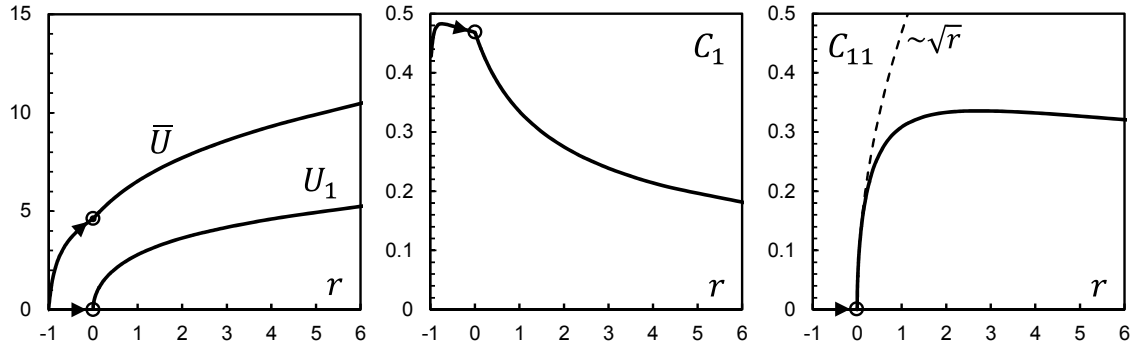

Figure 4.7. Bifurcation curves of the instability of photoabsorptive grid in the perpendicular configuration of the external field: calculated stationary amplitudes U_1 (left), C_1 (middle) and C_{11} (right).

The calculated evolution of the selected concentration modes C_1 and C_{11} and the averaged velocity magnitude $\overline{U}$ during the formation of the grid from the initially homogeneous state to the quasi-stationary state and then the eventual emergence of the destabilizing perturbations is plotted in Figure 4.6 for $l = 1$ and some arbitrary values of the magnetosolutal Rayleigh number Rs_m exceeding the threshold of the instability.

The appearance of the cross-grid flows leads to the lowering of the contrast of the grid in both of the primary directions as evidenced by the decrease of the amplitude C_1. The calculated bifurcation curves for the instability are plotted in Figure 4.7.

The character of the destabilization corresponds to the supercritical pitchfork instability, its properties are in many ways similar to the case of the undulatory instability in photoabsorptive gratings and the same principle conclusions apply here as well. The critical threshold corresponds to $Rs_m \approx 2\,820$.

The counterpart of the peristaltic instability of the photoabsorptive gratings was also observed in the numerical simulations of the bidirectional grids. Instead of the stretching of the grid element in the diagonal direction, the element is stretched in either of the primary directions of the modulation (Figure 4.8).

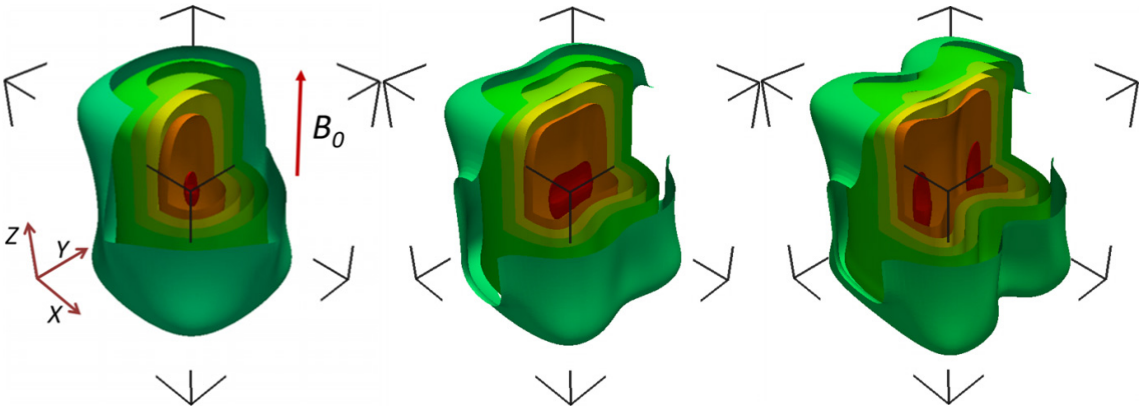

Figure 4.8. Development of the instability: concentration contours within the element of the bidirectional grid at $Rs_m = 10\,000$ (left), $Rs_m = 20\,000$ (middle), $Rs_m = 50\,000$ (right).

This type of instability develops at higher values of the magnetic Rayleigh number as the one previously described and the corresponding perturbation then is not the critical perturbation.

The state of the grid is characterized in this case by the modes C_{10} and C_{01} (4.3) and the appropriate corresponding mode U_{11} with

$$U_{11}(z,t) = \int_{-1}^{1}\int_{-1}^{+1} U_y(x,y,z,t)\cos(\pi x)\sin(\pi y)\,dx\,dy \tag{4.7}$$

The evolution of the selected modes during the formation of the grid from the initial homogeneous state is determined from the numerical simulations. While initially both the modes C_{10} and C_{01} coincide and at some point reach a seemingly stationary state, the eventual

appearance of the splitting of the mode amplitudes during the further evolution of the photoabsorptive microstructure evidences the loss of stability of the cuboid group and the reduction of the order of the rotational symmetry corresponding to the transition $D_{4h} \rightarrow D_{2h}$ above the corresponding threshold. The calculated bifurcation curves (Figure 4.9) evidence the divergence of the stationary values of the mode amplitudes with the increasing of the magnetic Rayleigh number.

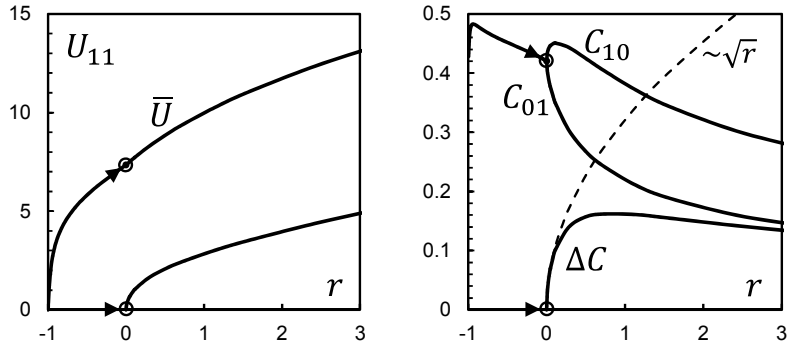

Figure 4.9. Bifurcation curves of the instability of photoabsorptive grid in the perpendicular configuration of the external field: calculated stationary amplitudes U_{11} (left) and C_{01}, C_{10}, C_{11} (right).

The bifurcation is identified by the splitting of the calculated amplitudes

$$\Delta C = |C_{10} - C_{01}| \tag{4.8}$$

The form of the symmetry breaking again corresponds to a supercritical pitchfork bifurcation. Extrapolating the calculated numerical values of the splitting ΔC by a square root dependence on the control parameter $\sim\sqrt{r}$, the critical threshold of the instability can be determined. Apparently, the growth of the destabilizing perturbations begins somewhere at around $Rs_m^{crit} \approx 11\,700$. The subsequent emerging anisotropy signifies the appearance of the stratification of the concentration distribution within the element of the photoabsorptive grid in one or the other direction.

In contrast to the photoabsorptive grating, the bidirectional grids are still scantily explored. At present, the development of the described instabilities and the subsequent reduction of order of the rotational symmetry have yet neither been looked for, nor observed in photoabsorptive concentration grids. In this regard, the experimental confirmation of the proposed mechanism of destabilization may help ascertain the crucial role of advective transport in the formation of photoabsorptive microstructures and will be expected in the future.

Localized structures

In the previous sections the presence and role of the magnetic microconvection were considered on the example of some model problems. The unifying feature of the examined model systems lies in the extended geometry of these problems and the eventual solutions in one or both orthogonal directions within the ferrofluid layer. Clearly, the real physical photoabsorptive gratings and grids created in the experiments are not infinite in these directions, but it is assumed that they are sufficiently extended to allow considering them such (the actual FRS gratings usually contain tens of periods) and the end effect can be disregarded.

The opposite situation is the case of the localized microstructures embedded in an infinite layer of otherwise quiescent ferrofluid. The purpose of this section then is to discuss some aspects of the formation and evolution of the localized photoabsorptive microstructures such as those, for example, formed in the beam spot of a laser by the complex magnetodiffusive and magnetoadvective interactions. While the principal mechanisms of the formation of magnetoconvective currents are similar and so, consequently, also will be the employed approach to elucidate their role, the localized microstructures are not constrained and not affected by the presence of the neighboring elements as the elements of the extended systems are and their shape and dynamics show notable differences.

Technically, gaining information about the structure of the localized photoabsorptive formations is more complicated in comparison with the extended ones. From the theoretical point of view, the problem of modeling of the unbounded flows possesses peculiarities. The symmetry of the localized microstructure also dictates the application of the appropriate coordinate system and frequently requires the use of the curvilinear coordinates. These factors complicate the form of the governing equations and the methods of obtaining their solution.

From the experimental side, while the formation of the localized photoabsorptive microstructures is relatively simple, in this case the reliable and powerful method of forced Rayleigh scattering is not easily applicable to the quantitative characterization of the ferroparticle concentration field. Still, some qualitative results are available in the literature and will be discussed.

5.1. Diffusive state

Assuming that a Gaussian beam illuminates an infinitely extended layer of ferrofluid, the formulation of the governing equations is more convenient in cylindrical coordinates (r, θ, z). To analyze the shape of the localized convective-diffusive microstructure formed by the absorption of the incident optical intensity and estimate the role of the microconvective fluxes, the previously established procedure is observed and the solution of the purely diffusive problem is initially obtained. Due to the separation of the timescales the thermal transport is purely conductive and the temperature equation obtained by substituting the Gaussian heat source in (2.5) has simple form, disregarding the secondary photoabsorption

$$\Delta T + \pi^2 e^{-\frac{r^2}{2\sigma^2}} = 0 \tag{5.1}$$

with $\Delta = \frac{1}{r}\frac{\partial}{\partial r}\left(r\frac{\partial}{\partial r}\right) + \frac{1}{r^2}\frac{\partial^2}{\partial \theta^2} + \frac{\partial^2}{\partial z^2}$ – the cylindrical Laplacian and the boundary condition (2.6) on the transversal walls. Additionally, the thermal perturbation should vanish as $r \to \infty$.

The problem (5.1) then yields an axially symmetric solution, which is obtained by applying the radial Hankel transformation

$$\hat{f}_\nu(s) = \mathcal{H}_\nu\{f(r)\} = \int_0^\infty r f(r) J_\nu(sr) dr \tag{5.2}$$

of order $\nu = 0$, with J_ν – Bessel's function of the same order, and making use of its principal property

$$\mathcal{H}_\nu\{\Delta_\nu f(r)\} = -s^2 \mathcal{H}_\nu\{f(r)\} \tag{5.3}$$

with $\Delta_\nu = \frac{1}{r}\frac{\partial}{\partial r}\left(r\frac{\partial}{\partial r}\right) - \frac{\nu^2}{r^2}$ to transform (5.1) to an ODE with constant coefficients. Taking account of the boundary condition (2.6) the transformed temperature field is expressed without difficulty

$$\hat{T}_0(s, z) = K_0(s)\left[1 - \frac{Bi}{f_s(s)}\cosh(sz)\right] \tag{5.4}$$

with

$$K_0(s) = \pi^2 \frac{\sigma^2}{s^2} e^{-\frac{\sigma^2 s^2}{2}} \tag{5.5}$$

and $f_s(s) = s\sinh(sl) + Bi\cosh(sl)$.

The corresponding stationary concentration field established by the equilibrium of thermophoretic, diffusive and magnetophoretic fluxes is governed by the condition (3.7) and the corresponding distribution of the demagnetizing field is described by (3.5).

In the following only the case of the transversally oriented external field $\boldsymbol{h} = (0,0,1)$ will be considered, because this configuration yields an axially symmetric solution. The zero-order Hankel transformation (5.2) is then applied to the problem (3.7), (3.5) and making use of the temperature distribution (5.4) the concentration and demagnetizing field perturbations are obtained in the *s*-domain

$$K_H(s) = -\frac{s_m}{\mathcal{M}_{ph}} \frac{Bi}{f_s(s)} K_0(s) \tag{5.6}$$

$$\hat{C}_0(s,z) = K_c(s)\cosh(r_s z) - s_m K_0(s) \tag{5.7}$$

$$\hat{H}_0(s,z) = K_H(s)\cosh(sz) + \frac{1}{\mathcal{M}_{ph}} K_c(s)\cosh(r_s z) \tag{5.8}$$

with $r_s(s) = \sqrt{\frac{s^2}{d_m}}$.

The coefficients K_c and K_H are expressed from the transversal boundary conditions (3.6) and (3.1)

$$K_c(s) = \frac{s_m}{d_m} \frac{s}{g_s(s)} K_0(s) \left[(d_m - 1) + \frac{Bi}{f_s(s)} e^{sl} \right] \tag{5.9}$$

$$K_H(s) = -\frac{s_m}{\mathcal{M}_{ph}} \frac{Bi}{f_s(s)} K_0(s) \tag{5.10}$$

with $g_s(s) = r_s \sinh(r_s l) + s\cosh(r_s l)$.

In turn, the inverse Hankel transformation is

$$f(r) = \mathcal{H}_\nu^{-1}\{\hat{f}_\nu(s)\} = \int_0^\infty s\hat{f}_\nu(s) J_\nu(sr) ds \tag{5.11}$$

and the spatial distributions of the fields in real variables are expressed by the integrals

$$T(r,z) = \int_0^\infty s\hat{T}_0(s,z) J_0(sr) ds \tag{5.12}$$

$$C(r,z) = \int_0^\infty s\hat{C}_0(s,z) J_0(sr) ds \tag{5.13}$$

$$H(r,z) = \int_0^\infty s\hat{H}_0(s,z) J_0(sr) ds \tag{5.14}$$

The set of integrals (5.12)-(5.14) can be evaluated numerically, in this case the upper limit is replaced by an appropriate cut-off radius depending on the required tolerance.

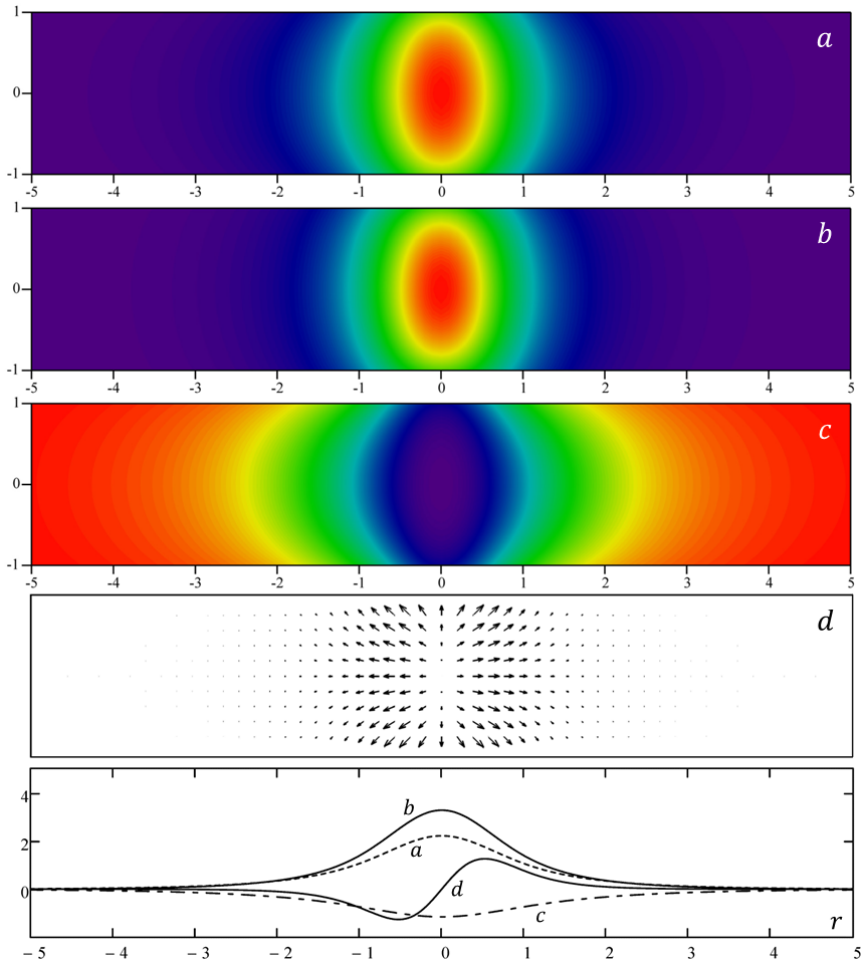

Figure 5.1. Diffusive base state of the localized photoabsorptive microstructure: from top to bottom - spatial distributions of *(a)* temperature T, *(b)* concentration C and *(c)* demagnetizing field H perturbations, *(d)* vector plot of the resulting magnetic force $C\nabla H$, corresponding radial profiles of the transversally averaged distributions: *(a)* $\langle T\rangle_z$, *(b)* $\langle C\rangle_z$, *(c)* $\langle H\rangle_z$, *(d)* $\langle C\rangle_z \frac{\partial}{\partial r}\langle H\rangle_z$.

The *r-z* distributions of the corresponding fields calculated according to (5.12)-(5.14) are plotted on Figure 5.1 for the case of the variance $\sigma^2 = 0.2$. The particular value $\sigma = \sqrt{0.2}$ is chosen because the resulting distribution of the absorbed optical intensity approximately corresponds to a single period of the $\frac{1}{2}[1 + \cos(\pi y)]$ distribution employed previously (2.5), which allows qualitative comparison with the extended systems. The obtained profiles show

the exponential decay of the field perturbations with the radial distance from the center of the beam and the microstructure is well localized.

There is notable difference between the structures of the localized and extended photoabsorptive formations calculated previously (Figure 3.4). The dissipation of the thermal energy within the localized microstructure is accomplished by two mechanisms – radial dissipation, which is suppressed in the extended gratings by the presence of the neighboring elements and the transversal dissipation through the boundaries of the layer. The later mechanism is limited to the area of a single period of the grating for each of its elements, while the localized element can technically dissipate heat through the whole boundary. Of course, the most intensive heat flux is located near the center of the beam. This distinction causes the presence of intensive transversal thermal gradients in the elements of the extended gratings and the corresponding mass fluxes. The decoupled thermophoretic flux is compensated by the coupled diffusive and magnetophoretic fluxes. The transversal magnetophoresis apparently plays a significant role in the formation of extended photoabsorptive microstructures, while on the other hand in the localized ones it is not so pronounced and the shape of the microstructure is determined mostly by the equilibrium of thermophoretic and diffusive fluxes.

Consequently, the calculated profile of the magnetic force in the localized microstructure (Figure 5.1 *(d)*) also differs from such within the element of the extended grating (Figure 3.4) in the perpendicular configuration of the external field. The near-wall contributions are not so pronounced in comparison with the bulk contributions and their direction is reversed. The bulk magnetic force is directed outward from the center of the localized microstructure, while in the extended gratings the bulk contributions are directed vertically, i.e. along the transversally applied external field. The distribution of the magnetic force is obviously not potential and will inevitably promote some form of magnetic microconvection leading to the redistribution of the ferroparticles, but evidently the non-potential component of the magnetic force is not defining and the advective contributions may not be very significant.

5.2. Stationary microconvection

The consideration of the presence of the magnetoconvective fluxes within the localized photoabsorptive microstructure leads again to the set of equations (1.36)-(1.39), (3.5) with the boundary conditions (3.1), (3.6) and (3.70). Additional constraint imposed on the solution is the condition of eventual vanishing of the field perturbations with the radial distance from the center of the Gaussian beam $r \to \infty$. Because the problem is axially symmetric in the configuration of the transversally applied external magnetic field $\boldsymbol{h} = (0,0,1)$ it is reasonable to look for the initial solution of the convective-diffusive problem with the same symmetry.

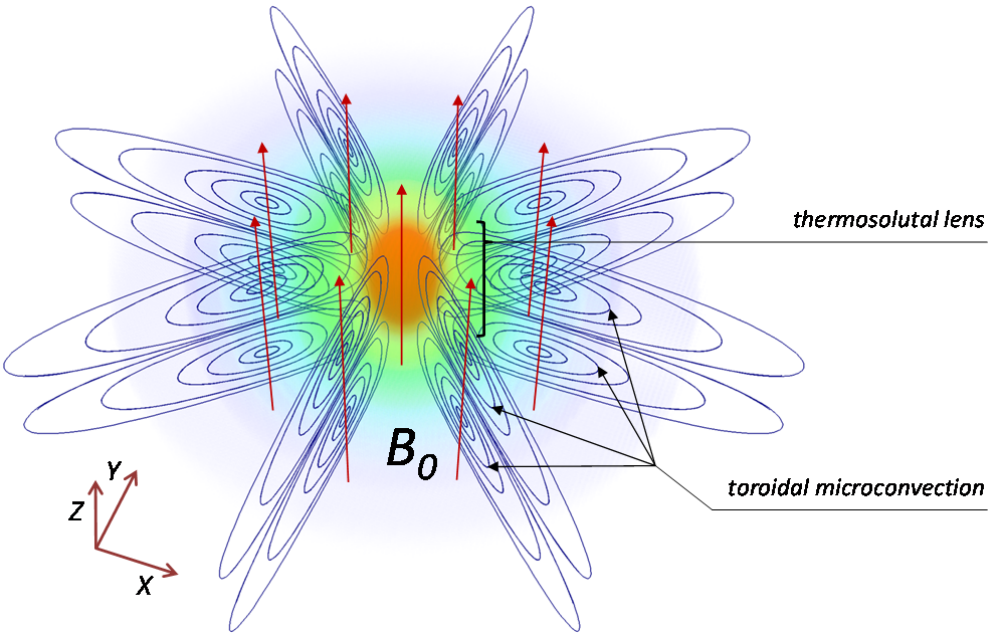

Figure 5.2. Definition of the problem: toroidal convective fluxes within the localized photoabsorptive microstructure formed by a Gaussian beam under the action of the perpendicular applied magnetic field.

The calculated magnetic force possesses no azimuthal component so initially the convective currents should take the form of a pair of coaxial toroidal vortices with their axis of rotation directed vertically along the applied field (Figure 5.2). This arrangement retains the full symmetry of the problem, the question of its stability is not considered at this point.

The obtaining of the spectral solution to the problem (3.64)-(3.70) is complicated for several reasons – unboundedness of the flow requiring the use of advanced numerical methods and the symmetry of the system necessitating the application of the cylindrical coordinates. The numerical solution is most convenient in finite volume formulation. The calculated

streamlines and stationary concentration profiles are plotted in Figure 5.3 for some values of the magnetosolutal Rayleigh number.

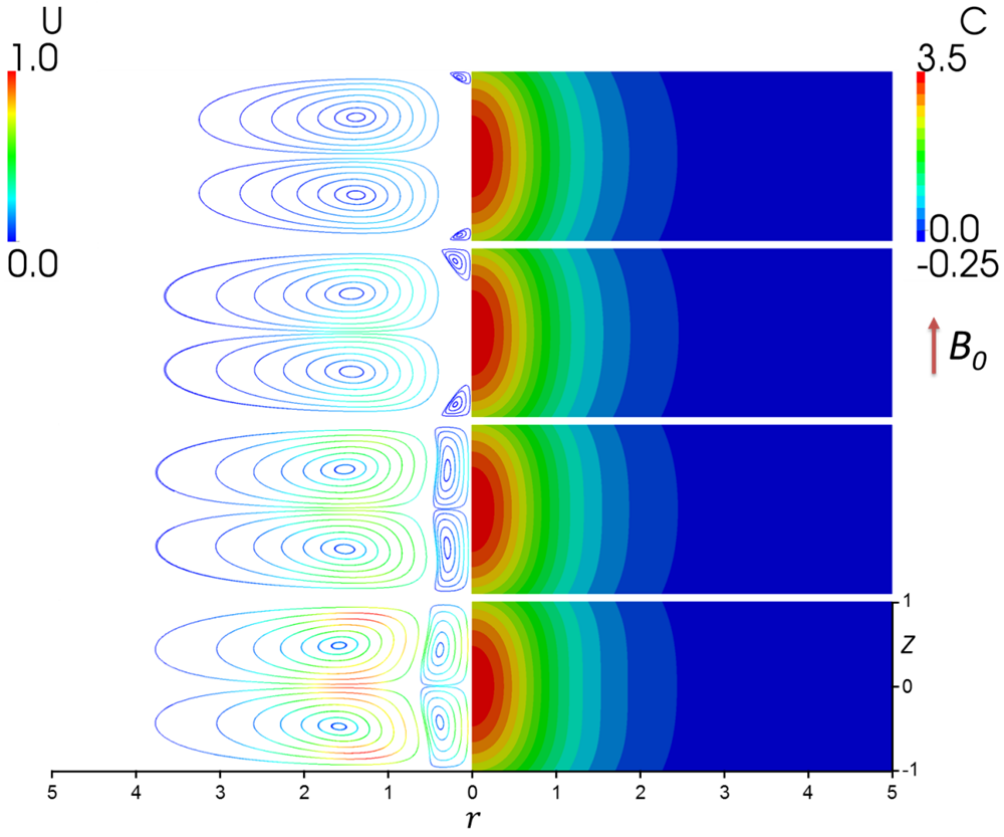

Figure 5.3. Computed streamlines (left) and concentration profiles (right) of the localized convective-diffusive microstructure for the values of the magnetosolutal Rayleigh number *(a)* $Rs_m = 100$ *(b)* $Rs_m = 200$ *(c)* $Rs_m = 500$ *(d)* $Rs_m = 1\,000$ (top to bottom)

The numerical simulations show that intensity of advective mass transport is not very substantial, it becomes comparable with the diffusive mechanism at approximately $Rs_m = 1\,000$ and in fact promotes slight homogenization of the concentration field in the transversal direction. The configuration of the convective flow is somewhat more interesting – as the value of the magnetosolutal Rayleigh number is increased a second pair of toroidal vortices appears near the symmetry axis of the microstructure. The secondary vortices begin to grow and eventually displace the original pair from the center of the Gaussian beam spot at some $Rs_m = 200 \ldots 500$. Intuitively, it is clear that such structure of the flow is unstable and is only realized in the numerical simulation due to the artificially imposed axial symmetry.

In fact, the formation of the corresponding secondary circulations has also been observed within the elements of the bidirectional grids (Figure 4.3) leading to the subsequent loss of stability. It can be hypothesized that the localized photoabsorptive formations can be similarly destabilized by the emergence of azimuthal convective currents.

5.3. Azimuthal instability

In order to determine the reliability of the previously obtained numerical solution its stability with respect to higher azimuthal modes must be examined. Such analysis requires the formulation of the linearized stability problem analogous to the previously solved system (3.162)-(3.164), (3.5) with the corresponding boundary conditions (3.1) and (3.6) and no-slip condition for velocity perturbation, which would eventually yield the dispersion relation and the neutral curves. Clearly, the direct approach to the formulation of this problem is prohibitively complex for the same reasons as were earlier described for the impracticality of the spectral solution of the stationary problem so some approximations would be desirable.

The previous calculations show that the stationary toroidal convective fluxes are not intense, do not exert significant influence on the concentration field and only cause a slight homogenization of its transversal profile. There is then the possibility to concentrate on the emerging lateral motions within the plane of the ferrofluid layer and decrease the complexity of the problem by reducing the transversal direction. At the same time, it is necessary to retain some degree of generality with respect to the thickness of the ferrofluid layer so as not to limit the validity of the assumptions to infinitely thick or very narrow layers, because in the conditions of real experiments neither is usually true.

To formulate a slightly simpler stability problem the equations (3.162) and (3.164) are averaged across the transversal direction, adopting the notation (3.159)-(3.161) for the convective-diffusive base state and the corresponding infinitesimal perturbations. The averaging of the Stokes equation (3.162) with account to the parabolic profile (2.11) for $\tilde{\boldsymbol{u}}$ yields the already familiar linearized Darcy-Stokes equation (2.21) with Brinkman's term

$$-\boldsymbol{\nabla}_\perp p + (\Delta_\perp - \beta)\langle\tilde{\boldsymbol{u}}\rangle_z + Rs_m\left(\tilde{c}\boldsymbol{\nabla}_\perp\langle H\rangle_z + \langle C\rangle_z\boldsymbol{\nabla}_\perp\tilde{h}\right) = \mathbf{0} \tag{5.15}$$

where it has been assumed that the infinitesimal perturbations $\tilde{c}(r,\theta)$ and $\tilde{h}(r,\theta)$ of the concentration and demagnetizing fields are independent of the transversal coordinate. While intuitively such assumption might seem rather coarse, numerical simulations of the evolution of the localized convective-diffusive microstructure above the threshold of the azimuthal instability show that it is surprisingly accurate even for finite amplitude perturbations.

In turn, the averaging of the concentration balance equation is straightforward

$$\frac{\partial \tilde{c}}{\partial t} = \Delta_\perp \tilde{c} - \langle \tilde{\boldsymbol{u}} \rangle_z \boldsymbol{\nabla}_\perp \langle C \rangle_z \tag{5.16}$$

taking into account that the term $\boldsymbol{U}\boldsymbol{\nabla}\tilde{c}$ vanishes after averaging due to the axial symmetry of the primary toroidal convective circulation and the assumed transversal homogeneity of the concentration perturbation. The influence of the lateral magnetophoresis also disappears for the same reason by virtue of the equation (3.5).

Taking the *curl* of the equation (5.15) and introducing the polar stream function $\tilde{\psi}$ in the following form

$$u_r = \frac{1}{r}\frac{\partial \tilde{\psi}}{\partial \theta},\ u_\theta = -\frac{\partial \tilde{\psi}}{\partial r} \tag{5.17}$$

with $\langle \tilde{\boldsymbol{u}} \rangle_z = u_r \mathbf{e}_{\boldsymbol{r}} + u_\theta \mathbf{e}_{\boldsymbol{\theta}}$, the equation for $\tilde{\psi}$ is obtained after some transformations

$$(\Delta_\perp - \beta)\Delta_\perp \tilde{\psi} + Rs_m \left(\frac{1}{r}\frac{\partial \tilde{c}}{\partial \theta}\frac{\partial}{\partial r}\langle H \rangle_z - \frac{1}{r}\frac{\partial \tilde{h}}{\partial \theta}\frac{\partial}{\partial r}\langle C \rangle_z \right) = 0 \tag{5.18}$$

The numerical solution to (5.16) and (5.18) can be found by applying the Galerkin method and the following ansatz is adopted

$$\tilde{c}(r,\theta) = \sum_{m=0}^{N_c} \hat{c}_m \cos\left(\frac{\pi m r}{R_c}\right) \cos(\mathrm{K}\theta) \tag{5.19}$$

$$\tilde{\psi}(r,\theta) = \sum_{m=1}^{N_\xi} \hat{\psi}_m F_{Km}(r) \sin(\mathrm{K}\theta) \tag{5.20}$$

which transforms the unbounded problem into a bounded one with R_c – the cut-off radius and K is the azimuthal wavenumber. The convergence of the solution with respect to the size of the expansions N_c, N_ξ and R_c is required.

The radial expansion of the polar stream function is performed making use of the Chandrasekhar's cylindrical functions $F_{Km}(r)$ [95]

$$F_{Km}(r) = J_K\left(\alpha_m \frac{r}{R_c}\right) + B_m Y_K\left(\alpha_m \frac{r}{R_c}\right) + C_m I_K\left(\alpha_m \frac{r}{R_c}\right) + D_m K_{\mathrm{K}}\left(\alpha_m \frac{r}{R_c}\right) \tag{5.21}$$

where J_K, Y_K, I_K, K_{K} are the Bessel and modified Bessel functions of the first and second kind of order K, following the conventional notation; the coefficients B_m, C_m and D_m depend on α_m and K. The characteristic values α_m and the corresponding functions $F_{Km}(r)$ satisfy the characteristic equation

$$\left(\frac{d^2}{dr^2}+\frac{1}{r}\frac{d}{dr}-\frac{\mathrm{K}^2}{r^2}\right)^2 F_{Km}=\alpha_m F_{Km}(r) \tag{5.22}$$

and the boundary conditions

$$[\partial_r F_{Km}=F_{Km}=0]_{\substack{r\to 0\\ r=R_c}} \tag{5.23}$$

What remains is the determining of the relationship between the perturbations of the demagnetizing field and concentration. It follows from the equations (3.5) along with the boundary conditions (3.6) and can be obtained by several methods – either as the boundary integral by the application of the Green's function method [96] or by integral transform. For the problems in cylindrical coordinates the latter approach seems more convenient because it allows separating the azimuthal modes in a straightforward way.

The application of the Henkel transformation to the problem (3.5)-(3.6) simplifies the cylindrical Laplacian and the solution is not complicated

$$\tilde{h}(r,\theta)=-\tilde{\alpha}_c\sum_{m=0}^{N_c}\hat{c}_m H_m(r)\cos(\mathrm{K}\theta) \tag{5.24}$$

with

$$H_m(r)=\frac{1}{2l}\int_0^\infty(1-e^{-2ls})J_{\mathrm{K}}(sr)\int_0^\infty r\cos\left(\frac{\pi m r}{R_c}\right)J_{\mathrm{K}}(sr)dr\,ds \tag{5.25}$$

where the transversal coordinate has been reduced by averaging across the gap of the layer.

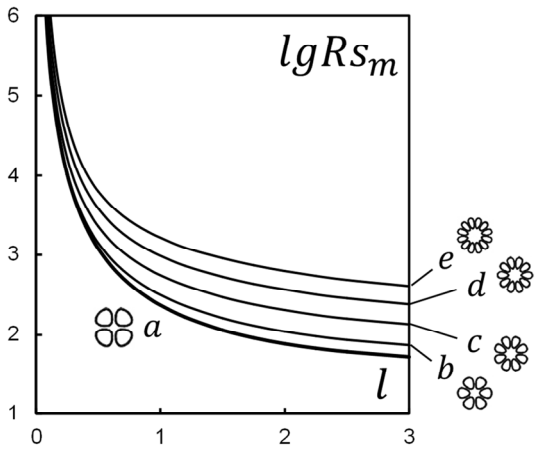

Figure 5.4. Neutral curves of the azimuthal instability for different azimuthal modes: *(a)* $\mathrm{K}=2$, *(b)* $\mathrm{K}=3$, *(c)* $\mathrm{K}=4$, *(d)* $\mathrm{K}=5$, (e) $\mathrm{K}=6$.

Projecting the governing equations (5.16) and (5.18) onto the modes of the expansions (5.19), (5.20) and (5.25) the dispersion relation is obtained and the neutral curves are determined for different azimuthal modes (Figure 5.4). The solutions corresponding to different values of the azimuthal wavenumber K consist of a set of vortices positioned symmetrically around the axis of the laser beam. The number of the vortices corresponds to the value 2K and the primary critical mode is the one with $\mathrm{K}=2$, corresponding to a set of 4 vortices.

The motions described by different arbitrary values of the azimuthal wave-number K along with the expected deformations of the concentration field are shown in Figure 5.5.

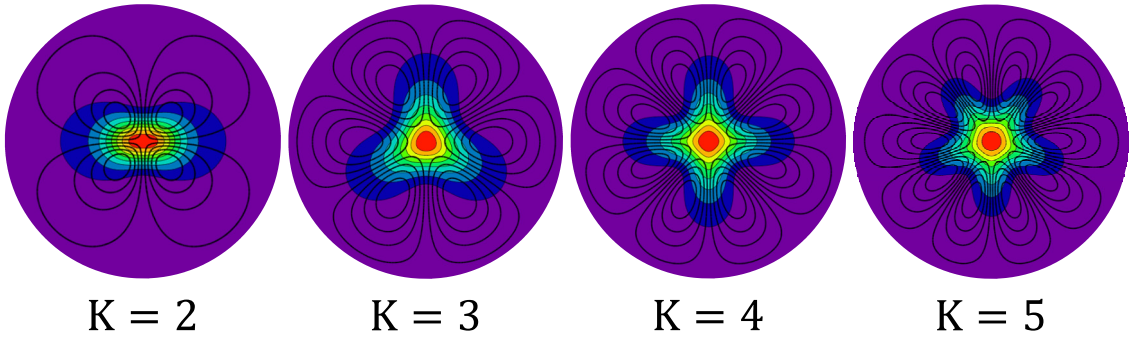

Figure 5.5. Calculated azimuthal motions and the corresponding expected deformations of the concentration field.

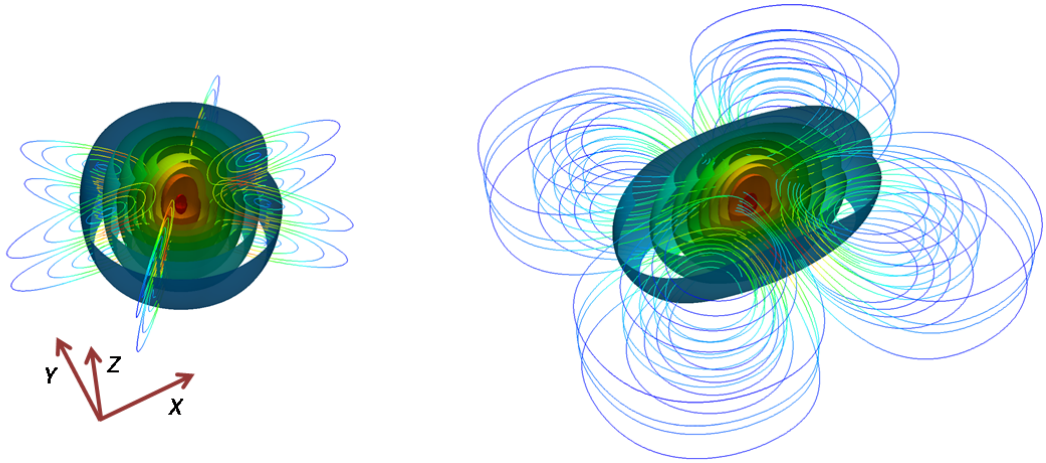

Figure 5.6. Numerical simulation of the localized photoabsorptive microstructure above the threshold of the azimuthal instability at $Rs_m = 500$: left – symmetric base state, right – convective symmetry breaking (convective streamlines and concentration contours).

It seems that the concentration field can form different shapes above the threshold of the instability. Apart from simple elongations of the concentration distribution, more complicated configurations are possible with higher azimuthal wave-numbers – triangular, quadratic, pentagonal and others.

The numerical simulations of the evolution of the localized photoabsorptive microstructure above the threshold of the instability confirm the principal conclusions of the approximate linear model. The establishing of the stationary lateral circulation was observed at certain arbitrary values of the control parameter (Figure 5.6). The calculations evidence that the mode $K = 2$ is indeed the most unstable one.

Discussion

In the previous sections the problems of formation, evolution and stability of the extended and localized convective-diffusive microstructures formed by photoabsorption and the subsequent simultaneous interactions of the gradients of temperature, concentration and demagnetizing field in non-isothermal and inhomogeneous ferrodispersions have been consequently considered. By the application of theoretical and numerical methods it was demonstrated that rather than simple modulations of concentration and magnetic field the fotoabsorptive formations can possess complex internal structure generated by the reciprocal interactions of phoretic and advective currents.

Yet, the discussed possibility of the existence of magnetoconvection within the photoabsorptive microstructures does not necessarily imply its presence or significance in the conditions of real experiments. Many of the results of the experimental measurements seemingly signifying the influence of magnetic microconvection in photoabsorptive systems can well be interpreted in terms of phoretic transport or magnetostatic effects. Also, the presence of transversal microconvection is not easily discerned by the direct visualizations of the regular photoabsorptive formations, as it initially possesses the same symmetries unless the destabilization of the microstructures takes place. It is then the purpose of this section to interpret some available experimental observations of the formation and evolution of the magnetic photoabsorptive microstructures accommodating the influence of the magnetoadvective transport.

Extended grating

Firstly, the formation of the extended concentration grating with interfringe 30 μm was observed in a 100 μm thick ferrofluid cell under the influence of a uniform external magnetic field with adjustable magnitude oriented along the direction of the imposed photoabsorptive thermal modulation [94], i.e. in the parallel direction. The experiments were performed by Dr. A. Mezulis (Laboratory of Heat and Mass Transfer, IPUL).

The employed ferrofluid was a magnetite based solution in n-tetradecane, with steric stabilization (oleic acid was used as surfactant). The relevant parameters of the sample TD-5 are summarized in Table 5.1., the volume concentration of the ferroparticles was 2.3%.

Table 5.1. Parameters of the ferrofluid samples [94]

Parameter	TD-5	207BNE	
solvent density ρ_s	800	875	kg m^{-3}
viscosity η	0.002	$5.9 \cdot 10^{-4}$	Pa s
thermal conductivity λ	0.12	0.14	W (m K)$^{-1}$
specific heat capacity c_p	2100	1670	J (kg K)$^{-1}$
particle density ρ_p	5200	5200	kg m^{-3}
diffusivity D	$1.2 \cdot 10^{-11}$	$6.2 \cdot 10^{-11}$	m^2 s^{-1}
Soret coef. S_T	0.16	0.16	K^{-1}
magnetic diameter d_m	7.3	9.1	nm
spontaneous magnetization M_s	$4.9 \cdot 10^5$	$4.9 \cdot 10^5$	A m^{-1}

Instead of the usual FRS setup, the photoabsorptive grating was created by illuminating the metallic mask with periodically spaced slits by a high pressure mercury lamp. The total incident intensity of the optical grating was $\sim 27\ mW$ focused in a circle of diameter $\sim 1\ mm$. The evaluation of the characteristic temperature difference has yielded the value of about $\sim 0.1\ K$. The values of the dimensionless parameters calculated for the intensities of the magnetic field employed in the series of experiments are summarized in Table 5.2.

The measured quantity in a FRS setup is the diffracted intensity of the probe laser beam, which illuminates the index grating corresponding to the forming concentration microstructures. Figure 5.7 shows the time dependence of the square root of the measured diffracted intensity in a series of experiments with different field strengths. The value of this quantity is proportional to the magnitude of first parallel mode of the induced concentration perturbation $\sqrt{I_d} \sim C_1$ [93]. The value $\sqrt{I_d}$ is compared to the L^2-norm $J(t)$ (3.157), which is obtained from the numerical calculations by finite volume integration of (3.64)-(3.70).

Table 5.2. Dimensionless parameters (grating experiments)

$\mathbf{B_0} \parallel \nabla T$	0 mT	20 mT	30 mT	40 mT	60 mT	80 mT	120 mT
$\tilde{\alpha}_c$	-	1	1	1	1	1	1
$\mathcal{M}_{ph}$	-	0.01	0.02	0.03	0.05	0.08	0.12
s_m	-	1.01	1.02	1.03	1.05	1.08	1.13
Rs_m	-	5	11	16	30	43	62
$\frac{\overline{\Delta c}[H]}{\overline{\Delta c}[0]}$	1.0	0.99	0.98	0.97	0.95	0.92	0.89

The time evolution of $J(t)$ is determined from the simulations of the formation stage of the concentration grating for the parameters in Table 5.2. Much information can be gained from the comparison of the experimental and calculated data (Figure 5.7). For convenience all series have been normalized by the corresponding zero-field saturation values.

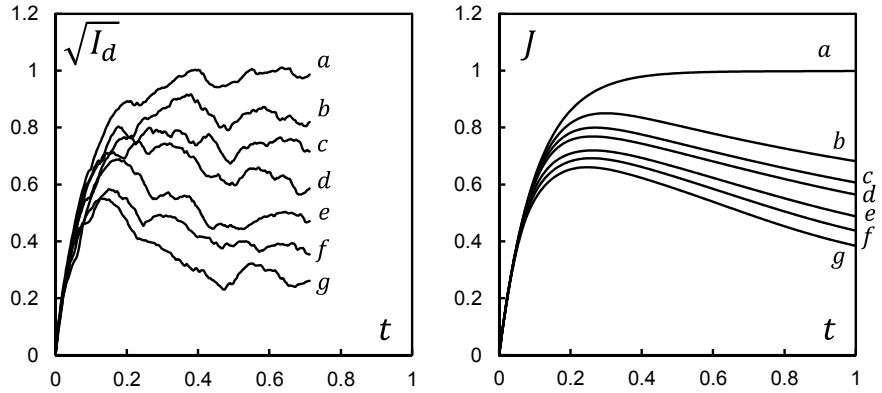

Figure 5.7. Formation of the concentration grating, establishing of the stationary state in the parallel applied field: experimental measurements of the diffracted intensity (left, courtesy of Dr. A. Mezulis) and corresponding numerical calculations (right) at *(a)* zero field *(b)* $20\ mT$, *(c)* $30\ mT$, *(d)* $40\ mT$, *(e)* $60\ mT$, *(f)* $80\ mT$, *(g)* $120\ mT$.

The notable evidence of the influence of microconvective transport is the somewhat relaxational character of the measured diffracted signal after the initially attained maximum. In fact, despite rather small values of the magnetic solutal Rayleigh numbers, such behavior cannot be explained by any phoretic process and is a clear sign of microconvection. Comparing the calculated and measured time dependencies of the appropriate quantities it is possible to conclude that the correspondence is not perfect, but is still meaningful, taking into account the absence of the approximation parameters. Certainly, the qualitative comparison is possible at the least.

Some of the main factors for the quantitative discrepancy between the calculations and the experimental measurements seem to be the large aspect ratio of the thickness of the ferrofluid layer to the interfringe of the induced photoabsorptive grating as well as the polydispersity of the studied sample. The magnetic core size distribution can be obtained by the method of magnetic granulometry. In fact the magnetic diameters were approximately in the range between 5 and 10 *nm* yielding the averaged value of 7.3 *nm*. This leads to two notable conclusions. First of all, larger magnetic nanoparticles have greater magnetophoretic mobility.

Secondly, the relative contribution of the certain size fraction to the diffracted intensity is proportional to the sixth power of its diameter $\sim d^6$ [94]. Then the visibility of the larger particles is far greater than that of the smaller ones. The models of the polydisperse mixtures are, however, outside the scope and focus of this work and will not be discussed further.

Considering the dynamics of the evolution of the grating, it seems that the presence of microconvection significantly slows down the formation of the stationary state, especially at lower values of the magnetic solutal Rayleigh numbers as compared with the phoretic process alone. At higher fields, the evolution of the measured diffracted signal reaches the stationary state rather quickly, somewhat faster than predicted by the theory. It can then be concluded that in this case the effective value of the Rayleigh number is greater than the one predicted due to the presence of some contributing factor. Additional calculations show that the observed rapid establishing of the stationary regime takes place at $Rs_m \sim 250$. Such discrepancy can be explained by the deformation of the assumed symmetric configuration of the perturbations with respect to the midplane of the layer, since the dependence of the solutal Rayleigh number on the characteristic dimensions is very strong (Section 2.1). This effect should be more pronounced in photoabsorptive gratings with larger aspect ratios, such as the one considered here.

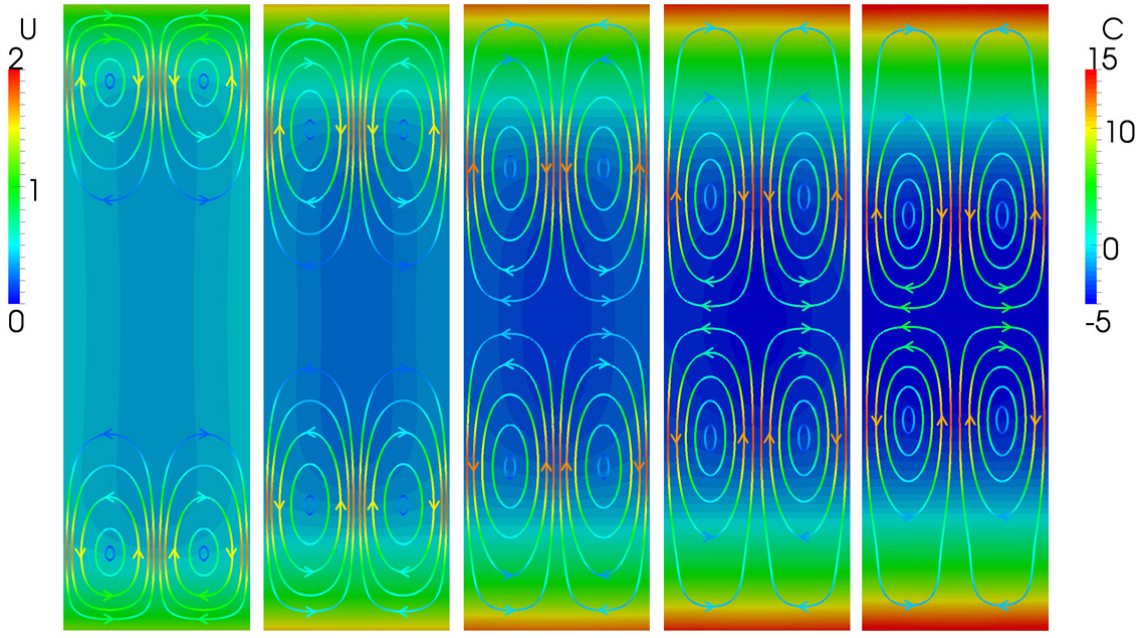

Figure 5.8. Formation of the concentration grating, establishing of the stationary state in the parallel applied field of $120\,mT$. The calculated contours of the concentration field and convective streamlines at time moments $t = 0.2, 0.4, 0.6, 0.8, 1.0$.

For the purpose of gaining understanding of the dynamics of the measured diffracted signal during the formation stage of the concentration grating it is appropriate to consider the microscopic evolution of the element photoabsorptive convective-diffusive microstructure. In the large aspect ratio structures the process of formation of the concentration profile possesses peculiarities and begins at the boundary regardless of the sign of the Soret coefficient.

Initially, the interaction of the concentration boundary layer with the gradient of the corresponding demagnetizing field creates two sets of convective rolls near the opposite sidewalls of the ferrofluid layer (Figure 5.8). The concentration front, which is advanced by the interaction of the thermophoretic and magnetophoretic fluxes, then, drives these rolls to the center of the layer, all the while the microconvection acting to homogenize the concentration perturbation that creates it and slow down the evolution of the concentration profile.

If the symmetry of the field perturbations across the midplane of the layer is broken then the asymmetric contributions cannot be neglected anymore. Qualitatively this means that one of the pairs of the convective rolls will begin to suppress the other pair with the increase of the control parameter, leading to the increase of the effective Rayleigh number for the dominating set of rolls. In fact, the measurements of the intensity of the beam exiting the ferrofluid layer show considerable decrease as compared with the entering beam, which can as well lead to the asymmetry of the field profiles across the midplane of the layer. Unfortunately, the present model cannot account for the asymmetric terms, but their presence does not seem to change the qualitative picture of the process.

Bidirectional grid

In turn, a bidirectional photoabsorptive grating can be created in the same fashion by illuminating the ferrofluid layer through an array of square openings in a metallic stencil. A ferrofluid sample 207BNE, magnetite based solution in toluene (Table 5.1) with 3.3% volume fraction of the solid phase, was employed for this particular experiment. The optical grid formed by the metallic stencil was focused within the ferrofluid layer. The period of the imposed optical modulation constituted $75\mu m$ in both directions, the thickness of the layer remained at $100\mu m$. The calculations of the photoabsorptive thermal nonhomogeneities predict the characteristic temperature difference in the range ~0.5-0.6K.

The measurements were performed in the parallel configuration of the external magnetic field, applying the field along one of the preferred orientations. During the set of experiments the

intensity of the optical pumping remained unchanged and the magnitude of the external field was varied from $3mT$ to $50mT$. The calculated values of the necessary dimensionless parameters corresponding to magnetic field strengths employed during the series of the measurements are summarized in Table 5.3.

Table 5.3. Dimensionless parameters (grid experiments)

$\mathbf{B_0} \parallel \nabla T$	0 mT	3 mT	10 mT	20 mT	30 mT	40 mT	50 mT
$\tilde{\alpha}_c$	-	1	1	1	1	1	1
$\mathcal{M}_{ph}$	-	0.0	0.02	0.06	0.12	0.17	0.23
s_m	-	1.0	1.02	1.06	1.12	1.18	1.24
Rs_m	-	95	1670	4530	7680	10 450	12 390
$\frac{\overline{\Delta c}[H]}{\overline{\Delta c}[0]}$	1.0	1.0	0.98	0.94	0.89	0.85	0.81

The dimensional analysis predicts rather weak magnetophoretic effects, the diffusive mobility of the ferroparticles is increased by not more than approximately 20% in the direction of the field, but the magnetosolutal Rayleigh number reaches considerable values, owing to the larger characteristic temperature difference and interfringe than in the grating experiments.

The intensity of the diffracted component of a scanning laser beam was measured in both directions – parallel $I_d^{\parallel}$ and longitudinal $I_d^{\llcorner}$. The square root of these signals is compared with the corresponding quantities $J_{\parallel}$ and $J_{\llcorner}$ (4.1) calculated from the numerical model for the parameters of the experiment (Figure 5.9). The experimental setup did not allow the measurements in zero field, but the imposed magnetic field could be reduced to the lowest value of $3mT$. To exclude the coefficients of proportionality between the measured and calculated values the measured diffracted intensities are normalized by the maximum value in the lowest field and the same is done with the calculated curves, which are normalized by the maximum of the parallel signal $J_{\parallel}$.

The observations of the formation stage of the bidirectional photoabsorptive grid already point to the strong influence of the microconvective effects. The longitudinal signal is affected very little at higher fields comparing with its dynamics in low fields, but the mixing in the direction of the imposed external field is significantly enhanced causing the attenuation of the amplitude of the concentration modulation in that direction. The characteristic primary maximum and consequent relaxation to the stationary state evidencing the presence of

microconvection is observed in the evolution of both the diffracted signal $I_d^{\parallel}$ and the calculated signal $J_{\parallel}$.

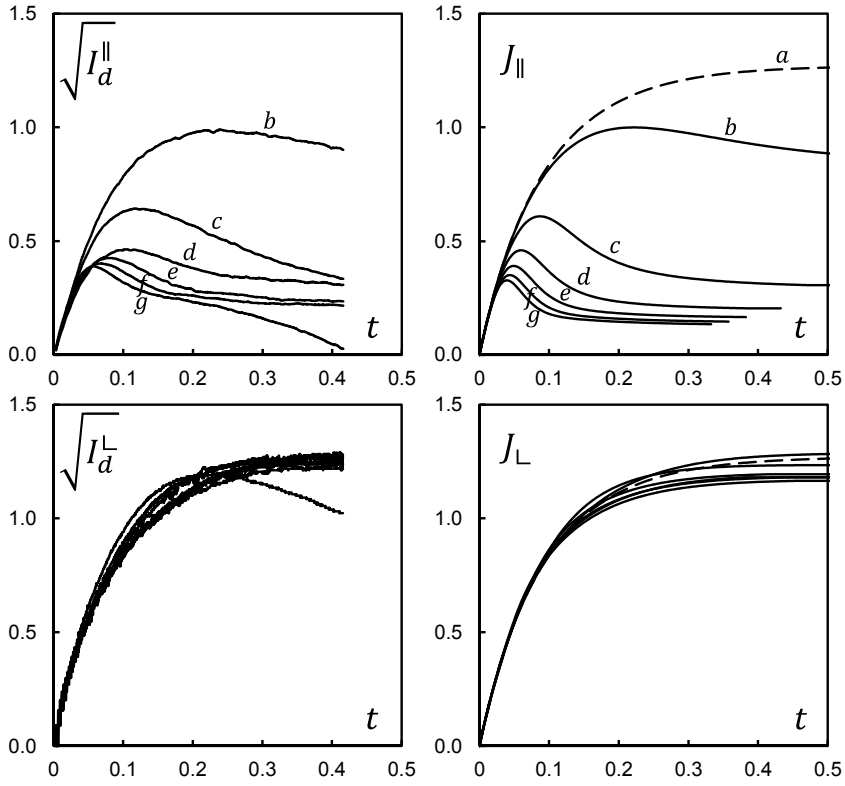

Figure 5.9. Formation of the bidirectional concentration grid, establishing of the stationary state in the parallel applied field: experimental measurements of the parallel $I_d^{\parallel}$ and longitudinal $I_d^{\perp}$ diffracted intensity (left, courtesy of Dr. A. Mezulis) and the corresponding numerical calculations of $J_{\parallel}$ and $J_{\perp}$ (right) at *(a)* zero field *(b)* $3\ mT$, *(c)* $10\ mT$, *(d)* $20\ mT$, *(e)* $30\ mT$, *(f)* $40\ mT$, *(g)* $50\ mT$.

Generally, the relaxation of the measured parallel diffracted intensity is slower than that of the calculated dependencies $J_{\parallel}$. This perhaps can be attributed to the polidispersity of the employed ferrofluid sample and different dynamics of the fractions. Otherwise, the correspondence is sufficient to confirm the presence and direction of the magnetic microconvection. Although in this case the similarity is much better than in the situation of the photoabsorptive grating, owing most probably to the lower aspect ratio of the induced microstructures, it can in part be accidental.

Symmetry breaking

The linear analysis of the stability of the extended photoabsorptive convective-diffusive microstructures, similar to those formed in ferrofluid layers in the framework of forced

Rayleigh scattering experiments, has yielded the limits for the values of the magnetic Rayleigh number within which the stability of the gratings is retained. Above the threshold of the instability the growth of the longitudinal perturbations is not dampened but is instead amplified and in parallel applied magnetic field the peristaltic stratification develops in the longitudinal direction, while in the perpendicular field the instability assumes the form of undulatory bending of the concentration front. In this regard, the parallel configuration of the external field seems to be relatively stable, while the perpendicular orientation is much less so. Still, the relatively high values of the magnetic Rayeligh number, which are necessary to cross the threshold of the peristaltic instability in parallel field, are quite reachable in the FRS experiments without significant difficulties.

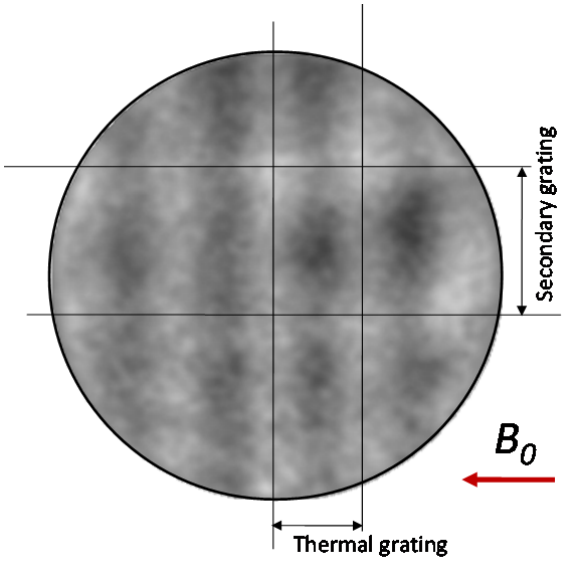

Figure 5.10. Holographic visualization of the photoabsorptive grating in parallel magnetic field (courtesy of Dr. A. Mezulis): the emergence of the secondary grating near the threshold

The formation of the peristaltic instability of the photoabsorptive grating was ascertained experimentally by the FRS procedure in a ferrofluid sample TD-5 [94] under the action of the parallel magnetic field. The period of the primary grating was 80μm and estimations showed that the induced thermal difference constituted about 0.5K-0.6K. The thickness of the ferrofluid cell was as previously 100μm. At the magnitude of the applied field of approximately 150mT the emergence of a microstructure similar to a secondary perpendicular concentration grating was observed (Figure 5.10).

The dimensional analysis shows that the critical threshold for the peristaltic instability in the parallel field corresponds to the imposed temperature difference of approximately 1K, which is slightly higher than the estimations. The ratio of the periods of the primary thermal and the emerging secondary gratings determined from the experiment was ~0.59. This corresponds very well with the longitudinal period of the critical peristaltic perturbation ~0.54 calculated from the stability analysis (Figure 3.14).

In turn, the loss of stability of a photoabsorptive concentration microstructure localized in a beam spot of a laser was observed by Luo, Du and Huang [68]-[69] upon the application of uniform vertical magnetic field. The ferrofluid layer with thickness 100 μm was illuminated by a focused laser beam with radius of 6.7 μm and power of 10 mW. Their employed magnetic fluid was a magnetite based solution in kerosene with 6% volume fraction of the solid component. The high intensity of the incident beam has produced rather large thermal differences due to photoabsorption. The authors reported the results of their numerical simulations of the temperature distribution within the layer: the temperature difference of ~15K was obtained between the center of the hot spot and the edge of the beam. The total fall off constituted approximately 40K at several beam widths. Such strong thermal gradients cause the formation of pronounced concentration inhomogeneities in colloidal dispersions. The Soret coefficient of the ferrofluid was large and positive ~0.1 K^{-1} as is characteristic for mixtures with steric stabilization.

In the absence of magnetic field the formation of a concentric interference pattern similar to Newton's rings was observed due to the reciprocal interaction between the incident laser beam and the photoabsorptive thermal lens, which is formed by the radial gradients of temperature and concentration contributing to the variation of the refractive index.

Upon the application of the vertical magnetic field in the direction along the beam axis, the transformation of the interference rings took place if the strength of the external field exceeded some threshold value. A triangle-shaped instability was reported and observations of differently shaped polygons – tetragons and pentagons - have been claimed.

The authors of [68] interpret the observed evolution of the interference patterns in terms of the *magnetoconvective instability* of the flat photoabsorptive concentration profile with initially circular symmetry. The proposed model is that of a system of six (eight or ten in the case of tetragons or pentagons) convective rolls with axes parallel to the axis of the beam emerging

within the concentration microstructure due to the bifurcation from the diffusive state. The deformation of the concentration profile is then the influence of the microconvective fluxes.

An alternative explanation was offered in [70], where it was pointed out that the intense thermal gradients can eventually cause significant thermophoretic depletion of the ferroparticles in the beam spot. The expulsion of the ferroparticles from the heated region leads to the formation of a non-magnetic "bubble" immersed in magnetic liquid. The magnetic forces on the surface of the bubble can be interpreted in terms of the magnetic surface tension. The observed formation of the polygons can then be explained in terms of the magnetostatic *shape instability*.

While both approaches seem to be valid and have been observed in principle in different systems, additional considerations evidence in favor of the hydrodynamic effects driving the instability [71].

Although the formation of different shapes via azimuthal hydrodynamic instability of a localized photoabsorptive microstructure is consistent with the analysis of Section 5.3, the interpretation of the observed effect in terms of the magnetic microconvection is neither simple nor clear. The experimental procedure employed considerable thermal differences and very strong thermal gradients owing to the focusing of the laser beam. In such conditions the thermomagnetic effect may be sufficiently strong to influence the convective motion. Also, the optical index variation was formed generally by the thermal contribution and not the concentration contribution as it was in the case of the previously discussed FRS procedures in the application to ferrofluids. In this regard the visualization of the beam spot yields information exclusively about the shape of the thermal perturbation, while the solutal constituent remains concealed. The intensity of the convective motion is then sufficient to deform also the temperature field. It remains to conclude that the model based on just the magnetosolutal convection cannot describe the observed effects.

At this time it is unclear, what is the character of interactions of the solutal and thermal mechanisms of the magnetic buoyancy in such localized systems and the relative role of the respective contributions in the formation of magnetoconvection. While some attempts have been made to approach the magnetic convection in cylindrical systems [103]-[104] the conclusions are not readily applicable to localized photoabsorptive microstructures and more specific investigations are required.

Final remarks

In this work the formation, evolution and stability of extended and localized photoabsorptive microstructures in non-isothermal and inhomogeneous ferrodispersions have been consequently considered in the presence of the applied uniform magnetic field in different configurations on the grounds of the pseudohomogeneous mixture model.

The starting point for the investigation was the plane hydrodynamic instability of a flat array of periodic concentration stripes. The formulation of this problem should qualitatively correspond to the application of a Forced Rayleigh scattering technique in very thin ferrofluid layers. A nonlinear Lorenz-type model based on selective truncation of the modes was proposed for the formation and relaxation scenarios in a weakly nonlinear regime.

1. It was ascertained that the emergence of the lateral circulation would lead to the enhancement of the mass transport in both parallel and perpendicular configurations of the applied magnetic field manifesting in the increase of the measured diffusion coefficient and the corresponding decrease of the Soret coefficient.
2. In turn, the formation of the convective currents can occur only through the breaking of the translational symmetry of the grating and implies the presence of the critical threshold.

The limits of applicability of the thin layer approximation are very narrow and degenerated microstructures are rarely observed in the real conditions. The subsequent consideration of the transversal profile was found to be crucial to the understanding of the mass transport processes in photoabsorptive microstructures in magnetizable dispersions and leads naturally to the notion of the photoabsorptive convective-diffusive microstructures.

3. It was determined that the magnetic microconvection is an important and integral component of the photoabsorptive mass transport in ferrofluids under the action of the external magnetic field.
4. The calculations show the significant role of the transversal boundary and in this regard the two principal driving mechanisms of magnetoconvection have been observed.

In parallel field the convective fluxes are driven by the induced bulk nonhomogeneities of the ferroparticle concentration and the associated gradients of the demagnetizing field. In turn, in the perpendicular field configuration the main mechanism is related to the interaction of the concentration perturbation with the discontinuity of the normal component of the magnetic field.

The calculations of the formation and relaxation of the extended photoabsorptive microstructures with account to the transversal microconvection demonstrate the considerable role of the magnetoadvection in the lateral mass transport.

5. It was concluded that the principal direction of the lateral magnetoadvective currents corresponds both to the magnetophoretic mass fluxes and to the expected influence of the interparticle interactions on the mass transport coefficients, which considerably complicates the separation and interpretation of these effects in the conditions of the experiment.
6. The transversal circulation emerges without the presence of a distinct threshold and does not violate the initial symmetry of the photoabsorptive microstructures, in contrast to the appearance of the previously considered lateral convective circulations in very narrow layers.

Consequently, it was recognized that the magnetic fotoabsorptive formations possess complex internal structure generated by the reciprocal interactions of phoretic and advective currents.

In turn, the subsequent consideration of the problem of stability of the extended and localized photoabsorptive microstructures has shown richness of behavior and diverse bifurcating regimes.

7. It was shown that the translational symmetry of the extended convective-diffusive microstructures in parallel applied field can be broken by a peristaltic perturbation leading to the eventual longitudinal stratification; while in the perpendicular field the undulatory bending of the concentration front may occur.
8. The comparing of the results of stability analysis in thin layer approximation and with account for the transversal direction has revealed the existence of the regime of efficient mixing responsible for the enhanced stability of the photoabsorptive gratings in the parallel configuration of the applied magnetic field.

In this regard, the normal field configuration is unstable and the parallel configuration is somewhat stable.

9. The destabilization of the bidirectional photoabsorptive grid and the eventual reduction of the order of its rotational symmetry in the configuration of the perpendicular external field were noted in numerical calculations, but are yet to be established in real observations.

The formation of the bidirectional grids of the photoabsorptive convective-diffusive microstructures was considered by numerical simulations and the principal similarities between the grids and extended gratings were noted.

In turn, the simulations of the localized photoabsorptive formations within the beam spot of a Gaussian beam showed small influence of the transversal microconvection in vertical magnetic field.

10. The loss of stability of the localized photoabsorptive microstructure occurred through the emergence of the azimuthal perturbations.

The subsequent establishing of the lateral circulations causes the eventual deformations of the concentration field and the formation of polygonal shapes within the beam spot.

The comparison of the theoretical calculations with the available experimental data strongly evidences the presence of magnetic microconvection in photoabsorptive concentration microstructures subjected to an external magnetic field. The process of the formation of the extended gratings and the bidirectional grids is interpreted in terms of the convective-diffusive processes and the microscopic evolution of the photoabsorptive structures is explained on these grounds. The principal applicability of the current model and its limits in relation to the experimental systems are then discussed. The principal success of the hydrodynamic approach is the correct prediction of the parameters of the observed peristaltic instability due to the growth of the cross-roll perturbation.

In conclusion, the principal theses, which summarize the findings of this work are formulated and submitted for defense:

I. The formation of invisible magnetic microconvection within the photoabsorptive microstructures is claimed upon the application of external magnetic field.

The shape and direction of the microconvective currents completely correspond to the action of lateral magnetophoretic transport and the two transport mechanisms are almost indistinguishable in this regard.

II. The presence of magnetic microconvection is evidenced by the destabilization of the photoabsorptive convective-diffusive microstructures and the consequent symmetry breaking.

In principle, we consider that the existence of magnetoconvection in photoabsorptive concentration microstructures under the action of the applied magnetic field is highly probable, although substantial experimental investigations are still required. The possibility of fine magnetic control over the transport processes is one of the main features of ferrodispersions. Even relatively low thermal differences can cause intensive magnetoadvective mixing, enhancing the efficiency of the phoretic transport many times. Given the very recent interest in photoabsorptive thermogravitational microconvection for efficient phoretic trapping of macromolecules or crystal growth, ferrocolloids may prove invaluable for these purposes, especially under the conditions when the process is sensitive to the employed temperature range.

Bibliography

[1] Blums E., Cebers A., Maiorov M., *Magnetic fluids* (Walter de Gruyter, 1997)

[2] Rosensweig R.E., *Ferrohydrodynamics* (Dover Publications, 1997)

[3] Gogosov V.V., Naletova V.A., Shaposhnikova G.A. (1981), Hydrodynamics of magnetizable fluids, Advances in Science and Technology: Mechanics of Fluids and Gases 16

[4] Neuringer J.L., Rosensweig R.E. (1964), Ferrohydrodynamics, Phys. Fluids 7 (12), doi:10.1063/1.1711103

[5] Shliomis M.I. (1974), Magnetic fluids, Sov. Phys. Usp. 17 (2), doi:10.1070/PU1974v017n02ABEH004332

[6] Lenglet J., Bourdon A., Bacri J.C., Demouchy G. (2002), Thermodiffusion in magnetic colloids evidenced and studied by forced Rayleigh scattering experiments, Phys. Rev. E 65 (3), doi: 10.1103/PhysRevE.65.031408

[7] Bean C. P., Livingston J. D. (1959), Superparamagnetism, J. Appl. Phys. 30 (4), doi:10.1063/1.2185850

[8] Piazza R., Parola A. (2008), Thermophoresis in colloidal suspensions, J. Phys.: Condens. Matter 20 (15), doi:10.1088/0953-8984/20/15/153102

[9] Hort W., Linz S.J., Lucke M. (1992), Onset of convection in binary gas mixtures: Role of the Dufour effect, Phys. Rev. A 45 (6), 3737-3748, doi:10.1103/PhysRevA.45.3737

[10] Hollinger St., Lucke M. (1995), Influence of the Dufour effect on convection in binary gas mixtures, Phys. Rev. E 52 (1), 642-657, doi:10.1103/PhysRevE.52.642

[11] Blums E., Mezulis A., Maiorov M., Kronkalns G. (1997), Thermal diffusion of magnetic nanoparticles in ferrocolloids: Experiments on particle separation in vertical columns, JMMM 169 (1-2), 220-228, doi:10.1016/S0304-8853(96)00730-5

[12] Blum E.Ya. (1979), Thermomagnetophoresis of particles in magnetic suspensions, Magnetohydrodynamics 15 (1), 18-21

[13] Blums E., Odenbach S., Mezulis A., Maiorov M. (1998), Soret coefficient of nanoparticles in ferrofluids in the presence of a magnetic field, Phys. Fluids 10 (9), 2155-2163, doi:10.1063/1.869737

[14] Blums E. (1999), Mass transfer in nonisothermal ferrocolloids under the effect of a magnetic field, JMMM 201 (1-3), 242-247, doi:10.1016/S0304-8853(99)00014-1

[15] Voelker T., Odenbach S. (2005), Thermodiffusion in ferrofluids in the presence of a magnetic field, Phys. Fluids 17 (3), doi:dx.doi.org/10.1063/1.1864092

[16] Benard H. (1900), Les tourbillons cellulaires dans une nappe liquid, Rev. Gen. Sci. pures et appl. 11

[17] Strutt J.W. (3rd Baron Rayleigh, 1916), On Convection Currents in a Horizontal Layer of Fluid, when the Higher Temperature is on the Under Side, Phil. Mag. 32, 529-546

[18] Pearson J.R.A. (1958), On convection cells induced by surface tension, J. Fluid Mech. 4 (5), 489-500, doi:10.1017/S0022112058000616

[19] Busse F.H. (1978), Non-linear properties of thermal convection, Rep. Prog. Phys. 41 (12), doi:10.1088/0034-4885/41/12/003

[20] Cross M.C., Hohenberg P.C. (1993), Pattern formation outside of equilibrium, Rev. Mod. Phys. 65 (3), 851-1112, doi:10.1103/RevModPhys.65.851

[21] Platten J.K., Legros J.C., *Convection in Liquids* (Springer-Verlag, 1984)

[22] Gershuni G.Z., Zhukovitskii E.M. (1977), Convective Stability of Incompressible Fluids, J. Fluid Mech. 82 (4), doi:10.1017/S0022112077210986

[23] Le Gal P., Pocheau A., Croquette V. (1985), Square versus Roll Pattern at Convective Threshold, Phys. Rev. Lett. 54 (23), 2501-2504, doi:10.1103/PhysRevLett.54.2501

[24] Huke B., Lucke M. (2002), Convective Patterns in Binary Fluid Mixtures with Positive Separation Ratios, Lecture Notes in Physics 584, 334-354, doi:10.1007/3-540-45791-7_16

[25] Jung Ch., Huke B., Lucke M. (1998), Subharmonic Bifurcation Cascade of Pattern Oscillations Caused by Winding Number Increasing Entrainment, Phys. Rev. Lett. 81 (17), 3651-3654, doi:10.1103/PhysRevLett.81.3651

[26] Walden R.W., Kolodner P., Passner A., Surko C.M. (1985), Traveling waves and chaos in convection in binary fluid mixtures, Phys. Rev. Lett. 55 (5), 496-499, doi:10.1103/PhysRevLett.55.496

[27] Barten W., Lucke M., Kamps M., Schmitz R. (1995), Convection in binary fluid mixtures. I. Extended traveling-wave and stationary states, Phys. Rev. E 51 (6), 5636-5661, doi:10.1103/PhysRevE.51.5636

[28] Barten W., Lucke M., Kamps M., Schmitz R. (1995), Convection in binary fluid mixtures. II. Localized traveling waves, Phys. Rev. E 51 (6), 5662-5680, doi:10.1103/PhysRevE.51.5662

[29] Jung D., Lucke M. (2005), Traveling wave fronts and localized traveling wave convection in binary fluid mixtures, Phys. Rev. E 72 (2), doi:10.1103/PhysRevE.72.026307

[30] Ryskin A., Muller H.W., Pleiner H. (2003), Thermal convection in binary fluid mixtures with a weak concentration diffusivity, but strong solutal buoyancy forces, Phys. Rev. E 67 (4), doi:10.1103/PhysRevE.67.046302

[31] Ryskin A., Pleiner H. (2005), Thermal convection in colloidal suspensions with negative separation ratio, Phys. Rev. E 71 (5), doi:10.1103/PhysRevE.71.056303

[32] Odenbach S., Volker T. (2005), Thermal convection in a ferrofluid supported by thermodiffusion, JMMM 289, 122-125, doi:10.1016/j.jmmm.2004.11.036

[33] Shliomis M.I., Souhar M. (2000), Self-oscillatory convection caused by the Soret effect, Europhys. Lett. 49 (1), doi:10.1209/epl/i2000-00119-4

[34] Cerbino R., Vailati A., Giglio M. (2002), Soret driven convection in a colloidal solution heated from above at very large solutal Rayleigh number, Phys. Rev. E 66 (5), doi:10.1103/PhysRevE.66.055301

[35] Mazzoni S., Cerbino R., Brogioli D., Vailati A., Giglio M. (2004), Transient oscillations in Soret-driven convection in a colloidal suspension, Eur. Phys. J. E 15 (3), 305-309, doi:10.1140/epje/i2004-10070-8

[36] Shevtsova V.M., Melnikov D.E., Legros J.C. (2006), Onset of convection in Soret-driven instability, Phys. Rev. E 73 (4), doi:10.1103/PhysRevE.73.047302

[37] Huke B., Pleiner H., Lucke M. (2007), Convection patterns in colloidal solutions, Phys. Rev. E 75 (3), doi:10.1103/PhysRevE.75.036203

[38] Finlayson B.A. (1970), Convective instability of ferromagnetic fluids, J. Fluid Mech. 40 (4), 753-767, doi:10.1017/S0022112070000423

[39] Schwab L., Hildebrandt U., Stierstadt K. (1983), Magnetic Benard convection, JMMM 39 (1-2), doi:10.1016/0304-8853(83)90412-2

[40] Schwab L., Stierstadt K. (1987), Field-induced wavevector-selection by magnetic Bénard-convection, JMMM 65 (2-3), doi:10.1016/0304-8853(87)90059-X

[41] Bozhko A., Putin G. (2009), Thermomagnetic Convection as a Tool for Heat and Mass Transfer Control in Nanosize Materials Under Microgravity Conditions, Microgravity Science and Technology 21 (1-2), 89-93, doi: 10.1007/s12217-008-9059-7

[42] Chukhrov A.Yu. (1985), Formation of free convection in magnetodiffusion, Magnetohydrodynamics 21 (2), 154-158

[43] Blum E.Ya., Rimsha A.Ya., Chukhrov A.Yu. (1987), Convection and mass transfer in the high-gradient magnetic separation of colloidal particles, Magnetohydrodynamics 23 (2), 139-149

[44] Shliomis M.I., Smorodin B.L. (2002), Convective instability of magnetized ferrofluids, JMMM 252, 197-202, doi:10.1016/S0304-8853(02)00712-6

[45] Ryskin A., Pleiner H. (2004), Influence of a magnetic field on the Soret-effect-dominated thermal convection in ferrofluids, Phys. Rev. E 69 (4), doi:10.1103/PhysRevE.69.046301

[46] Shliomis M.I., Smorodin B.L. (2005), Onset of convection in colloids stratified by gravity, Phys. Rev. E 71 (3), doi:10.1103/PhysRevE.71.036312

[47] Ryskin A., Pleiner H. (2007), Magnetic Field Driven Instability in Stratified Ferrofluids, Phys. Rev. E 75 (5), doi:10.1103/PhysRevE.75.056303

[48] Smorodin B.L., Cherepanov I.N., Myznikova B.I., Shliomis M.I. (2011), Traveling-wave convection in colloids stratified by gravity, Phys. Rev. E 84 (2), doi:10.1103/PhysRevE.84.026305

[49] Maiorov M.M., Tsebers A.O. (1983), Magnetic microconvection on the diffusion front of the ferroparticles, Magnetohydrodynamics 19 (4), 376-380

[50] Tsebers A.O., Chukhrov A.Yu. (1986), Numerical modeling of hydrodynamic phenomena in the diffusion processes of magnetizable media, Magnetohydrodynamics 22 (3), 231-235

[51] Chukhrov A.Yu. (1986), Convective stability of dilute colloid in the presence of magnetic diffusion in an inhomogeneous field, Magnetohydrodynamics 22 (3), 254-258

[52] Lykov A.V., Berkovsky B.M., *Konvektsiya i teplovye volny [Convection and heat waves]* (Energy, 1974)

[53] Bacri J.C., Cebers A., Bourdon A., Demouchy G., Heegaard B.M., Perzynski R. (1995), Forced Rayleigh Experiment in a Magnetic Fluid, Phys. Rev. Lett. 74 (25), 5032-5035, doi:10.1103/PhysRevLett.74.5032

[54] Bacri J.C., Cebers A., Bourdon A., Demouchy G., Heegaard B.M., Kashevsky B., Perzynski R. (1995), Transient grating in a ferrofluid under magnetic field: Effect of magnetic interactions on the diffusion coefficient of translation, Phys. Rev. E 52 (4), 3936-3942, doi:10.1103/PhysRevE.52.3936

[55] Demouchy G., Bourdon A., Bacri J.-C., Da Cruz F., Mezulis A., Blums E. (2000), Forced Rayleigh scattering determination of the Soret coefficient and of the

thermodiffusion mobility of ferrofluids under applied magnetic field, Proc. of the 4th Int. PAMIR Conference 2, 433-438

[56] Cebers A., Igonin M. (2002), Convective instability of magnetic colloid and forced Rayleigh scattering experiments, Magnetohydrodynamics 38 (3), 265-270

[57] Igonin M. (2004), On the microconvective instability of an inhomogeneous magnetic fluid in a Hele-Shaw cell, Magnetohydrodynamics 40 (1), 53-64

[58] Mezulis A., Blums E. (2003), Two-dimensional determing of the transport coefficients under an applied magnetic field, Magnetohydrodynamics 39 (3), 369-375

[59] Mezulis A., Blums E. (2004), Experimental investigations of the microconvective instability in optically induced gratings, Magnetohydrodynamics 40 (4), 337-344

[60] Mezulis A., Blums E. (2005), Experimental investigations of the microconvective instability in optically induced gratings, Magnetohydrodynamics 41 (4), 341-348

[61] Mezulis A., Blums E. (2006), On the microconvective instability in optically induced gratings, Phys. Fluids 18 (10), doi:10.1063/1.2243337

[62] Mezulis A., Blums E. (2006), The Presence of Microconvective Instability in Optically Induced Gratings, J. Non-Eq. Thermodyn. 32 (3), 331-340, doi:10.1515/JNETDY.2007.025

[63] Lange A. (2004), Magnetic Soret effect: Application of the ferrofluid dynamics theory, Phys. Rev. E 70 (4), doi:10.1103/PhysRevE.70.046308

[64] Du T., Yuan S., Luo W. (1994), Thermal lens coupled magneto-optical effect in a ferrofluid, Appl. Phys. Lett. 65 (14), doi:10.1063/1.112861

[65] Du T., Luo W. (1995), Dynamic interference patterns from ferrolfuids, MPLB 9 (25), doi: 10.1142/S0217984995001650

[66] Cebers A., Du T., Luo W. (1996), Photoabsorptive magnetic instability of a magnetic liquid under uniform heating by a laser, Magnetohydrodynamics 32 (3), 315-321

[67] Cebers A., Du T., Luo W. (1996), Temperature-concentration (activator-inhibitor) model of magnetic fluid free surface autooscillations induced by absorption of light, Magnetohydrodynamics 32 (3), 303-314

[68] Luo W., Du T., Huang J. (1999), Novel Convective Instabilities in a Magnetic Fluid, Phys. Rev. Lett. 82 (20), 4134-4137, doi:10.1103/PhysRevLett.82.4134

[69] Luo W., Du T., Huang J. (1999), Field-induced instabilities in a magnetic fluid, JMMM 201 (1-3), 88-90, doi:10.1016/S0304-8853(99)00152-3

[70] Shliomis M.I. (2001), Comment on "Novel Convective Instabilities in a Magnetic Fluid", Phys. Rev. Lett. 87 (5), doi:10.1103/PhysRevLett.87.059801

[71] Luo W., Du T., Huang J. (2001), Reply to the Comment by Mark I. Shliomis, Phys. Rev. Lett. 87 (5), doi:10.1103/PhysRevLett.87.059802

[72] Liu M. (2000), Range of Validity for the Kelvin Force, Phys. Rev. Lett. 84 (12), 2762-2762, doi:10.1103/PhysRevLett.84.2762

[73] Luo W., Du T., Huang J. (2000), Reply to the Comment by Mario Liu, Phys. Rev. Lett. 84 (12), 2763-2763, doi:10.1103/PhysRevLett.84.2763

[74] Odenbach S., Liu M. (2001), Invalidation of the Kelvin Force in Ferrofluids, Phys. Rev. Lett. 86 (2), 328-331, doi:10.1103/PhysRevLett.86.328

[75] Engel A. (2001), Comment on "Invalidation of the Kelvin Force in Ferrofluids", Phys. Rev. Lett. 86 (21), 4978-4978, doi:10.1103/PhysRevLett.86.4978

[76] Braun D., Libchaber A. (2002), Trapping of DNA by Thermophoretic Depletion and Convection, Phys. Rev. Lett. 89 (18), doi:10.1103/PhysRevLett.89.188103

[77] Duhr S., Braun D. (2006), Optothermal Molecule Trapping by Opposing Fluid Flow with Thermophoretic Drift, Phys. Rev. Lett. 97 (3), doi:10.1103/PhysRevLett.97.038103

[78] Braun D., Goddard N.L., Libchaber A. (2003), Exponential DNA Replication by Laminar Convection, Phys. Rev. Lett. 91 (15), doi:10.1103/PhysRevLett.91.158103

[79] Braun D. (2004), PCR by Thermal Convection, MPLB 18 (16), 775-784, doi:10.1142/S0217984904007049

[80] Duhr S., Braun D. (2005), Two-dimensional colloidal crystals formed by thermophoresis and convection, Appl. Phys. Lett. 86 (13), doi:10.1063/1.1888036

[81] Dobran F., *Theory of Structured Multiphase Mixtures* (Springer-Verlag, 1991)

[82] Ishii T., Hibiki T., *Thermo-Fluid Dynamics of Two-phase Flow* (Springer, 2006).

[83] Batchelor G.K. (1972), Sedimentation in a dilute dispersion of spheres, J. Fluid Mech. 52 (2), 245-268, doi:10.1017/S0022112072001399

[84] Batchelor G.K. (1977), The effect of Brownian motion on the bulk stress in a suspension of spherical particles, J. Fluid Mech. 83 (1), 97-117, doi:10.1017/S0022112077001062

[85] Cowley M.D., Rosensweig R.E. (1967), The interfacial stability of a ferromagnetic fluid, J. Fluid Mech. 30 (4), 671-688, doi:10.1017/S0022112067001697

[86] Shaposhnikov I.G., Shliomis. M.I. (1975), Hydrodynamics of magnetizable media, Magnetohydrodynamics 11 (1), 37-46

[87] Gogosov V., Naletova V., Shaposhnikova G. (1980), Hydrodynamics of dispersive magnetizable media including Brown motion, IEEE Transactions on Magnetics 16 (2), 301-308, doi:10.1109/TMAG.1980.1060580

[88] Blums E. (2003), Magnetic Soret effect in ferrocolloids: Experimental results and new problems, Magnetohydrodynamics 39 (3), 353-360

[89] Blum E.Ya., Rimsha A.Ya., Chukhrov A.Yu. (1987), Convection and mass transfer in the high-gradient magnetic separation of colloidal particles, Magnetohydrodynamics 23 (2), 139-149

[90] Landau L.D., Lifshitz E.M., *Course of Theoretical Physics 6: Fluid Mechanics* (Butterworth-Heinemann, 1987)

[91] Tynjala T., Bozhko A., Bulychev P., Putin G., Sarkomaa P. (2006), On features of ferrofluid convection caused by barometrical sedimentation, JMMM 300 (1), doi:10.1016/j.jmmm.2005.10.078

[92] Blums E., Mezulis A., Bourdon A. (1999), Some heat and mass transfer problems related to the measurements of a Soret effect in ferrofluids, Progress in Engineering Heat Transfer 247

[93] Mezulis A., Blums E., Bourdon A., Demouchy G. (2000), Thermodiffusion-induced optical index grating in ferrocolloids: determination of transport coefficients, Proc. of the 4th Int. PAMIR Conference 2, doi:10.1063/1.869737

[94] Dr. A. Mezulis, Private communication

[95] Chandrasekhar S., *Hydrodynamic and Hydromagnetic Stability* (Dover, 1981)

[96] Tsebers A.O. (1981), Dynamics of magnetostatic instabilities, Magnetohydrodynamics 17 (2), 113-121

[97] Cebers A. (1994), A numerical simulation of the dynamics of bending deformations of the magnetized stripes in Hele-Shaw cells, Magnetohydrodynamics 30 (1), 20-26

[98] Cebers A. (1997), Stability of diffusion fronts of magnetic nanoparticles in porous media (Hele-Shaw cell) under the action of an external magnetic field, Magnetohydrodynamics 33 (1), 48-55

[99] Cebers A., Drikis I. (1996), A numerical study of the evolution of quasi-two-dimensional magnetic fluid shapes, Magnetohydrodynamics 32 (1), 8-17

[100] Fernandez J., Kurowski P., Limat L., Petitjeans P. (2001), Wavelength selection of fingering instability inside Hele-Shaw cells, Phys. Fluids 13 (11), 3120-3125, doi:10.1063/1.1410120

[101] Fernandez J., Kurowski P., Petitjeans P., Meiburg E. (2002), Density-driven unstable flows of miscible fluids in a Hele-Shaw cell, J. Fluid Mech. 451, 239-260, doi:10.1017/S0022112001006504

[102] Graf F., Meiburg E., Hartel C. (2002), Density-driven instabilities of miscible fluids in a Hele-Shaw cell: linear stability analysis of the three-dimensional Stokes equations, J. Fluid Mech. 451, 261-282, doi:10.1017/S0022112001006516

[103] Zebib A. (1996), Thermal convection in a magnetic fluid, J. Fluid Mech. 321, 121-136

[104] Lange A. (2002), Thermomagnetic convection of magnetic fluids in a cylindrical geometry, Phys. Fluids 14 (7), 2059-2064